2010

# Utilizing reactive capability of doubly fed induction generators to enhance system voltage performance and withstand wind variability

Pradip Vijayan
*Iowa State University*

# Utilizing reactive capability of doubly fed induction generators to enhance system voltage performance and withstand wind variability

by

Pradip Vijayan

A thesis submitted to the graduate faculty

in partial fulfillment of the requirements for the degree of

MASTER OF SCIENCE

Major: Electrical Engineering

Program of Study Committee:
Venkataramana Ajjarapu, Major Professor
James D McCalley
Umesh Vaidya

Iowa State University

Ames, Iowa

2010

# Table of Contents

# LIST OF FIGURES

## LIST OF TABLES

# CHAPTER 1: INTRODUCTION

## 1.1 Growth of Wind-based Power Generation

The fluctuating global fuel prices, concerns with the depleting fossil fuel reserves and apprehension relating to climate change has resulted in an increasing focus on renewable sources to satisfy rising global energy requirements. Amongst the available renewable sources of energy wind and hydro are the most feasible for utility scale power generation. With a majority of the hydro reserves around the world reaching the maximum capacity in terms of available power there is an increasing shift towards wind power generation to satisfy the need of a clean renewable source [1], [2]. The year 2008 was a record year for wind generation in the United States with a total increase of 8,360 MW which is 50% of the total wind capacity at the end of 2007 [3]. Wind energy accounted for 42% of the total new capacity added. In 2008, the United States overtook Germany to become the country with the largest installed wind power capacity in the world. The total wind power capacity of the United States is at 25,170 MW [4].

Federal policy in the form of production tax credits and state regulations in the form of renewable portfolio standards (RPS) [5] have contributed to encouraging the development of wind generation in the United States [6]. Over 25 states have accepted RPS by requiring a substantial contribution from renewable sources of energy to their power generation portfolio [7].

## 1.2 Wind Generation Technologies

There are two major classifications amongst wind generation units: fixed speed generation and variable speed generation [8]. The fixed speed generators have a design speed for which they have maximum efficiency whereas for other speeds their efficiency is lower. But variable speed generators have the maximum power tracking capability that extracts maximum available power out of the wind at different speeds thereby resulting in more efficient operation. Also the variable speed generators reduce mechanical stresses on the turbine thus increasing the lifetime of the turbine. It also helps damp out oscillations in torques more efficiently. Thus variable speed generators are more commonly installed.

Amongst the variable speed generators there are two major kinds, synchronous generators with direct power electronic converters and doubly fed induction generators with rotor side power electronic converters. Both have the above mentioned advantages of variable speed generators but the power electronic ratings of the two machines are different. In a doubly fed induction generator the power electronic converter has a rating of about 30% of the machine rating whereas for the synchronous generator the rating of the power electronic converter is the same as machine rating thereby resulting in higher costs. Thus DFIGs are the preferred choice for installation.

## 1.3 Doubly-Fed Induction Generators

The Doubly Fed Induction Machine is shown in figure 2[9]. It consists of a wind turbine that is connected via a gear train to the rotor shaft of the induction generator. The rotor terminals of the induction machine are connected to the four-quadrant power electronic converter capable of both supplying real/reactive power from the grid to the rotor as well as supplying power from the rotor to the grid [5]. The converter consists of two separate devices with different functions, the generator side converter and the grid side converter. The generator side converter controls the real and reactive power output of the machine and the grid side converter maintains the DC link voltage at its set point. These converters are controlled respectively by the Generator side controller and the Grid side controller. The DFIG also has a wind turbine control that maximizes the power output from the turbine via pitch control and sends this computed maximum power output $P_{grid}^{conv,ref}$ to the converter.

The Power electronic converter is connected to the grid via a transformer that steps up the voltage to the grid. The stator side of the induction generator is also connected to the grid via a step up transformer. The point of interconnection with the grid is the point used to measure the active and reactive power output of the wind farm. In case the system reliability requires that additional reactive power be injected a STATCOM may be connected at this point of interconnection.

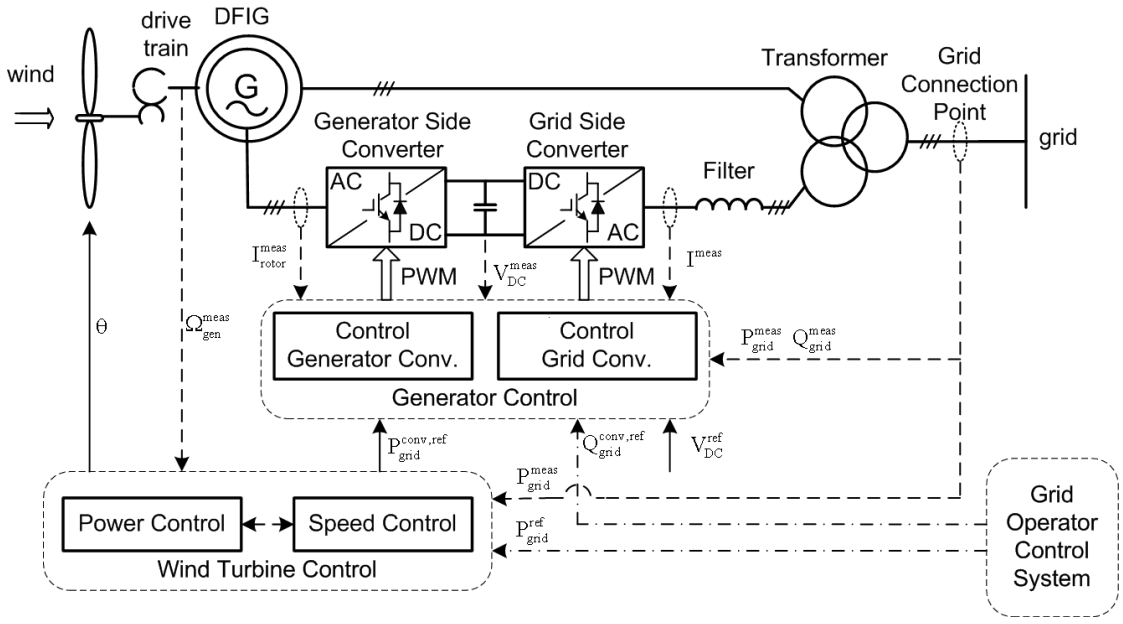


**Figure 1: Schematic of a Doubly Fed Induction Generator [9]**

The doubly fed Induction generator consists of a three phase induction generator with three phase windings on the rotor. The rotor is connected to a converter which supplies power to the rotor via the slip rings. The power electronic converter is capable of handling power flow in both directions which permits the DFIG to operate at both sub synchronous and super synchronous speeds. The DFIG produces controlled voltage $V_1$ at grid frequency $f_1$ at the stator and variable voltage $V_2$ is provided at the rotor at variable frequency$f_2$. The frequency of the rotor depends on the angular velocity of the rotor which in turn depends on the wind speed. Let $f_r$ be the electrical frequency of revolution of the rotor. The following relation holds between the various frequencies:

$$f_r = f_1 \pm f_2 \tag{1}$$

The positive sign above is for the super synchronous operation where rotor speed exceeds rated speed and negative sign is for sub synchronous operation when rotor speed is

less than rated speed. At super synchronous speed the phase sequence of the rotor currents is the same as the stator and power is supplied from the rotor to the grid. In the sub synchronous operation power is drawn by the rotor from the grid and the phase sequence of rotor currents is opposite to the phase sequence of the stator currents.

The steady state operation of the DFIG is only restricted by the converter ratings of the rotor side converter. The maximum power rating of the rotor side converter ($P_{max}$) is generally 25%-30% of the Induction machine ratings. Thus if the converter is operated such that all magnetizing power is provided by the stator, the maximum rotor power supplied/absorbed is $P_{max}$, and the maximum magnitude of slip for operation is given by

$$s_{max} = {}^{P_{max}}/_{P_{rated}} \tag{2}$$

Where, $P_{rated}$ is the rated power output of the DFIG.

This means that the DFIG can provide an operating range of 75% to 125% of the rated wind speed. Also the pitch control with maximum power tracking allows the DFIG to produce maximum power at different wind speeds thus increasing overall efficiency of the unit.

### 1.3.1 Control of a Doubly Fed Induction Generator

The space phasor equivalent circuit of a DFIG is given below:

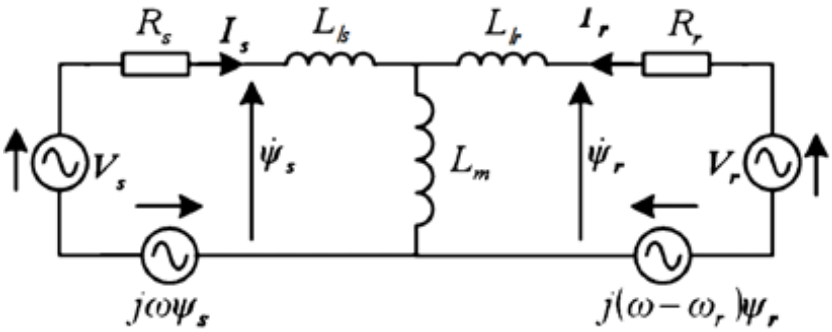


**Figure 2 : Space Phasor Equivalent Circuit [9]**

Considering a synchronously rotating reference frame with $\omega = \omega_1$ , and converting to time domain, the following equations are obtained:

$$I_s R_s + V_s = -\frac{d}{dt}\Psi_s - j\omega\Psi_s \quad (3)$$

$$I_r R_r + V_r = -\frac{d}{dt}\Psi_r - j(\omega - \omega_r)\Psi_r \quad (4)$$

### 1.3.2 Control of Generator Side Converter

Now the stator flux is more or less constant and thus is assumed to be a constant. It is also assumed that saturation does not occur. Also stator resistance is negligible and hence the stator resistance is assumed to be zero. Now we select the d-q axis such that the stator flux $\Psi_s$ is along the d axis. Therefore $\Psi_q = 0$. Also since we assume that $\Psi_d$ is constant $\frac{d}{dt}\Psi_d = 0$. Now using these values in the stator equation of (3) we obtain:

$$V_d = 0 \tag{5}$$

$$V_q = -\omega_1 \Psi_d \tag{6}$$

Now, rearranging the stator flux equation to obtain $I_s$ in terms of the other values:

$$I_s = \Psi_s - \frac{L_m}{L_s} I_r \tag{7}$$

Where $L_s = L_{sl} + L_m$

Now power delivered at stator is given by:

$$S_s = V_s * I_s \tag{8}$$

Thus,

$$P_s = \frac{3}{2}(V_d I_d + V_q I_q) = \frac{3}{2} V_q I_q = \frac{3}{2} \omega_1 \Psi_d \frac{L_m}{L_s} I_{qr} \tag{9}$$

$$Q_s = \frac{3}{2}(V_d I_q - V_q I_d) = -\frac{3}{2} V_q I_d = \frac{3}{2} \omega_1 \Psi_d \left(\Psi_d - \frac{L_m}{L_s} I_{dr}\right) \tag{10}$$

From the above equation it is observed that $P_s$ can be controlled by the $I_{qr}$ component and the $Q_s$component can be controlled by the $I_{dr}$ component, assuming the stator flux is constant. Thus the appropriate control can be applied to the rotor side converter to obtain the required $I_{dr}$ and $I_{qr}$ for the set point $P_s$ and $Q_s$ values. This is the decoupled control of the active and reactive power in a DFIG.

### 1.3.3 Control of Grid Side Converter

The objective of the supply side converter is to maintain the DC link voltage at its set point value irrespective of the flow direction of power to the rotor. The supply side

converter maintains the DC link voltage constant irrespective to direction of rotor current and draws a sinusoidal current from the supply. The real power drawn from the supply maintains the DC link voltage at a constant value and this is controlled by the $i_{dc}$ component of the supply current drawn and the $i_{qc}$ component provides the requisite reactive power. For operation in which all reactive power is obtained from the stator side $i_{qc}$ is set to 0.

### 1.3.4 Summary of DFIG Controls

The rotor side converter controls the rotor currents to obtain the required real and reactive power outputs at the stator side. The real power setting is usually obtained using a maximum power tracking scheme [8]. The reactive power setting can vary depending on the control mode of the DFIG. The two popular control modes are:

Power Factor Control

Voltage Control

In the power factor control mode the stator real and reactive power are controlled so as to maintain a constant power factor at the point of interconnection. In the voltage control mode the reactive power is controlled to maintain the voltage at the Point of Interconnection to a fixed value.

The grid side converter is usually set at unity power factor.

# CHAPTER 2: IMPACT OF DFIG CAPABILITY CURVE ON STEADY STATE OPERATION

## 2.1 Reactive Power Requirements in a Power System

A majority of the newly installed wind generation consists of doubly fed induction generators (DFIG) [10]. As more units start coming online, increasing levels of wind penetration has generated a widespread concern over its impact on power system performance. There are primarily two reasons for such a concern, the variability of wind and the nature of the generator which is different from conventional units [11]. The effect of high wind penetration levels on system performance becomes critical in the planning of future units and to accomplish the requirements of the various states RPS.

The precise modeling of DFIG units is important for both static and dynamic analysis of power system performance [1]. To accurately assess the stability of a system and to prevent voltage violations, computation of available reactive power in the system is essential [12]. Reactive power is essential for the stable operation of the power system. It facilitates flow of active power from generation sources to load centers [13]-[15] and maintains bus voltages within prescribed limits [16]. Stable operation of power systems requires the availability of sufficient reactive generation [17]. Both static and dynamic reactive power sources play an important role in voltage stability [18], [19].

Traditional wind generation units consisting of Simply Fed induction generators (SFIG) do not allow for reactive support, but on the contrary are reactive power consumers. To mitigate this reactive demand SFIG wind parks are typically equipped with external sources of reactive power. Static sources like shunt capacitors are relatively inexpensive

compared to dynamic resources such as SVCs [20]. In contrast newer wind parks consisting of DFIG units have reactive power capability [21]. The presence of power electronic controls in DFIGs makes them a fast acting dynamic reactive resource as compared to direct grid connected synchronous generators [22] used in conventional power plants. This allows for voltage control and reactive power regulation of the wind park [23], [24].

In 2005, FERC orders 661 and 661A [25], [26] were released which mandate the interconnection requirements for large wind parks over 20MW. According to this order, a key requirement for plant operation is that the power factor at the point of interconnection (POI) must remain between 0.95 leading and 0.95 lagging. Reference [26] states that the reason for this ruling is that reactive power capability for a wind plant is a significant additional cost compared to conventional units which possess inherent reactive capability.

Imposing this power factor restriction limits the performance of DFIG wind parks. As penetration levels continue to increase the impact from the loss in performance translates into higher operating costs. This work demonstrates that utilization of the capability curve can lead to improved system performance. This will also reduce the amount of committed conventional reactive reserve. The FERC order 661-A gives general guidelines for interconnecting wind parks, but for specific parks employing DFIG units the restriction on power factor can be lifted because additional performance may be obtained at no extra cost to the wind farm owner.

## 2.2 Capability Curve of a DFIG Machine

### 2.2.1 Reactive Capability Limitations

The reactive power capability of any generation unit on the power system is essential in studying long term stability and voltage stability. Traditional synchronous generators have limitations in terms of maximum current and heating of the machine. The active power of the machine is limited by the prime mover capability. The reactive current output capability is dependent on the armature current limit, field current limit and heating limit of the coils. The armature current limit is the maximum temperature limit on the stator winding coils. Similarly, the field current limit is the maximum temperature limit on the field coil. Thus, the reactive capability of the synchronous generator depends on the machine limitations.

A Doubly Fed Induction Generator (DFIG) has advantages over the Singly Fed Induction Generator in its inherent capability to handle variable wind speed. The rotor side converter injects currents and voltages according to various wind speeds. The following figure indicates the variation in power output of a DFIG with respect to the wind velocity. It also indicates the variation in rotor slip with wind speed. This figure can be used to determine the rotor slip at different power output levels.

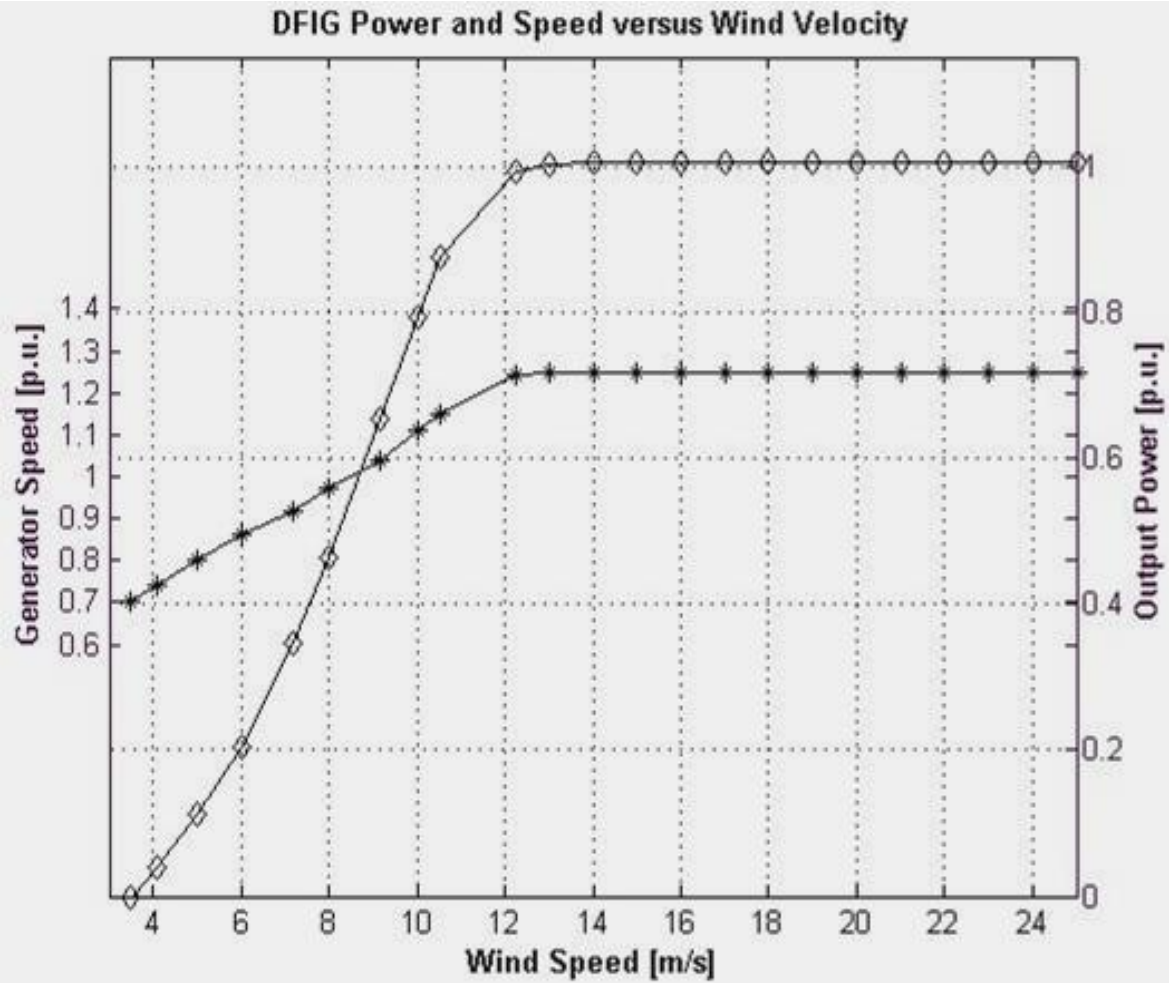


**Figure 3: Maximum Power Tracking Scheme**

The DFIG exchanges power through both the rotor and the stator. Majority of the power is passed through the stator, and a fraction of the power is passed through the rotor and the power converter. To determine the reactive power limits the electromechanical characteristics of the generator and the power converter have to be taken into consideration. Since the DFIG is a variable speed machine the rotor speed and the slip play an important role. The three limiting parameters for the reactive power capability of the DFIG are stator current, rotor current and rotor voltage [27]. The stator voltage is given by the grid, and is not influenced by the wind turbine design. The stator current limit depends on the generator

design, whereas the rotor voltage and rotor current limits depend on generator as well as power converter designs. The rotor voltage limitation is essential for the rotor speed interval, because the required rotor voltage to provide a certain field is directly proportional to the slip. Thus, the possible rotor speed is limited by the possible rotor voltage.

Figure 4 gives the T-equivalent of a Doubly Fed Induction Generator [27]. The equations describing the T model are given below. All variables are referred to the stator side.

$$(R_s + jX_s).I_s + jX_m(I_s + I_r) = V_s \tag{11}$$

$$\left(\frac{R_r}{s} + X_r\right)I_r + jX_m(I_s + I_r) = \frac{V_r}{s} \tag{12}$$

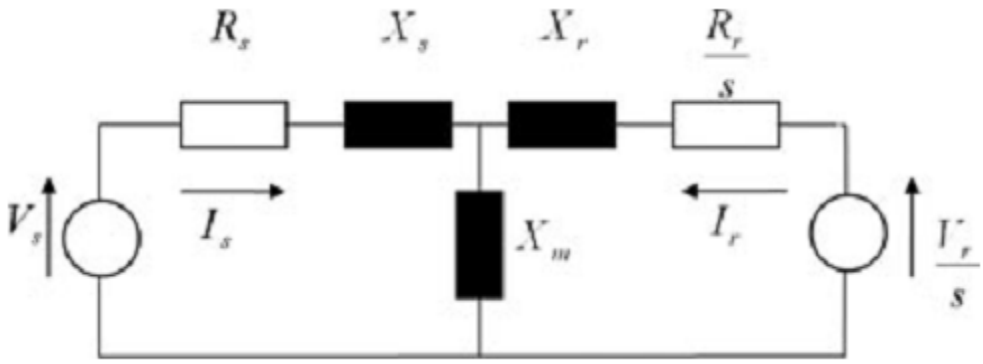


**Figure 4: T- Equivalent Circuit of DFIG [27]**

The rotor resistance and voltage can be divided into two components- Mechanical power and rotor loss. The mechanical power is represented in the following equation.

$$P_{mech} = Re\left\{V_r\left(\frac{1}{s} - 1\right)I_r^*\right\} - I_r I_r^* R_r\left(\frac{1}{s} - 1\right) \tag{13}$$

The division of power is reflected in the following figure.

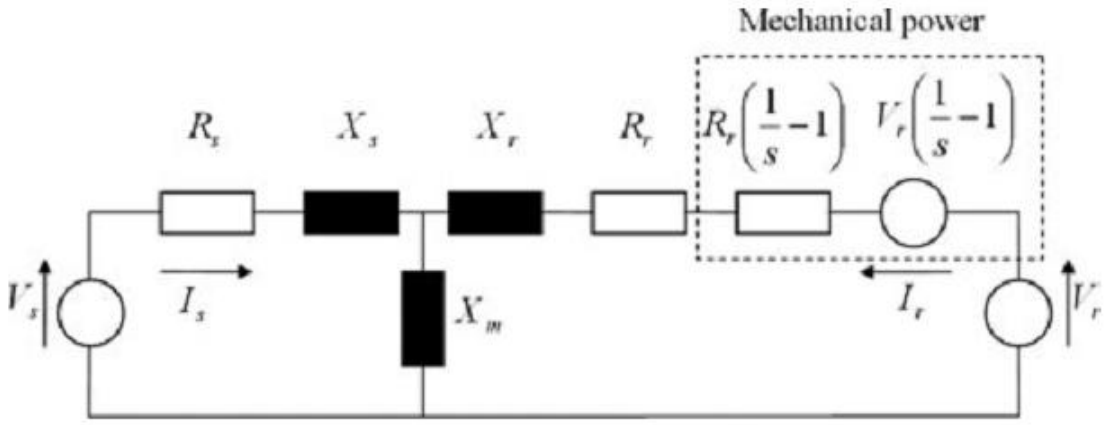


**Figure 5 : T- Equivalent Circuit with Mechanical Power [27]**

The power exchange in the above figure 5 [27] is considered positive coming out of the generator and rotor. Thus, the apparent stator and rotor powers are represented as:

$$S_s = -V_s I_s^* \tag{14}$$

$$S_r = -V_r I_r^* \tag{15}$$

The power delivered to the grid is given by the sum of the power delivered by the stator and the grid side converter. The grid side converter passes the real power delivered/absorbed through the rotor. Normally the grid side converter is set to operate at unity power factor. Hence the total power delivered to the grid can be given as:

$$S_{tot} = S_s + Re\{S_r\} - S_{loss} \tag{16}$$

In the above equation $S_{loss}$ consists of active and reactive losses in the generator and the converters.

### 2.2.2 Two-Port Parameters

The T-model for the Doubly Fed Induction Generator is represented in a two-port model to investigate the influence of the stator current, rotor current and rotor voltage on the reactive power capability.


**Figure 6 : Two Port Equivalent of DFIG [27]**

The above figure 6 [27] demonstrates the two port model. The following three equations describe the different correlations between the apparent power delivered to the grid and the rotor voltage, rotor current and the stator current respectively.

$$\begin{bmatrix} I_s \\ I_r \end{bmatrix} = Y. \begin{bmatrix} V_s \\ V_r/_s \end{bmatrix} \tag{17}$$

$$\begin{bmatrix} I_s \\ V_r/_s \end{bmatrix} = G. \begin{bmatrix} V_s \\ I_r \end{bmatrix} \tag{18}$$

$$\begin{bmatrix} V_r/_s \\ -I_r \end{bmatrix} = B. \begin{bmatrix} V_s \\ I_s \end{bmatrix} \tag{19}$$

The Y, G and B matrices are derived from the Z matrix. The Z matrix for the given 2 port system is

$$\begin{bmatrix} V_s \\ I_s \end{bmatrix} = Z. \begin{bmatrix} V_r/s \\ I_r \end{bmatrix} \tag{20}$$

Where, $Z = \begin{bmatrix} Z_s + Z_m & Z_m \\ Z_m & Z_r + Z_m \end{bmatrix}$ (21)

For a standard system:

$$Z = \begin{bmatrix} Z_{11} & Z_{12} \\ Z_{21} & Z_{22} \end{bmatrix} \tag{22}$$

$$Y = Z^{-1} = \frac{1}{\det(Z)} \begin{bmatrix} Z_{22} & -Z_{12} \\ -Z_{21} & Z_{11} \end{bmatrix} \tag{23}$$

For the two port system being considered, this equation transforms to:

$$Y = \begin{bmatrix} Z_r + Z_m/\det(Z) & -Z_m/\det(Z) \\ -Z_m/\det(Z) & Z_s + Z_m/\det(Z) \end{bmatrix} \tag{24}$$

For a standard two port system the G matrix is given by:

$$G = \frac{1}{Z_{11}} \begin{bmatrix} 1 & -Z_{12} \\ Z_{21} & \det(Z) \end{bmatrix} \tag{25}$$

For the DFIG two-port representation:

$$G = \begin{bmatrix} 1/Z_s + Z_m & -Z_m/Z_s + Z_m \\ Z_m/Z_s + Z_m & (Z_r + Z_s)Z_m + Z_s Z_r/Z_s + Z_m \end{bmatrix} \tag{26}$$

For a standard two port system the B matrix is given by:

$$B = \frac{1}{Z_{12}} \begin{bmatrix} Z_{22} & -\det(Z) \\ -1 & Z_{11} \end{bmatrix} \tag{27}$$

For the DFIG two-port representation:

$$B = \begin{bmatrix} Z_r + Z_m/Z_m & -((Z_r + Z_s)Z_m + Z_s Z_r)/Z_m \\ -1/Z_m & Z_s + Z_m/Z_m \end{bmatrix} \quad (28)$$

### 2.2.3 Rotor Current Limitation

To determine the reactive limits of a DFIG as a function of the rotor current, the PQ diagram is obtained by fixing the rotor current at its rated value and then varying the angle. By using the equation (18), the stator current can be represented in terms of the rotor current as:

$$I_s = G_{11} V_s + G_{12} I_r \quad (29)$$

$$I_s = \left(\frac{V_s - Z_m I_r}{Z_s + Z_m}\right) \quad (30)$$

The apparent power at the stator as a function of the rotor current ($S_{s\_Ir}$) is given by the following equation.

$$S_{s\_Ir} = - V_s I_s^* \quad (31)$$

$$S_{s\_Ir} = -V_s \left(\frac{V_s - Z_m I_r}{Z_s + Z_m}\right)^* \quad (32)$$

$$S_{s\_Ir} = -V_s \left(\frac{V_s - Z_m I_r}{Z_s + Z_m}\right)^* \quad (33)$$

The above equation is divided into two sections to isolate the section dependent on the rotor current.

$$S_{s\_Ir} = - V_s V_s^* \left(\frac{1}{Z_s + Z_m}\right)^* + I_r^* V_s \left(\frac{Z_m}{Z_s + Z_m}\right)^* \quad (34)$$

In the above equation, the first term is a constant since the stator voltage is assumed constant. The second term can be used to determine the reactive power limits by setting the magnitude of $I_r$ to its rated value and varying the angle. The equation for the stator apparent power can be represented as a circle with the center as $c_{s\_Ir}$ and a radius of magnitude $r_{s\_Ir}$.

$$c_{s\_Ir} = -|V_s|^2 \left(\frac{1}{Z_s+Z_m}\right)^* \tag{35}$$

$$r_{s\_Ir} = |I_r||V_s| \left|\frac{Z_m}{Z_s+Z_m}\right| \tag{36}$$

The power delivered to the grid is a combination of both stator and rotor powers. The rotor power component can be represented in terms of stator voltage and rotor current by replacing the rotor voltage equation from (18) and (26) in the rotor apparent power equation (15)

$$S_{r\_Ir} = -(G_{21}V_s + G_{22}I_r).s.I_r^* \tag{37}$$

$$S_{r\_Ir} = \left(\frac{Z_m V_s + I_r\left((Z_r+Z_s)Z_m + Z_s Z_r\right)}{Z_s+Z_m}\right).s.I_r^* \tag{38}$$

$$S_{s\_Ir} = -I_r.I_r^*.s.\frac{(Z_r+Z_s)Z_m + Z_s Z_r}{Z_s+Z_m} - I_r^*.V_s.s.\left(\frac{Z_m}{Z_s+Z_m}\right) \tag{39}$$

Since the grid side converter generally operates at unity power factor, the real power is of interest in the above equation. The first term is dominated by $Z_m$ , and since $Z_m$ is purely imaginary the first term can be approximated as purely imaginary and thus constituting reactive power. By comparing the real parts of (39) and (34), the following approximation can be made:

$$P_r = -s.P_s \tag{40}$$

The total real and reactive power output of the DFIG is given by:

$$P_{tot} = (1 - s).P_s \tag{41}$$

$$Q_{tot} = Q_s \tag{42}$$

The equation for the stator apparent power from (35) and (36) can be represented as:

$$\left(P_s - Re(c_{s\_Ir})\right)^2 + \left(Q_s - Im(c_{s\_Ir})\right)^2 = \left(r_{s\_Ir}\right)^2 \tag{43}$$

$$\left(\frac{P_{tot}}{(1-s)} - Re(c_{s\_Ir})\right)^2 + \left(Q_{tot} - Im(c_{s\_Ir})\right)^2 = \left(r_{s\_Ir}\right)^2 \tag{44}$$

Since $Z_m$ is purely imaginary and when connected to a strong grid $|Z_m| \gg |Z_s|$, the real part of (35) is small, and can be equivalence to the magnetizing losses. Since the slip $s$ is also small, the product of the slip and the real part of $c_{s_{Ir}}$ is small and can be neglected. By making this assumption the equation (44) can be modified as given below.

$$\left(\frac{P_{tot} - Re(c_{s_{Ir}})}{(1-s)}\right)^2 + \left(Q_{tot} - Im(c_{s_{Ir}})\right)^2 = \left(r_{s\_Ir}\right)^2 \tag{45}$$

The above equation is in the form of a standard ellipse and thus can easily be implemented for different values of slip. The assumption made in equation (45) and (41) will be utilized to determine the reactive power limits as a function of rotor voltage and stator current. With these assumptions it is sufficient to compute the stator side apparent power from equation (17) for the rotor voltage limitation.

### 2.2.4 Rotor Voltage Limitation

By using equation (17) the stator current can be represented in terms of the rotor voltage as:

$$I_s = Y_{11}V_s + Y_{12}\frac{V_r}{s} \tag{46}$$

$$I_s = \left( \frac{V_s\,(Z_r + Z_m) - \frac{V_r}{s} Z_m}{(Z_r + Z_s) Z_m + Z_r Z_s} \right) \tag{47}$$

Using equation (47) in the stator apparent power equation (31)

$$S_{s\_Vr} = -V_s \left( \frac{V_s\,(Z_r + Z_m) - \frac{V_r}{s} Z_m}{(Z_r + Z_s) Z_m + Z_r Z_s} \right)^* \tag{48}$$

By dividing the above equation into two parts, a constant function of the stator voltage and a variable function of the rotor voltage and slip are obtained. The stator apparent power can be represented as a circle with a center and radius provided below

$$c_{s\_Vr} = -|V_s|^2 \left( \frac{(Z_r + Z_m)}{(Z_r + Z_s) Z_m + Z_r Z_s} \right)^* \tag{49}$$

$$r_{s\_Vr} = \left| \frac{V_r}{s} \right| |V_s| \left| \frac{Z_m}{(Z_r + Z_s) Z_m + Z_r Z_s} \right| \tag{50}$$

By substituting the above values for center and radius in equation (45) the reactive power limits as a function of rotor voltage can be obtained.

$$\left( \frac{P_{tot} - Re(c_{s\_Vr})}{(1-s)} \right)^2 + \left( Q_{tot} - Im(c_{s\_Vr}) \right)^2 = \left( r_{s\_Vr} \right)^2 \tag{51}$$

### 2.2.5 Stator Current Limitation

From equation (30) the stator apparent power is directly available as a function of stator current. The center is at the origin.

$$c_{s\_Is} = 0 \tag{52}$$

$$r_{s\_Is} = |I_s||V_s| \tag{53}$$

By substituting (52) and (53) in equation (45) the following equation is obtained.

$$\left( \frac{P_{tot}}{(1-s)} \right)^2 + (Q_{tot})^2 = \left( r_{s\_Is} \right)^2 \tag{54}$$

### 2.2.6 Combination of Limitations

The capability curve is obtained by the most restrictive of the three limitations. For all the analysis a Doubly Fed Induction Generator with the following parameters is used. In addition to the above three limitations, the mechanical power limitation also exists. The mechanical power limitation is reflected in the slip. From figure 3 the corresponding Pmax for a given slip can be obtained.

**Table 1 : DFIG Wind Park Machine Simulation Parameters**

| Machine Parameter | Value |
|---|---|
| Rated mechanical power | 1.5 MW |
| Rated generator power | 1.3 MW |
| Rated stator voltage | 575 V |
| Rotor to stator turns ratio | 3 |
| Machine inertia | 30 $kgm^2$ |
| Rotor inertia | 610000 $kgm^2$ |
| Inductance: mutual, stator, rotor | 4.7351, 0.1107, 0.1193 p.u. |
| Resistance: stator, rotor | 0.0059, 0.0066 p.u. |
| Number of poles | 3 |
| Grid frequency | 60 Hz |
| Gearbox ratio | 1:72 |
| Nominal rotor speed | 16.67 rpm |
| Rotor radius | 42 m |
| Maximum slip range | +/- 30% |

At slip -0.25, the maximum power limit is hit. The figure 7 below demonstrates the various limitations on the reactive power capability. The most restricting value of $Q_{max}$ and $Q_{min}$ is used to obtain the capability curve. The maximum power tracking scheme in figure 3 is used to obtain the slips at 5%, 25%, 50%, 75% and 100% output levels. The following table summarizes the different slips at these output levels.

**Table 2 Slip Levels corresponding to different power outputs**

| Power Level | Slip Value |
|---|---|
| 0% | 0.25 |
| 25% | 0.12 |
| 50% | 0.03 |
| 75% | -0.08 |
| 100% | -0.25 |

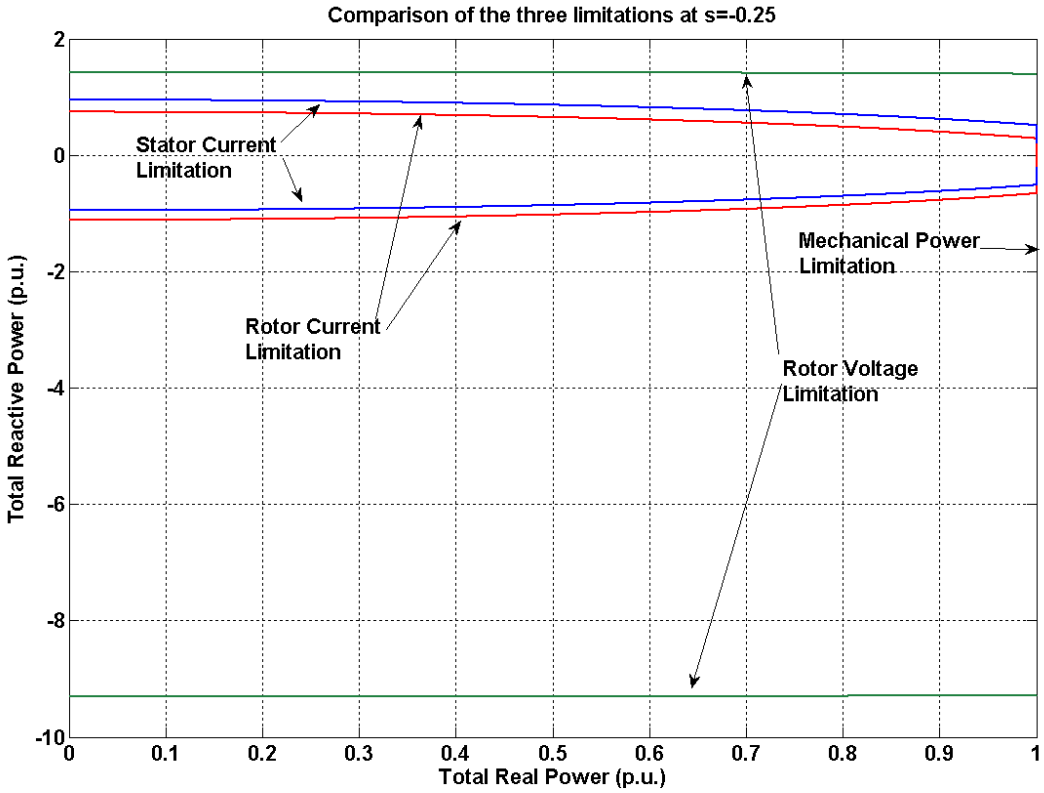


**Figure 7 : Comparison of the three limitations at slip = -0.25**

### 2.2.7 Sensitivity of reactive capability to stator voltage

Since the stator voltage is assumed to be constant in the above derivation, it is important to understand the sensitivity of stator voltage levels on the reactive power capability. This is necessary because if the DFIG is used to maintain remote voltage, then the reactive capability should be very close in the entire range of stator voltage variation. Figure 8 below demonstrates the reactive capability at 0.03 slip for stator voltage values on 0.95, 1.0 and 1.05 respectively. It can be seen that the stator voltage has a very minor effect on the reactive capability of the machine.

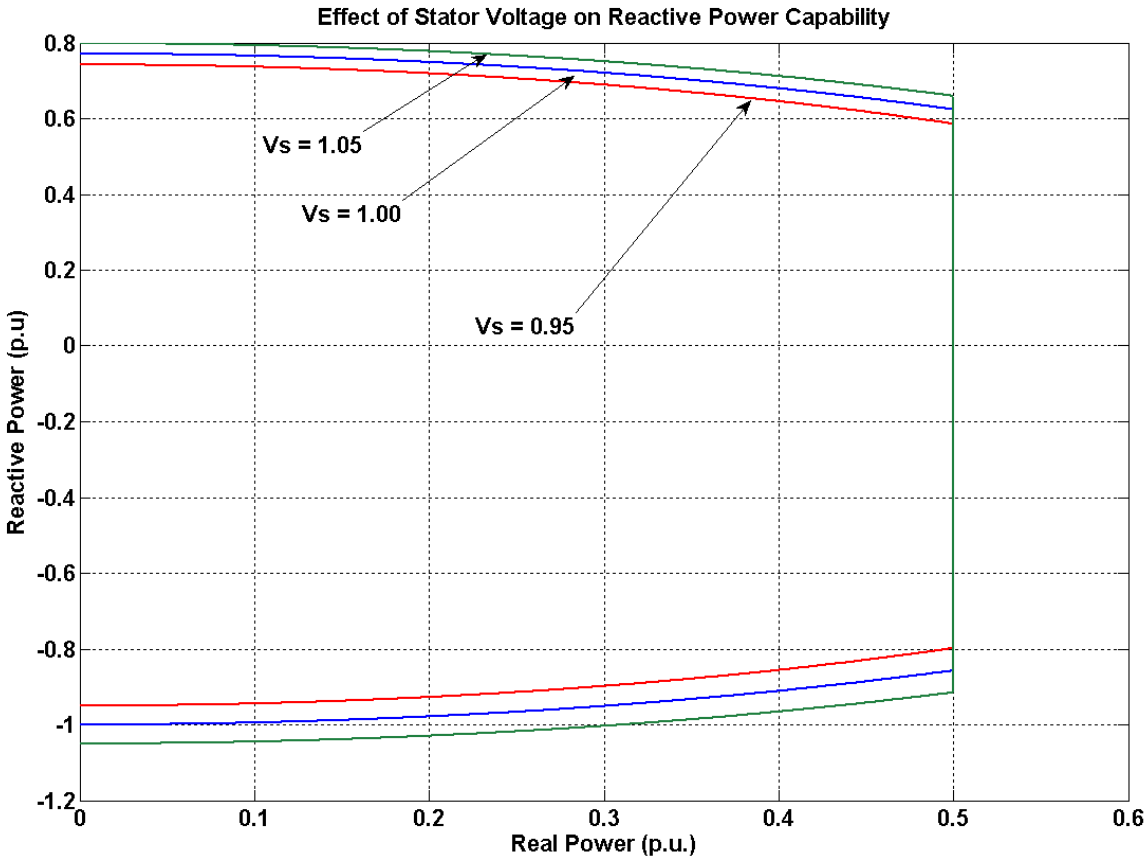


**Figure 8 : Effect of Stator Voltage on Reactive Capability**

A capability curve for a DFIG wind park was formulated using the method described above with a maximum power tracking characteristic given in figure 3. This technique is given for only a single machine, but it is assumed that the power capability of one machine can be scaled up to accurately aggregate the behavior of a DFIG wind park. The plot in figure 9 displays the operation of a DFIG within the specified 0.95 leading and 0.95 lagging power factors. Superimposed is the capability curve for the DFIG at different wind speeds corresponding to variable levels of power output. Given in the plot are the capability curves for the slip values in table 3.

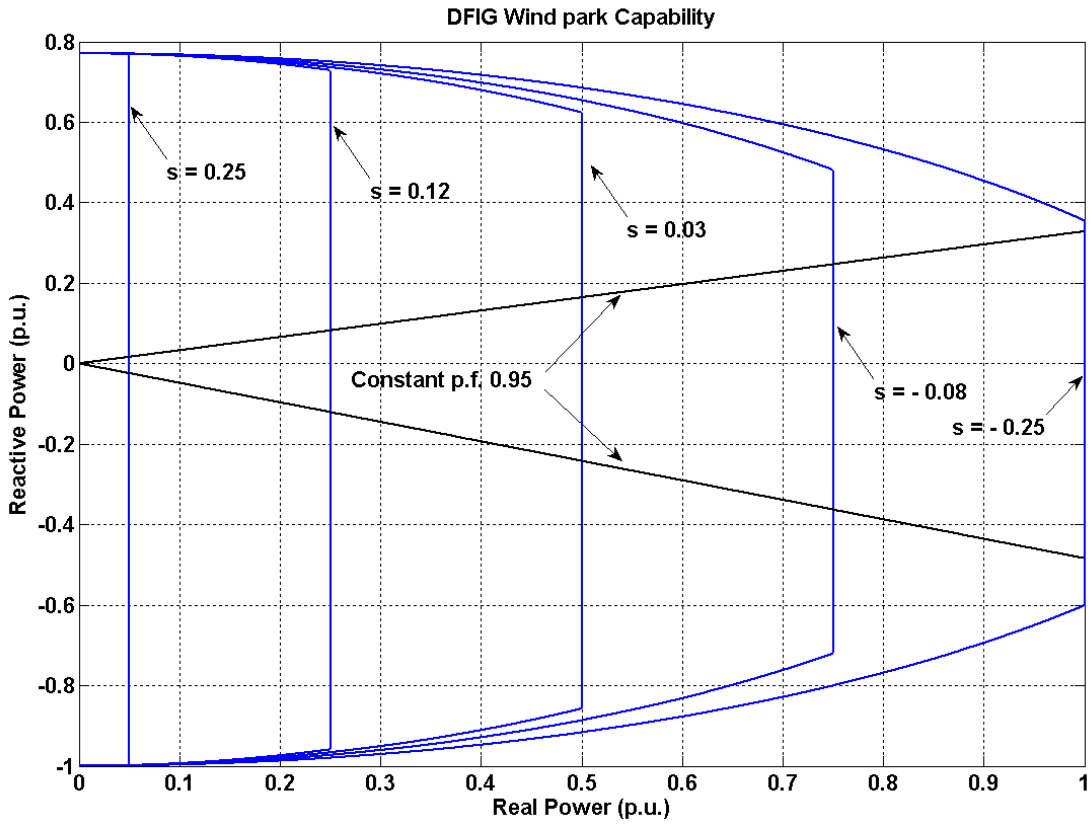


**Figure 9 : DFIG wind park static power capability curve in per units**

Thus by utilizing the capability curve in network analysis additional reactive power and hence improved power system performance may be attained over a regulated power factor. It is evident from the figure that at 100% plant output the use of the capability curve does not give much additional reactive support compared to the 0.95 leading operation. In contrast additional reactive consumption may be realized in lagging operation. Wind parks will very seldom operate continuously at 100% output and therefore in the periods of operation below 100% there is significant additional reactive power available that could aid in improved system performance.

## 2.3 Impact of Additional Reactive Power on System Dispatch

### 2.3.1 Optimal Power Flow Formulation

Optimal power flow (OPF) is a well developed tool and standard procedure in power system planning and operation [28], [29]. As part of this work it is used to study the impact of extended DFIG reactive capability on system operation as compared to regulated power factor operation. The objective of this OPF is to minimize system costs while adhering to operation constraints such as line flow, generation, and bus voltage limitations. The formulation is presented:

Minimize:

$$f(P_{gk}) = \sum_{k=0}^{n} C(P_{gk}) \tag{55}$$

Subject to:

$$\sum_{k=1}^{n} P_{gk} - \sum_{i=1}^{m} P_{di} - \sum P_{loss\_j} = 0 \tag{56}$$

$$\sum_{k=0}^{n} Q_{gk} - \sum_{i=0}^{m} Q_{di} - \sum Q_{loss\_j} = 0 \tag{57}$$

$$P_{gk,\min} \le P_{gk} \le P_{gk,\max} \tag{58}$$

$$Q_{gk,\min}(P_{gk}) \le Q_{gk} \le Q_{gk,\max}(P_{gk}) \tag{59}$$

$$V_{u,\min} \le V_u \le V_{u,\max} \tag{60}$$

$$-F_{\lim} \le F_j \le F_{\lim} \tag{61}$$

Where,

u $\in$ (1, 2…q), q – total no. of buses

j $\in$ (1, 2…p), p – total no. of branches

k $\in$ (1, 2…n), n – total no. of generators

i $\in$ (1, 2…m), m – total no. of load buses

Equation (55) indicates the total cost of production of power, where $C(P_{gk})$ is the price for $P_{gk}$ units of power from unit *k*. $Q_{gk}$ is the reactive injection of unit *k*. The real and reactive demand at bus *i* is $P_{di}$ and $Q_{di}$ and the real and reactive loss on line *j* is given by - $P_{loss\_j}$ and $Q_{loss\_j}$. Equations (56) and (57) are the power balance equations for real and reactive power. Equations (58) and (59) are the real and reactive power limits on the generators where the reactive limits are a function of the real power dispatch ($Q_{gk\_min/max}(P_{gk})$). This is done to capture the capability curve / restricted power factor regulations displayed in figure 2. The bus voltage constraints (0.95 – 1.05) and the line flow limits (<

1.0 p.u.) are given in equations (60) and (61). MATPOWER is the software tool used to conduct the OPF analysis [30].

This work addresses the impact of large scale DFIG wind generation on economic and reliability concerns in a power system. This representation aims to capture the major components of a large scale power system and emulate key system phenomena. The following section will elaborate on the system description.

### 2.3.2 Power System Description

A sample power network available in the PSS/E software was imported into MATPOWER and PowerFactory for system analysis. The original network consists of 6 conventional machines and 26 buses. The total load was modified to 3035 MW and 1230 MVAr. Refer to figure 4 for the schematic of the network. Shunt compensation (950 MVAr sum) is located at various buses throughout the system with a large 600 MVAr reactor at bus 151. The transmission voltages range from 230 – 500kV and the line parameters have been modified to reflect appropriate transmission distances [13].

In the base case the majority of generation is concentrated in the Northern region of the grid. The load centers are located in the South and South-East portion of the system with major concentration at buses 154 and 206. The South-West part of the network contains low load and low transmission capacity. Typical high wind regions have these characteristics and hence it is assumed a potential site for large scale wind facilities [31].

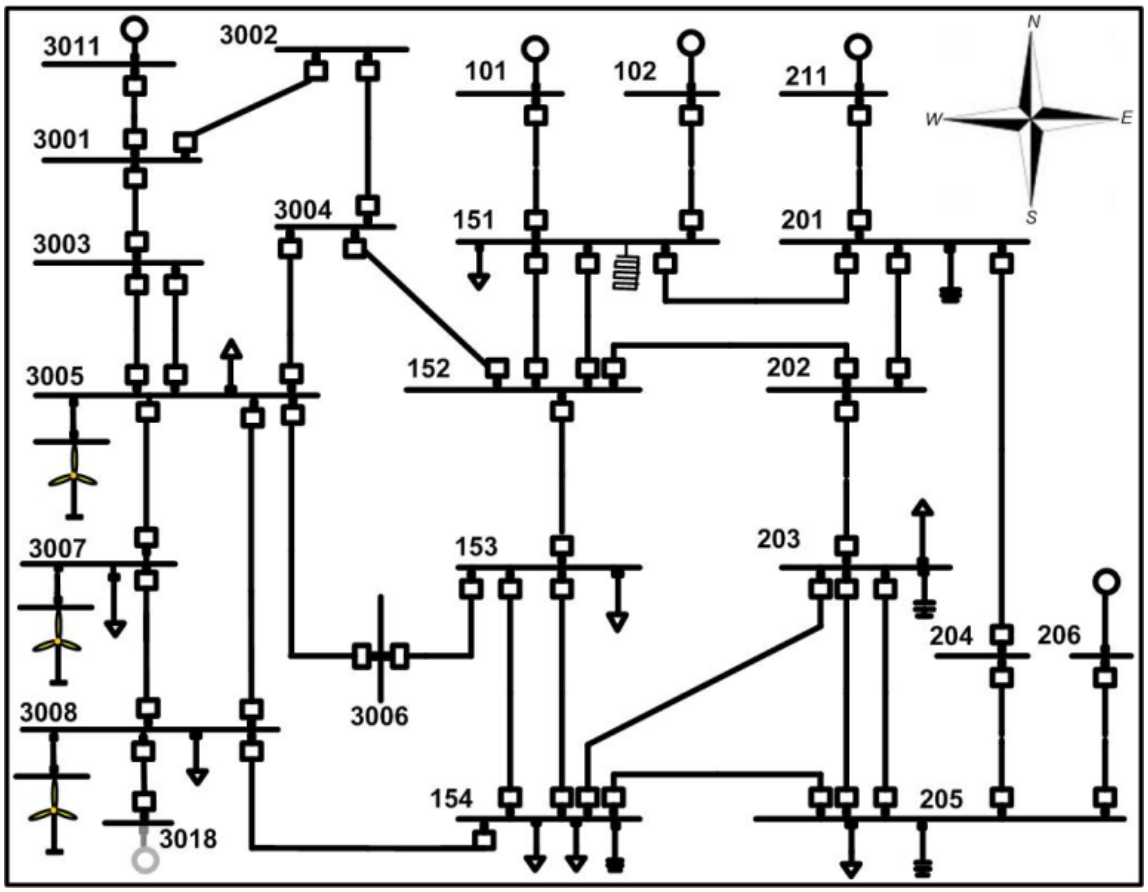


**Figure 10 : Simulated power** system **with park interconnection at bus 3008**

Since one of the underlying themes of this is to address the implementation of large DFIG penetration levels, unit 3018 has been taken off line. Installed in place of this unit are 3 DFIG wind facilities strategically placed at buses 3005/ 7/ 8. The replacement of this unit was to simulate disbursed wind generation that would emphasize the impact of high DFIG penetration on system performance. To facilitate the transfer of energy from these high wind regions to the load centers the lines (3008 – 154), (3005 – 3007), and (3007 – 3008) are upgraded to have sufficient transmission capacity.

### 2.3.3 OPF Analysis Description

The OPF analysis described in section 2.3.1 is used to assess the impact of extended reactive capability on system operating costs. The central goal of the analysis is to compare the system operation with restricted power factor versus the capability curve. The described system in figure 4 is studied with a load of 3340 MW and 1325 MVAr. At base case the depicted 5 conventional generators are online to satisfy this demand. The unit at bus 3011 is the slack bus and contains the most expensive generation. The production costs of all other generators are assumed to be the same. The wind parks are modeled to have a fixed production cost and are the least expensive generation. The units are modeled in the way to simulate the current practice of handling intermittent resources as price taking units, wherein all the available wind generation is purchased and no market is used to clear these bids. Due to the relative small scale of wind penetration in these markets their influence on setting the market price is considered negligible. [32, 33].

In this study wind penetration is defined as the total capacity of wind generation compared to the total load.

$$Penetration\ \ Level = \frac{\sum Installed\ \ wind\ \ capacity}{\sum Load} \tag{62}$$

To analyze the impact of increased DFIG wind penetration, various penetration levels at 15, 20, 25, and 30% are simulated. At each penetration level the total wind generation is simulated at 2, 15, 50, and 100% output in order to consider various production conditions from cut-in to cut-out wind speeds. Since wind is not a constant resource this study aims to capture the effect of wind variability on system operating costs.

**Table 3 Individual Plant Sizes at Different Penetration Levels**

| System Wind Penetration | Total Wind Capacity (MW) | Individual Plant Sizes (MW) |
|---|---|---|
| 15 % | 510 | 170 |
| 20 % | 680 | 227 |
| 25 % | 850 | 283 |
| 30 % | 1020 | 340 |

In this analysis the total wind generation at each penetration level is assumed to be equally distributed between the DFIG wind parks located at buses 3005/7/8. The total system load is 3340 MW and by utilizing equation (18) the plant sizes are obtained. The total wind capacity at the respective penetration levels are 510 MW, 680 MW, 850 MW and 1020 MW. At the described penetration levels the individual plant sizes are 170, 227, 283, and 340 MW. Table 3 summarizes the plant sizes at different penetration levels.

At 2% park output it is considered that the wind units have just cut-in and the real power output is at a minimum. When employing the capability curve, the reactive limits of the machines are the greatest at this output as compared the other output levels studied. As wind speeds increase the parks real output increases and consequently the reactive capability of the DFIG Park reduces. In contrast, the FERC regulation allows wind units to increase their reactive capability as the real output is increased. Again referring to figure 2, at 100% real output the leading reactive capability of both strategies is approximately equal.

### 2.3.4 System Loss Reduction

At each penetration level the total system operating costs are computed for each output level. The system operating costs are comprised of both the cost of generation to meet the demand and generation cost to satisfy losses. When a unit is unable to meet its local reactive load, remote generation compensates this requirement, but the system incurs additional line losses. Since the demand is fixed the reactive dispatch of the DFIG parks results in reduced system losses due to DFIG generation being able to meet the local reactive requirements. In this study the cost of system losses are minute as compared to the cost of generation. Thus even a substantial reduction in losses will not reflect a significant savings in total operating costs. Hence the reduction in system losses is used as a metric of comparison between the reactive control strategies.

**Table 4 : Percent Reduction in Losses Using Capability Curve Over 0.95 Leading/Lagging Power Factor**

| Penetration Level / Plant Output | 15% | 20 % | 25% | 30% |
|---|---|---|---|---|
| 2% | 15.82 | 15.46 | 15.10 | 14.74 |
| 15% | 8.54 | 7.17 | 6.54 | 7.06 |
| 50% | 3.75 | 2.80 | 2.19 | 1.62 |
| 100% | 0.34 | 0.35 | 0.11 | 0.02 |

Table 4 contains the percentage reduction in losses employing the capability curve as compared to an imposed 0.95 power factor limit. Observing the difference in the

reactive capacity between the two control strategies from figure 2, it is evident that as the real output of the wind park increases the additional reactive power available with the capability curve reduces. Correspondingly the percent reduction in system loss decreases with an increasing real power output.

DFIG wind parks implementing capability curve control may substantially reduce system losses especially at low plant output levels. This control strategy not only facilitates reductions in operating costs but avoids the necessity of additional reactive compensation required for secure operation of the power system. The combined savings in total system costs (losses+shunts) may help justify transmission investment for future wind installations [31].

## 2.4 Impact of Additional Reactive Power on Power Transfer Margin

The following analysis investigates the impact of the additional reactive power on power system transfer margin. The transfer margin is computed based on the minimum power transfer possible for various contingencies. For the above power system the contingencies considered are loss of transmission lines. Loss of generation is not considered in the analysis and hence generators and transformers connected to generators are not considered as contingencies. The base case load in the previous analysis does not provide a powerflow solution for all the contingencies. Hence the base case load level is reduced by 150 MVA to obtain the new base case for this analysis.

To compute the transfer margin the load and generation are increased in proportion to the base case load and generation dispatch. The base case generation dispatch is obtained based on the OPF formulation provided above. The penetration levels and output

levels used in the previous analysis are again utilized to obtain the different transfer margins. Table 5 summarizes the increase in transfer margin for the various scenarios.

The table demonstrates that with increasing system penetration of wind generation the increased power transfer margin increases. Given a base case load of 3200 MW the percentage increase in power transfer margin over the base case loading varies from 8.4% to 14.6% with increasing system penetration from 15% to 30% at low wind speeds. At 50% output the percentage increase in transfer margin varies from 4.8% to 8.5% with increasing system penetration. At 100% plant output there is very little increase in reactive power available and this translates into a very marginal increase in transfer margin.

**Table 5 : Increase in Transfer Margin (in MW) Using Capability Curve Over 0.95 Leading/Lagging Power Factor**

| Penetration Level / Plant Output | 15% | 20 % | 25% | 30% |
|---|---|---|---|---|
| 2% | 267.24 | 355.11 | 441.53 | 467.67 |
| 15% | 238.19 | 320.98 | 375.44 | 427.00 |
| 50% | 153.95 | 202.61 | 253.44 | 273.05 |
| 100% | 20.33 | 23.24 | 28.32 | 29.05 |

# CHAPTER 3: INCORPORATING WIND VARIABILITY INTO VOLTAGE SECURITY ASSESSMENT

## 3.1 Voltage Security Assessment Tools

According to [34], voltage stability refers to the ability of a power system to maintain steady voltages at all buses in the system after being subjected to a disturbance from a given initial operating condition. Voltage stability of a system depends on its ability to maintain/restore equilibrium between load demand and load supply from the power system. Any resulting instability occurs in the form of a progressive fall or rise of voltages of some buses. Major contributory factors to voltage instability are power system configuration, generation and load patterns [35-39]. A possible outcome of voltage instability is loss of load in an area, or tripping of transmission lines and other elements by their protective systems leading to cascading outages.

As mentioned in [40], the term voltage collapse is also often used. It is the process by which the sequence of events accompanying voltage instability leads to a blackout or abnormally low voltages in a significant part of the power system [37, 40, 41].

Voltage problems typically occur in power systems which are heavily loaded faulted and/or have reactive power shortages [37]. Among the various factors which affect voltage stability issues, there is a special correlation between voltage instability problems and insufficient reactive power reserves [42]. Voltage collapse is related to reactive power demands of loads not being met because of limitations on the available reactive power reserves and transmission of reactive power [43].

There are two general types of tools for voltage security assessment: dynamic and static. Dynamic analysis uses time-domain simulations to solve nonlinear system differential algebraic equations. Static analysis is based on the solution of conventional or modified powerflow equations.

Dynamic analysis provides the most accurate replication of the time responses of the power system [37, 44-46]. However, time-domain simulations are time consuming and computationally extensive. These limitations generally make dynamic analysis impractical for examination of a wide range of system conditions or for determining stability limits.

Static analysis [37, 47-52] involves only the solution of algebraic equations and therefore is computationally much more efficient than dynamic analysis. Voltage stability analysis often requires examination of lots of system states and many contingency scenarios. For this reason, the approach based on steady state analysis is more feasible.

For static voltage stability studies of a power system, the loading of the system is increased incrementally and slowly (in certain direction) to the point of voltage collapse. The MW-distance to this point is a good measure of system voltage stability limit. P-V analysis is a steady state-tool that develops a curve, which relates voltage at a bus (or buses) to load within an area. Bus voltages are monitored throughout a range of increased load.

The benefit of this methodology is that it provides an indication of proximity to voltage collapse throughout a range of load levels. Required input is standard power flow input data and the output is P-V curves for all specified buses. The voltage profile of the system is shown by the PV-curves which are plotted using power flow programs as the loading varies from the base values to the point of collapse.

Figure 11 demonstrates the P-V curves for a system. The three curves correspond to the base case (BC) and two contingencies (C1, C2). The PV margin reduces for contingencies (PV margin BC > PV margin C1 > PV margin C2), and hence including contingencies into voltage stability margin estimation is critical.

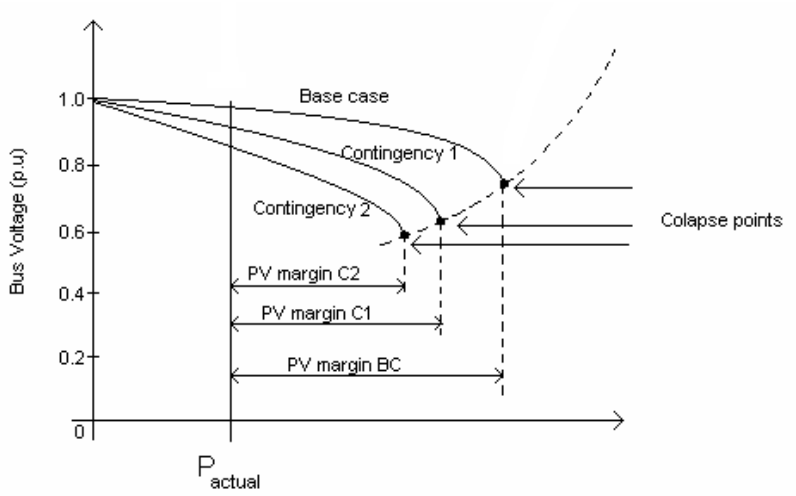


**Figure 11 : P-V Curve: Base Case and Contingencies**

## 3.2 Wind Variability Trends

Load variability affects power system operations in three different time frames. The following figure 12 demonstrates the three time frames [53]. Load variability affects voltage and frequency regulation in the power system. This is in the timeframe of a few seconds to a few minutes. The means of maintaining system operations in this time frame is Automatic Generation Control (AGC). The second timeframe of concern is the minutes to hour's time frame. This time frame is generally handled by spinning and non-spinning reserves. The final period of concern is the day ahead period and this is handled by committing units in advance to handle the uncertainty.

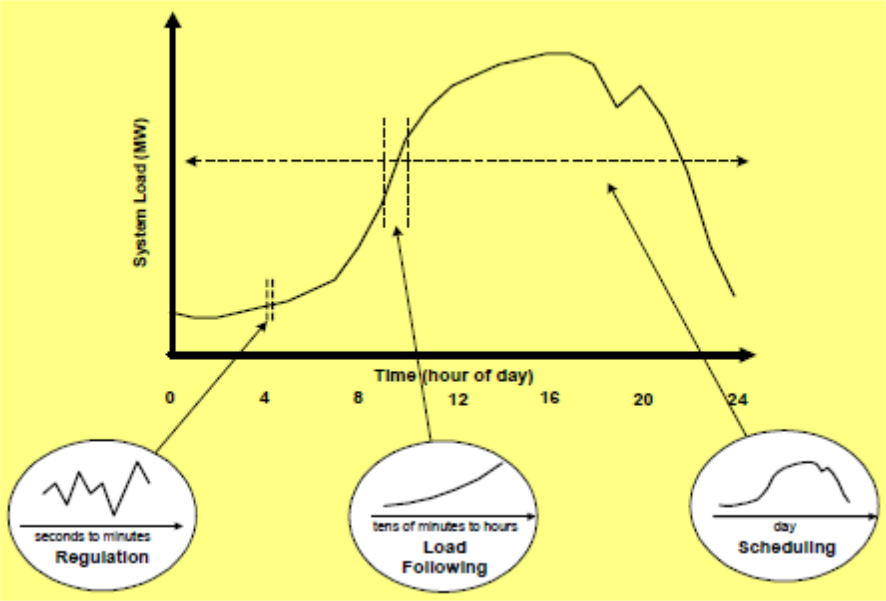


**Figure 12 : Different Time Frames for System Load Variation [53]**

The addition of large scale wind generation in the power system can affect all these time frames. A study conducted in 2004 studied the impact of high wind penetration on morning and evening load ramp events [11]. The study assumed a 15% wind penetration. The two plots indicate that during summer as load picks up, the presence of large scale wind penetration increases the ramp up requirements of the system, indicating that wind ramps down as load increases on a summer morning. The second plot indicates that in the evening as load ramps down, wind ramps up thereby causing other generation to ramp down to a greater degree. The second issue can be handled by spilling wind generation, but a greater concern for power system operations is the issue of wind ramp downs coinciding with load ramp ups.

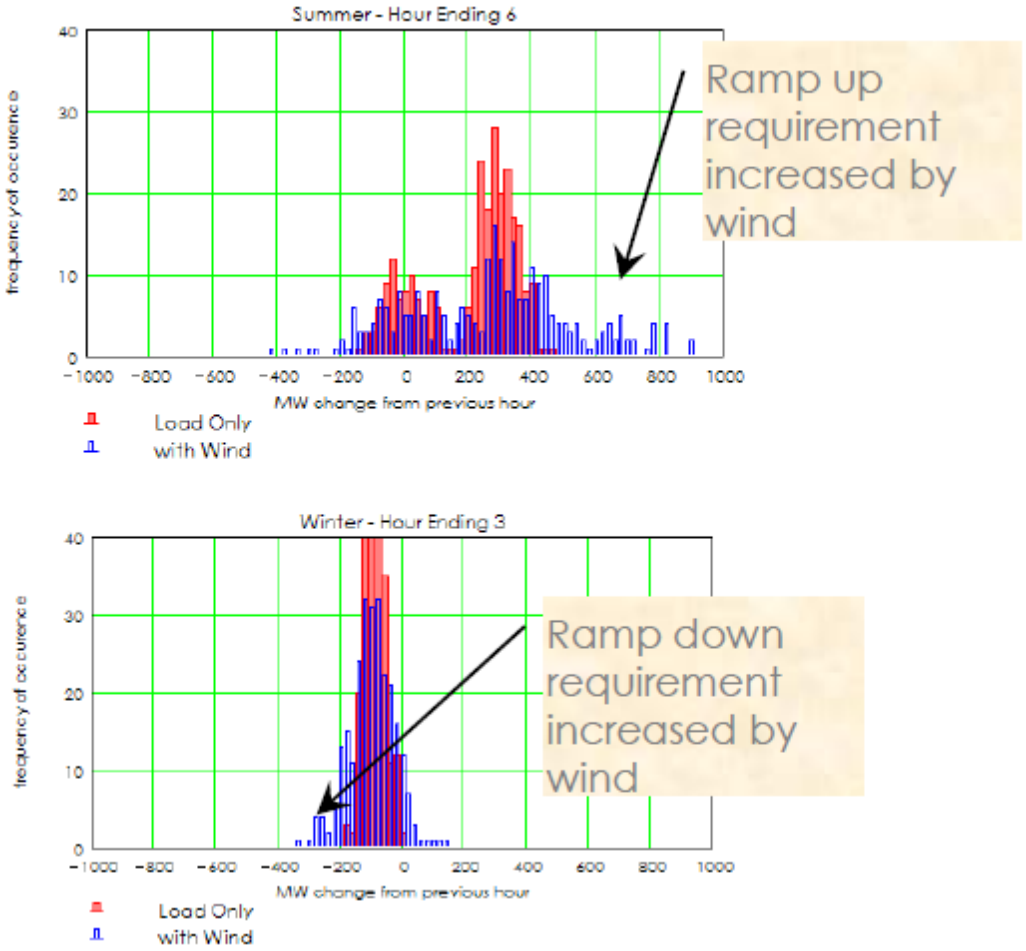


**Figure 13 : Impact of 15% wind penetration on System Ramping Requirements [11]**

The size of a wind farm affects the variability of the power output from the wind park in the various time frames of interest. The following figure 14 indicates that the percentage variability in wind power increases with increasing timeframe [53]. This indicates that large scale wind penetration will not require a large increase in regulation reserves, but will need more units available in terms of reserve in the minutes to hour's timeframe.

| | | 14 Turbines (%) | 61 Turbines (%) | 138 Turbines (%) | 250+Turbines (%) |
|---|---|---|---|---|---|
| **1-Second Interval** | | | | | |
| | Average | 0.4 | 0.2 | 0.1 | 0.1 |
| | Std. Dev. | 0.5 | 0.3 | 0.2 | 0.1 |
| **1-Minute Interval** | | | | | |
| | Average | 1.2 | 0.8 | 0.5 | 0.3 |
| | Std. Dev. | 2.1 | 1.3 | 0.8 | 0.6 |
| **10-Minute Interval** | | | | | |
| | Average | 3.1 | 2.1 | 2.2 | 1.5 |
| | Std. Dev. | 5.2 | 3.5 | 3.7 | 2.7 |
| **1-Hour Interval** | | | | | |
| | Average | 7.0 | 4.7 | 6.4 | 5.3 |
| | Std. Dev. | 10.7 | 7.5 | 9.7 | 7.9 |

Note: This table compares output at the start and end of the indicated time period in terms of the percentage of total generation from each turbine group. Std. Dev. is the abbreviation for standard deviation.

**Figure 14 : Average Wind Park Output Variation in Different Time Frames and for Different Plant Sizes [53]**

The accuracy of wind forecasts depends on the forecasting horizon. The figure 15 demonstrates the increasing forecasting uncertainty as the time horizon increases [54].

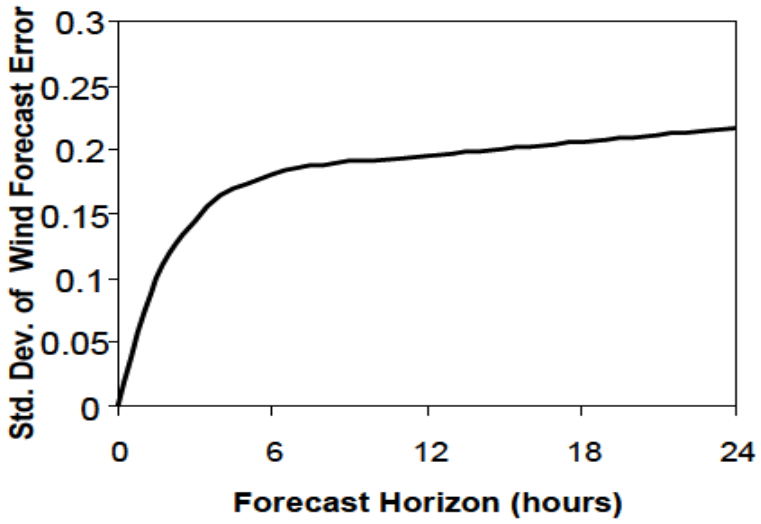


**Figure 15 : Impact of Forecast Horizon on Wind Forecast Error [54]**

## 3.3 Generator Ramp Rate Requirements

In section 3.2 the impact of wind variability on unit commitment and reserves was discussed. The impact of the variability and uncertainty of wind generation is minimized when the rest of the generation is flexible. The following table summarizes the different generation technologies and their flexibility in terms of ramping capability.

**Table 6 : Ramping Capability of Different Power Generation Technologies**

| Technology | Ramping Capability |
|---|---|
| Nuclear Power Plants | Very inflexible slow to change |
| Run-of-river hydro | Limited flexibility without wasting water |
| Large Coal Fired | Slow to start and ramp, better at base load |
| Combined Cycle Plants | Faster to start, fast to ramp; high efficiency at close to nominal |
| Conventional CT | Fast to start and ramp; costly |
| Advanced CCP | Fast to start and ramp; very efficient at many load levels |
| Pump storage | Faster to start, fast to ramp; need low cost energy |
| Storage Hydro | Fast to start and ramp; can virtual store |

A system which has a mix with more flexible resources (near the bottom of the list) is more equipped to handle large scale wind penetration. But even with a good mix of generation the choice of units that are held in reserve is important. This is especially important in a transmission constrained power system. The following methodology provides a means of assessing the different redispatch strategies and choosing one which provides most reliable operation of the power system.

## 3.4 Voltage Secure Region of Operation (VSROP) Methodology

PV curves are drawn to study the nature of the voltage profiles of a particular load bus given an assumed direction of increase of conventional generation. Existing static Voltage Stability analysis assumes all generation to be dispatchable. Wind generation cannot be considered to be dispatchable [55] and hence a different approach is needed to understand the impact of wind variability on Voltage Stability Margin.

With increasing environmental concerns and political mandates, wind energy is becoming the preferred choice of renewable energy. Wind energy dispatch will play a pivotal role in order to meet the renewable portfolio standard to make wind generation comprise 20% of the whole power generation portfolio in the US by 2030 [53].

Electricity generated from wind power can be highly variable with several different timescales - hourly, daily, and seasonal periods are present in wind energy. Since instantaneous electrical generation and consumption must remain in balance to maintain grid stability, this variability can present substantial challenges to incorporating large amounts of wind power into a grid system. With wind power generation being increasingly incorporated into the existing power system, the traditional PV curves are unable to capture

the stability margin for an integrated system which has high wind penetration (~20%). Intermittency and the non-dispatchable nature of wind energy production can raise various issues like increased regulation costs and operating reserves.

In order to include the wind variability, a P-V surface for secure operation is proposed. The developed surface is called the Voltage Secure Region of Operation (VSROp). The surface incorporates different levels of wind generation by representing different PV curves at different wind generation levels to obtain a three dimensional region of voltage secure operation. In the three dimensional region, the non-dispatchable wind generation (z axis) forms the additional axis along with the existing power generation, including losses of the system (x axis) and the per unit voltage (y axis).

Figure 16 below demonstrates a sample VSROp. The four PV curves corresponds to no wind and wind generations W1, W2 and W3 (W3>W2>W1). For each PV curve the amount of wind generation is kept constant and the load and generation is increased according to a set loading and generation increase scenario, which is kept constant for all PV curves. Another input to the PV surface calculation algorithm is the redispatch strategy for increase or decrease in wind generation.

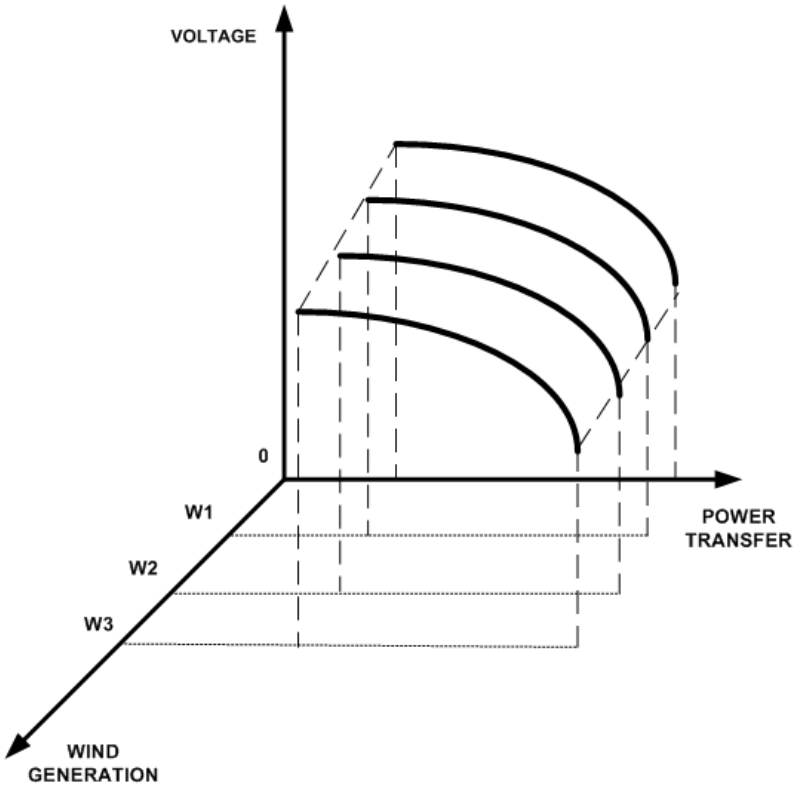


**Figure 16 : Voltage Secure Region of Operation (VSROp)**

The flowchart for the proposed methodology is shown in Figure 17. The proposed methodology includes the following steps:

**Step 1:** Obtain Input Data

This step basically involves obtaining the three inputs to the Voltage Security Assessment tool:

- The power flow data for the system under consideration.
- The assumed level of wind generation in the base case and wind variability that is to be studied.
- The redispatch strategy for increase or decrease in wind generation.

The power flow data includes the committed generations and their bid curves. It also includes the load increase direction and generation increase direction. The generation increase scenario is provided for all other generations except wind.

Historical wind speed data and load data is utilized to decide the amount of wind generation available in base case. The wind speed forecasts for maximum variability is utilized to decide at what values of wind variation PV curves are to be plotted.

The wind speed rate of variation along with the ramp rates of available generation is utilized to develop the generation redispatch strategy to compensate for variation in wind power in the system.

**Step 2:** Optimal Power Flow in the base case

Optimal power flow (OPF) methodology developed in Section 2.3 is utilized. MATPOWER is the software tool used to conduct the OPF analysis.

**Step 3:** Full Contingency based Margin Estimation

For a fixed wind energy dispatch, plot the PV curves using powerflow for all (n-1) contingencies. MATPOWER is used to obtain the PV curves. The contingency corresponding to the least power transfer margin is noted and the corresponding PV plot is stored. The set of all PV curves is plotted in the previously mentioned three dimensional space to obtain the Voltage secure PV surface.

The series of PV curves on different planes corresponding to a particular wind penetration level will constitute a hyperspace which will represent the stable voltage operating zone The base case dispatch is then utilized to estimate the least available margin in the PV surface.

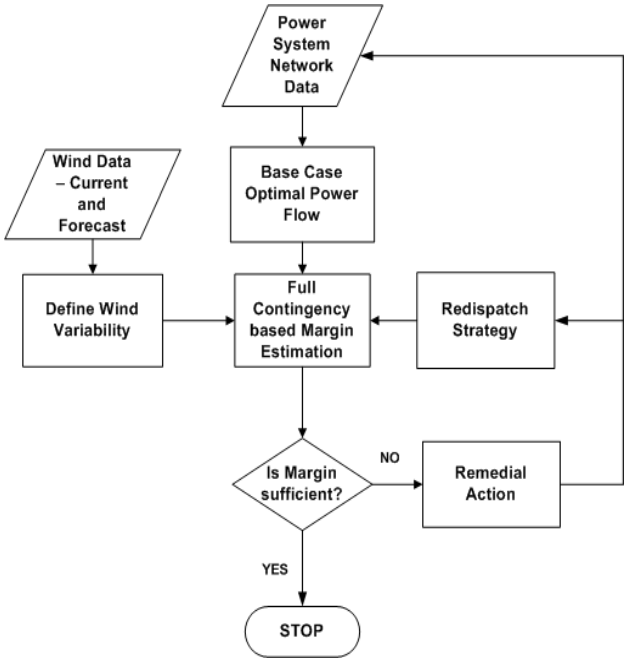


**Figure 17 : Flowchart for Voltage Security Assessment**

**Step 4:** Margin Check and Remedial Action

The margin obtained in Step 3 is verified to meet the power margin requirements. If the margin requirements are not met then remedial actions are taken to increase the margin and the modified load flow data is fed into step 1 and the entire process is iteratively repeated until the desired margin is obtained.

The remedial actions that can be taken include but are not restricted to capacitor switching, commitment of additional generation units or load shedding. This hyperspace would give the power system operators a given region which might be too conservative, but is the perfectly safe operating zone. Also given current wind dispatch and estimated variability in the next hour, the operator would be able to quickly determine the amount of the margin that would be available for the system.

## 3.5 Test Case

The 26-bus test system from PSS/E described in section 2.3.2 is considered and shown in figure 18. To negate the locational advantage of generation, all generators are assumend to have the same rating of 900 MW. Reactive limits on all generators areset to be 500 MVar and -150 MVar. The objective of this study is to examine the impact of wind variability on voltage stability margin and the location of wind generation w.r.t reserves, and its impact on the power trnsfer capability.

Two locations are chosen for wind generation. One is located at bus 3008 and the second at bus 3002.The wind park of size 800 MW is chosen. Base case plant output is assumed to be 560 MW which is 20% of the base case load. The location at bus 3008 is not transmission constrained whereas the location 3002 is in a high generation low load area of the power system.

Two different redispatch strategies are assumed. One with the residual generation being picked up by Gen 3011 and Gen 101(marked in red). These generators are more remote w.r.t the load.The second redispatch strategy assumes the generators at 211 and 206 to pe the pick up generators(marked in blue). These generators are closer to the load.

For each wind park location and redispatch strategy both Capability curve and FERC mandated restricted power factor is used to analyze the impact on transfer margin. All line out contingencies are tested and for each maximum transfer margin obtained the most critical contingency is recorded.

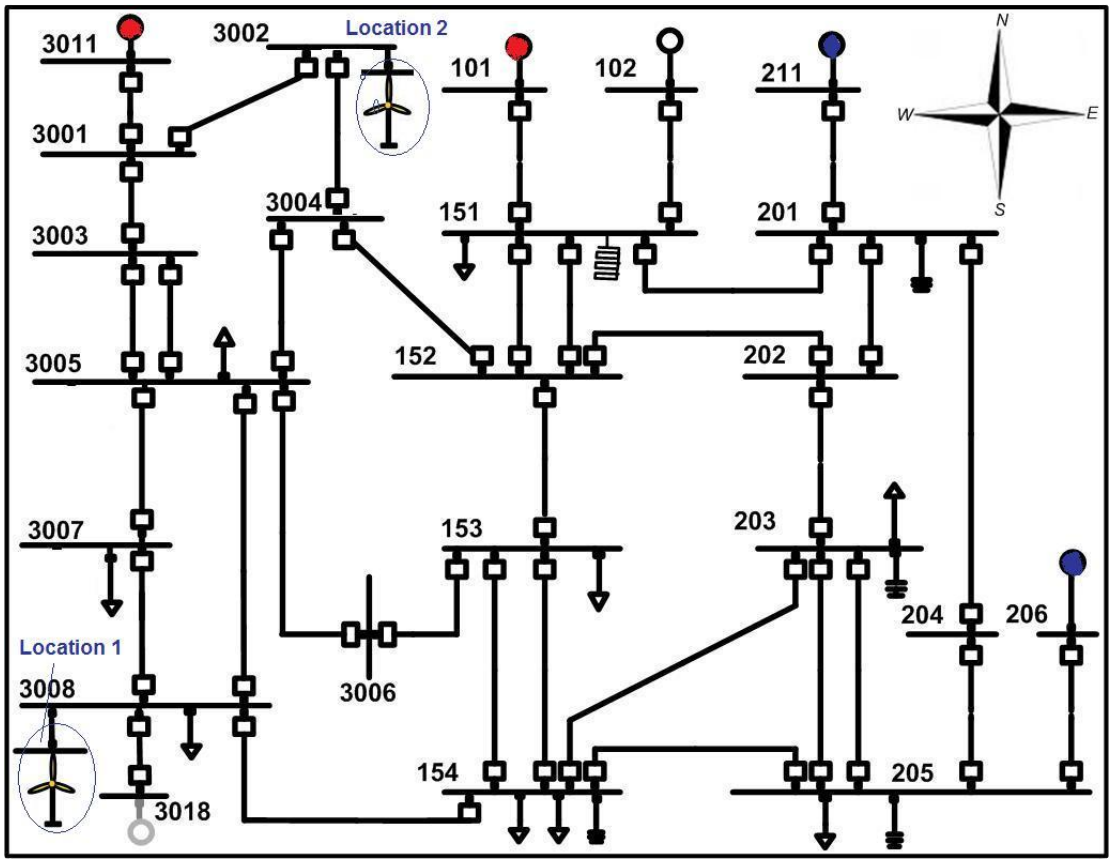


**Figure 18 : System Layout with Different Wind Locations and Redispatch Strategies**

### 3.5.1 Location 1

The following figures 19 and 20 demonstrate the variation in power transfer margin variation as the wind power is varied between 0 and 800 MW. The two redispatch strategies are used to obtain two separate plots. The general trend at location 1 is that the power transfer peaks at between 160-240 MW and the next peak is at approximately 640 MW.

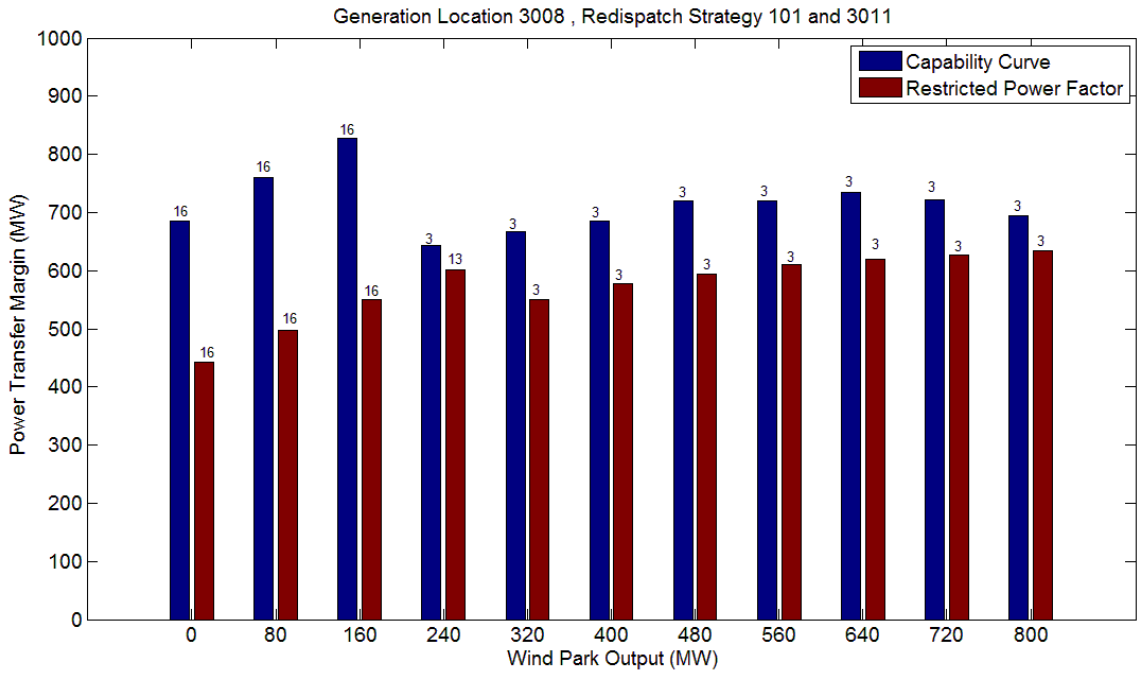


**Figure 19 : Location 1 Redispatch Strategy 1**

At location 1, the critical contingencies vary with varying wind levels. At lower wind levels the critical contingencies are 16, 26 and 13 whereas for higher wind speeds it s contingency 3. At location 1, for different reactive power limits on wind generations the critical contingency varies especially at low wind speeds.

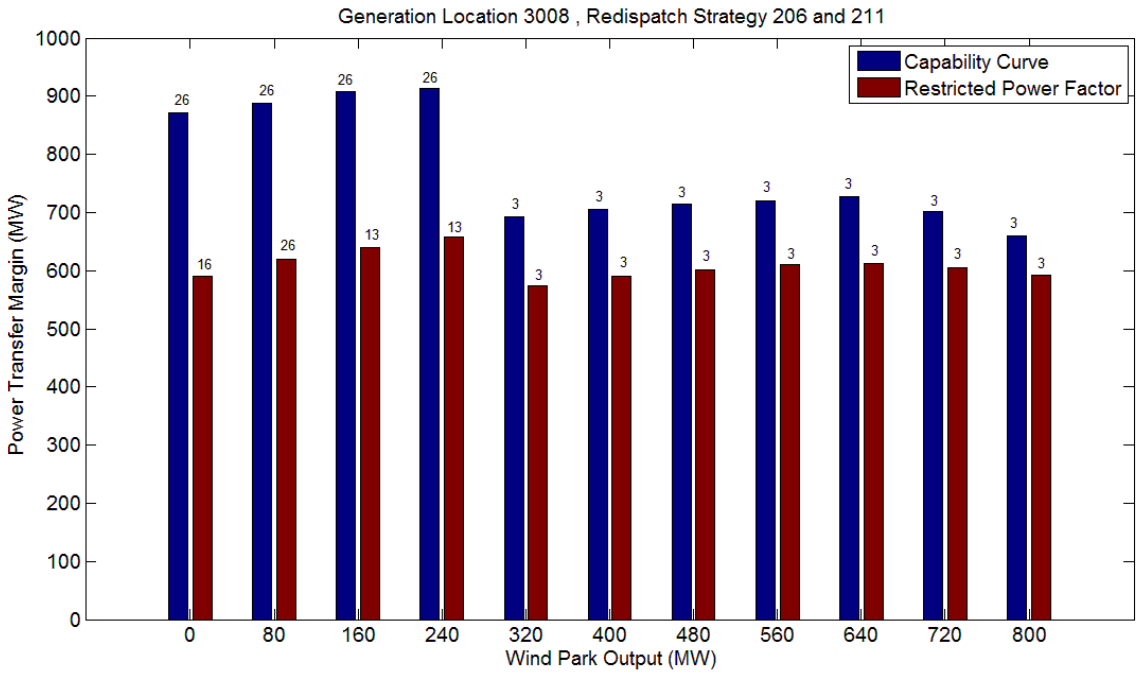


**Figure 20 : Location 1 Redispatch Strategy 2**

At location 1, the maximum margin for redispatch strategy 2 is obtained around 240 MW wind power output and for redispatch strategy 1 maximum margin is obtained at 160 MW plant output. At location 1, even though maximum transfer margin is less for redispatch strategy 1, the variation in transfer margin over the entire range of variability is lesser than strategy 2. The reason for the two peak power transfer margins is the peculiar trend obtained for the transfer margins for contingency 3 [line outage 151-201].

The following figure 21 demonstrates the variation in power transfer margin for the two most restrictive contingencies. In case of contingency 3 in the base case as the wind level increases the lower reactive limit of the generator at bus 211 is hit. Beyond this limit a bus acts as a PQ bus and thus the reactive capability of the generator at bus 211 is not utilized in the power transfer margin.

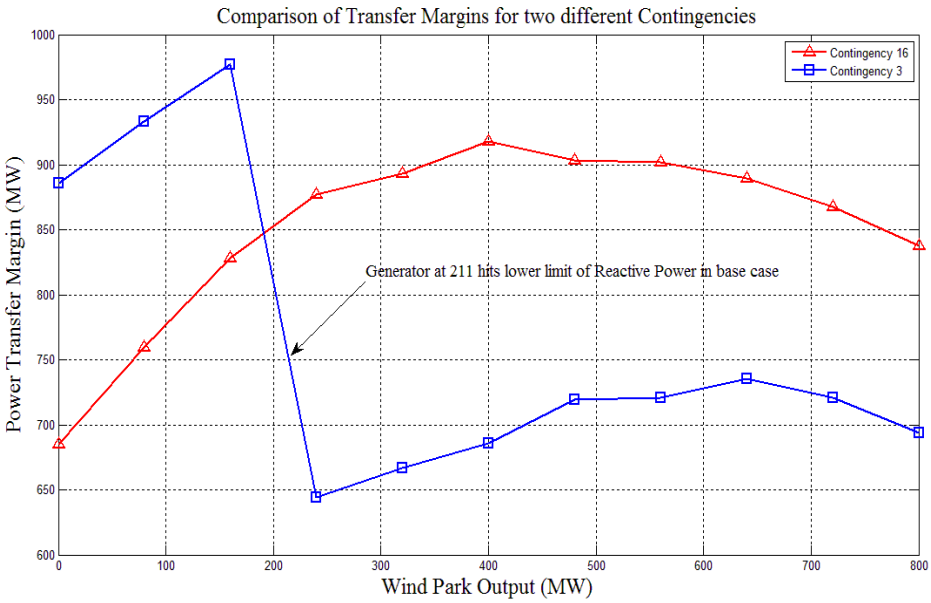


**Figure 21 : Comparison of two contingencies (3 and 16)**

### 3.5.2 Location 2

The following figures 22 and 23 demonstrate the variation in power transfer margin variation as the wind power is varied between 0 and 800 MW. The general trend for the transfer margin at location 2 is that the transfer margin decreased with increasing wind levels.

At location 2 there is no change in critical contingency over the entire range of variability. However at this location at higher wind outputs, for redispatch strategy 2 there is no convergence in base case for the critical contingency 16 at 90% and 100% output.

At location 1, by utilizing the capability curve a minimum power transfer margin of 100 MW is obtained. The restricted power factor operation restricts the power transfer margin to zero at 90% and 100% operation. Thus by using the capability curve the system can accommodate 800 MW whereas with the restricted power factor we can only accommodate 640 MW irrespective of the redispatch strategy employed.

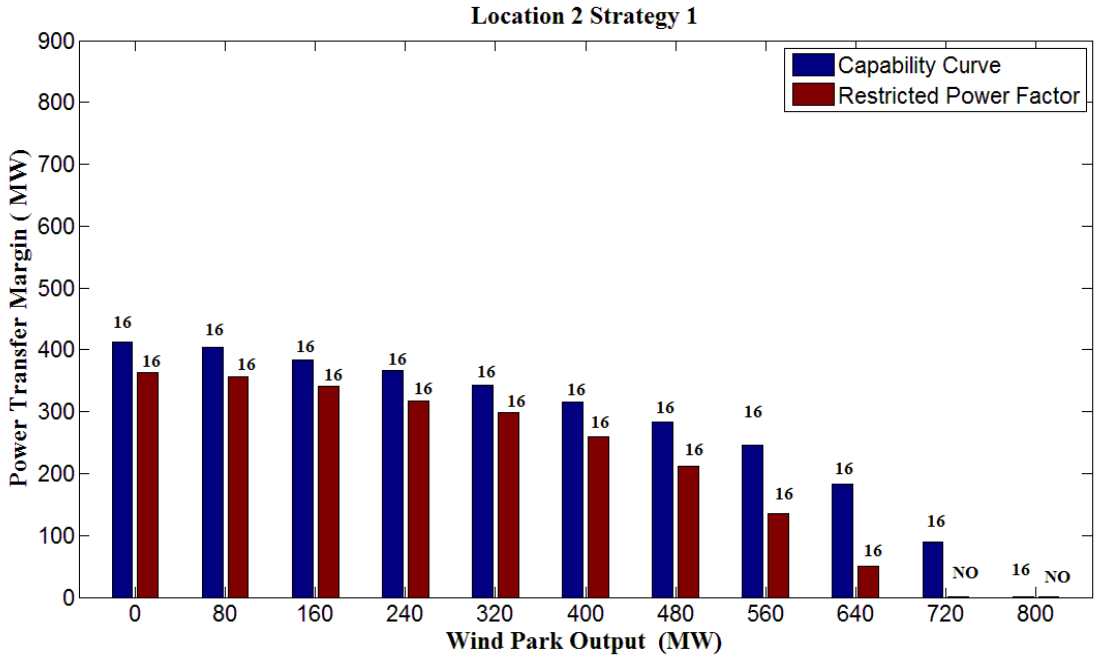


**Figure 22: Location 2 Redispatch Strategy 1**

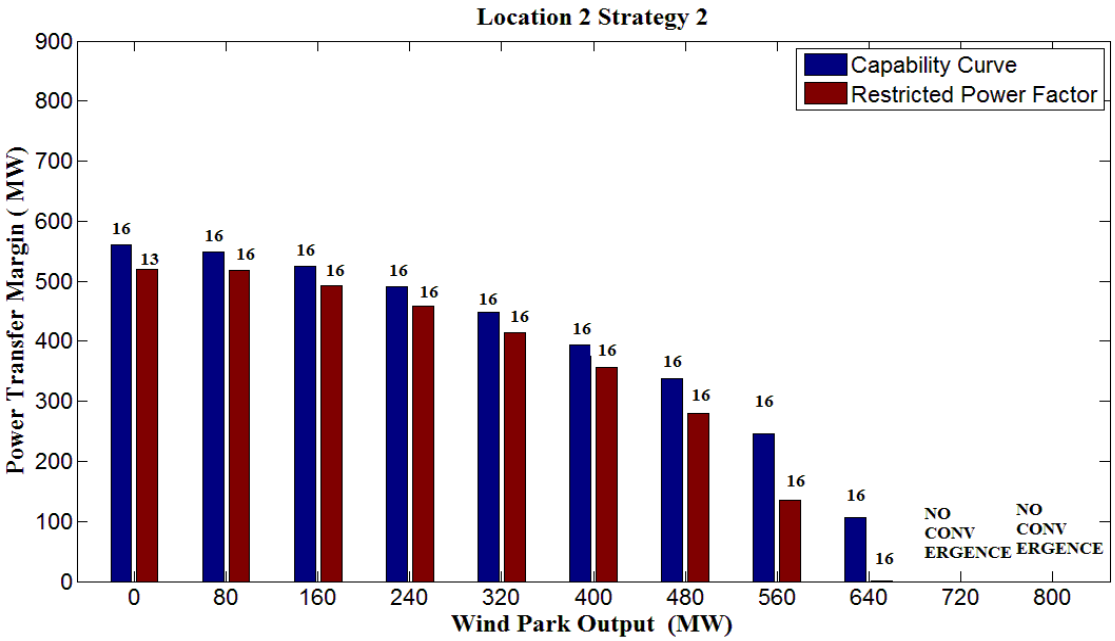


**Figure 23 : Location 2 Redispatch Strategy 2**

## 3.6 Wind Variability and Redispatch Strategy

In a power system with large levels of wind generation the choice of redispatch strategy has an important impact on the transfer margin of a system. In the above case study, redispatch strategy 2 gives the maximum power transfer margin at a given wind speed level, but is also the redispatch strategy that has maximum deviation. On the other hand redispatch strategy 1 gives a flatter profile for the transfer margin which is more desirable, as the wind variation does not affect the load serving capability of the system.

In the case of location 2, the redispatch strategy 2 is especially preferred because the wind generation is located in a high generation transmission constrained region and the redispatch strategy that utilizes generation in the vicinity of the wind generation is very favorable. It gives a balanced variation in power transfer margin. This is because by ramping up the surrounding generation when wind reduces and ramping down that generation when wind increases results in maximum transmission utilization.

This tool helps determine the wind level at which minimum power transfer margin is obtained. This power level need not be at minimum wind or maximum wind. The most severe contingencies on a system depend on the level of wind generation.

# CHAPTER 4: LARGE SYSTEM IMPLEMENTATION – OFFSHORE WIND FARM

## 4.1 Motivation

In this chapter, the impact of the capability curve on the large scale power system is considered. In a standard power system, the contribution of any reactive power source is directly proportional to its proximity to the load. In most regions, the coastal areas are thickly populated and are hence high load centers [56]. At the same time the high population density and the various environmental regulations, makes it very difficult to site generation close to these coastal load centers.

The United States has large load pockets along the eastern coast. There is considerable interest in developing off shore wind sites, especially with many states having renewable portfolio standards. Figure 24 below shows the availability of wind power in the Northeastern part of the United States. One area of particular interest for wind energy development is the coast of South Eastern Massachusetts. A major offshore wind project that has been in the pipeline is the Cape Wind Project [58].

The area of Southeastern Massachusetts (SEMA) is a high load pocket with limited generation. Recent operational experiences of the local independent system operator, ISO-NE indicate that some older expensive generating units in lower SEMA had to be kept online in peak conditions to facilitate reliable system operation [59]. The Cape Wind project plans the addition of wind units in the lower SEMA region which would serve load in the aforementioned load pocket. A detailed representation of the system is provided in section 4.2.

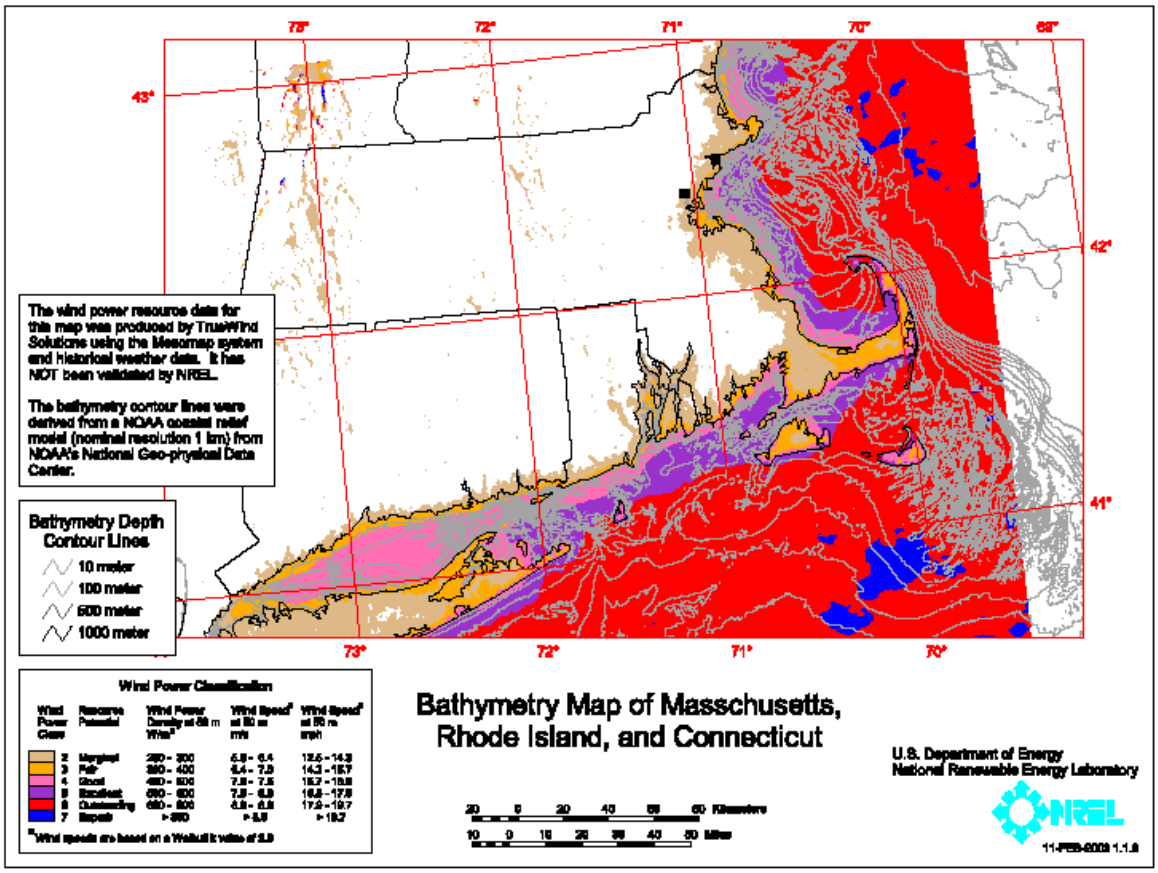


**Figure 24 : Wind Power Potential in the Northeastern USA [57]**

The Cape Wind project is planning to add an offshore wind park in the Nantucket Sound. Figure 25 indicated the location of cape wind. The following sections detail the modeling of a wind farm in a similar East Coast region, and investigate the impact of the additional reactive power at low wind levels.

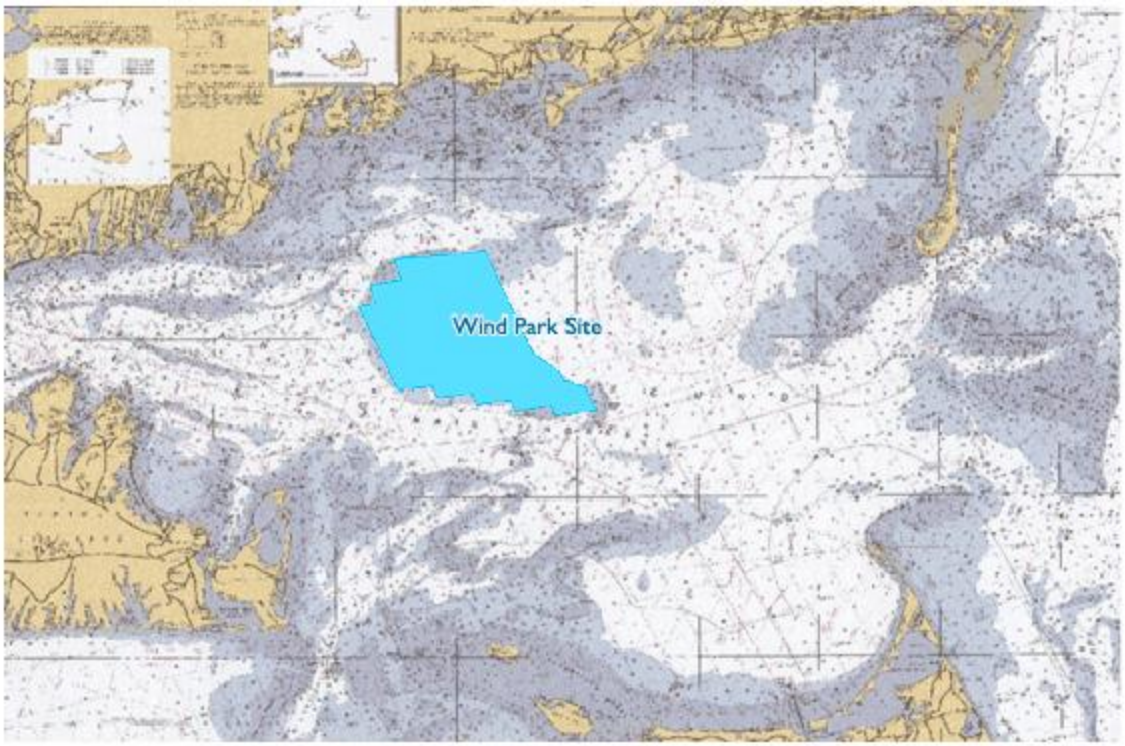


**Figure 25 : Cape Wind Location [58]**

## 4.2 System Modeling

The 22,000 bus Eastern Interconnection system is used to obtain static and dynamic data for the region being considered. The study region is restricted to an eastern coastal region of the system. The area is chosen based on generation sufficiency to serve the area load. The matching of area generation and load allows for the equivalence of the remaining system.

The reduced region consists of 648 buses. The total load in the region is 7100 MW. There are 57 units online serving the load. Within this area, the region of East Coast is indicated in figure 26. All buses over 115kV are modeled. The total load in the region in the base case is 600 MW. The region is fed by 5 major 115kV lines from the

northern area. The buses T-1, C-1, C-2 and C-3 are fed by a strong 345 kV network north of the region. The base case system has no generation in the East Coast load pocket.

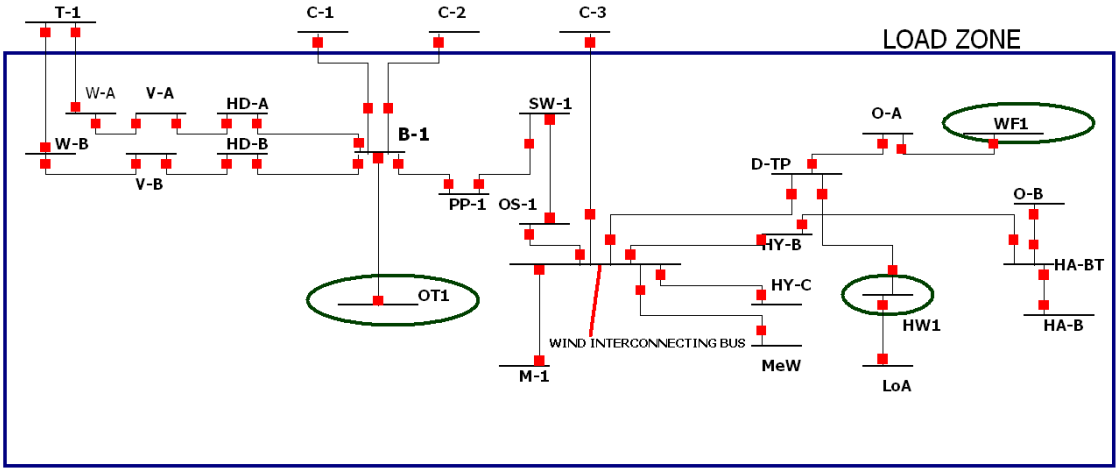


**Figure 26 : East Coast Region 115kV Network**

In the figure above, the interconnecting bus for the off shore wind farm is indicated. The figure 27 below indicates the steady state model of the wind park. The wind farm consists of two units of 126 MW units. Each unit is an aggregation of 84 units of maximum real power output of 1.5 MW. To accurately model the wind farm, the collector system is also modeled. The 115 kV lines that interconnect the wind farm to the 115 kV network is also modeled. The 115 kV lines have two segments, an underground segment from the collector 115kV bus to the mainland and an overhead segment on the mainland to the interconnecting substation. The collector network is modeled at 33kV. The terminal voltage at the wind units is 575V.

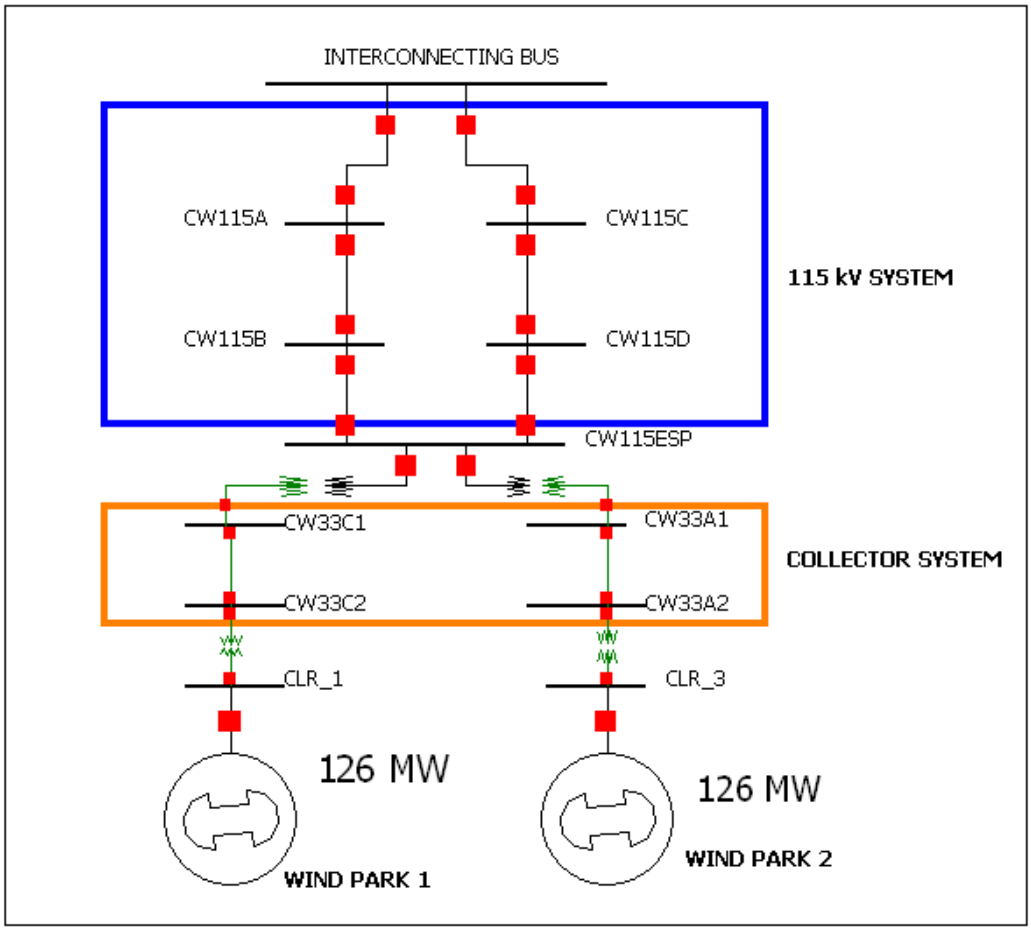


**Figure 27 : Wind Park Steady State Model**

Since the region is a load pocket and an import area, it is important to determine the import limit into the region. Three cases are considered in the analysis. The base case, with the system as it exists without the off shore wind park. A case in which the wind park provides rated output. A final case with the wind park at 5% output level. The third case is a typical summer day with low wind levels. In the following sections a static and dynamic analysis of the system is conducted to analyze the impact of the additional reactive capability. Since the region is known to require out of merit generation to be run for reliability, the region is an import constrained region.

Three buses in the system are monitored. The monitored buses are OT1, WF1 and HW1. The three buses are circled in figure 26 in green. There buses are used to analyze the results in sections 4.3 and 4.4.

The addition of conventional generation in such scenarios is helpful because it provides local generation and less imports is required to serve load. But the inherent variability of wind and the inverse nature of diurnal load and wind variation raise concerns about the effectiveness in a wind farm to enhance system reliability.

## 4.3 Static Voltage Stability Analysis

The system described in the above section is utilized to conduct a static transfer analysis. The initial load level in the load zone is maintained at 600 MW. Generation outside the load zone is used to import power into the load zone. The load is increased while maintaining a constant power factor.

The voltage criteria used for the system is that all pre contingency voltage should be above 0.95 p.u and below 1.05 p.u. on all buses over 115kV. For post contingency scenarios, the minimum voltage is extended to 0.9 p.u. and the maximum voltage is increased to 1.1 p.u.

All the imported power is delivered to the load zone through the 5 import lines emanating from T-1, C-1, C-2 and C-3. All line out contingencies are considered. The five most restricting contingencies are screened and are determined to be the outages of any one of the five import lines. VSAT is the tool used to carry out the PV analysis [60].

Of the three buses monitored WF1 bus is the most susceptible to low voltage violation. Of the five contingencies considered the most restricting contingency is the loss of

the line from C-3 to the wind interconnection bus. Figure 28 demonstrates the pre contingency voltage at WF1 bus as the load is increased. The first voltage violation for the cases with wind occurs in pre contingency. The maximum load in the load pocket with the wind generation at full output is 770 MW. The maximum loading possible with the wind at 5% is 830 MW. With no wind present in the system the maximum loading without any voltage violations is 650 MW.

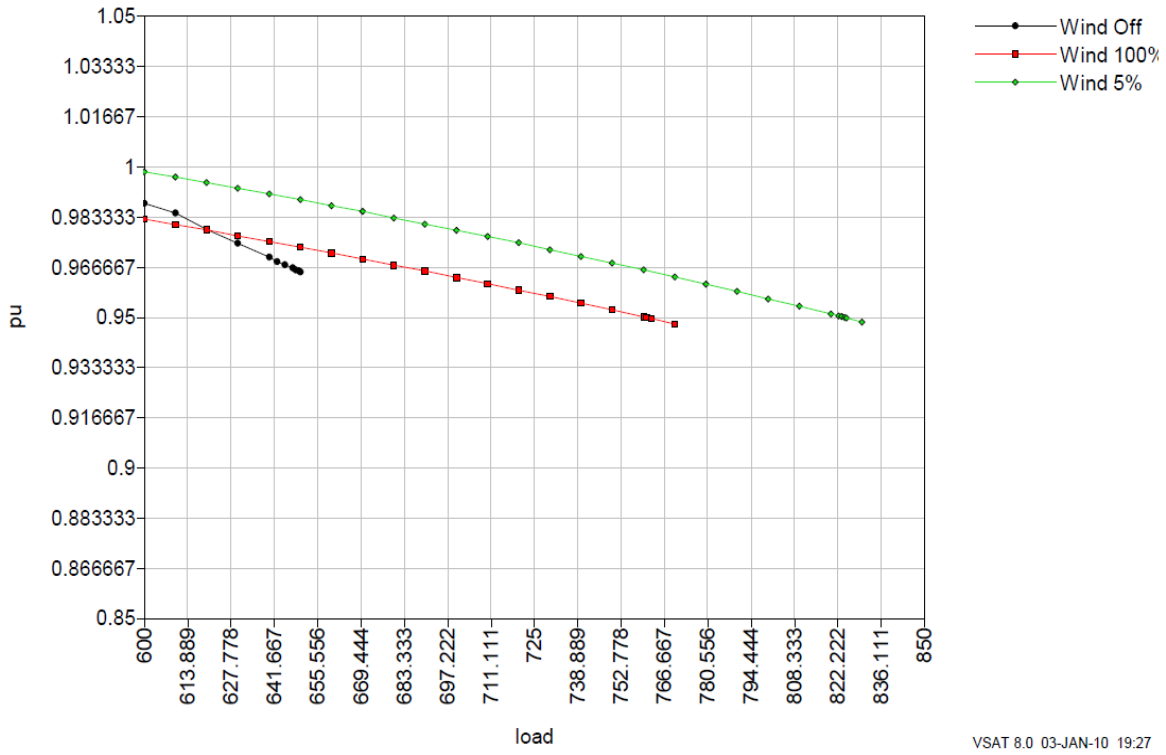


**Figure 28 : Pre-contingency Voltage Variation at WF1 Bus**

Figure 29 indicates the voltage variation at WF1 bus for the three different cases. The first voltage violation for the case without wind is at 650 MW. This violation occurs for the post contingency voltage. The post contingency voltage dips below 0.9 p.u. beyond this load level.

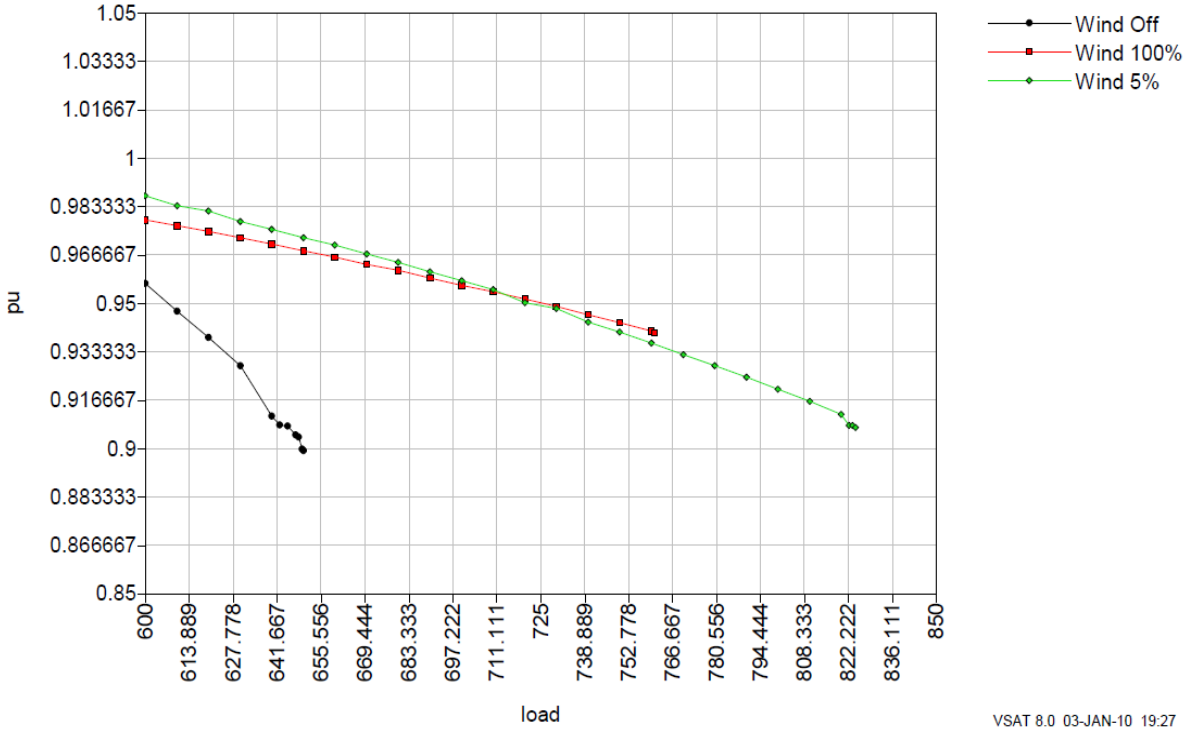


**Figure 29 : Post-contingency Voltage Variation at WF1 Bus**

The voltage profiles for the cases with wind again indicate that the post contingency voltages at WF1 are higher for the cases with wind present. The additional reactive power available at low wind levels allows for more loads to be served in the load pocket. The additional transfer capability provided by the wind park in this case is about 80 MW. Thus at low wind levels 10% additional load can be served in the load zone by imported power. This is especially important because at peak load levels on the system the wind speeds are minimal. Thus wind power output is very low during system peak and this lack of wind results in increased requirement of imported power from outside the load zone.

The above analysis indicates that even though wind power peaks at periods of relatively low loads, the incorporation of the capability curve of the wind park can enable the load zone to import higher levels of power to serve the load pocket reliably. The power

transfer margin without any wind is 50 MW. If the capability curve were not employed, then to reliably serve the load that the wind park supplies, additional system fixes in the form of either transmission lines or reactive devices will be required. The use of the capability curve in this analysis clearly demonstrates the cost savings for the power system by utilizing the capability curve.

## 4.4 Dynamic Simulation Setup

This section examines the impact of the additional reactive capability on dynamic voltage performance. The same three cases utilized in section 4.3 are utilized in this section as well. The following sections describe the different components that are modeled in the dynamic simulation.

The purpose of this analysis is to verify the results obtained in the steady state analysis described in section 4.3.

### 4.4.1 Generator Modeling

The dynamic model for the above system is obtained from the Eastern Interconnection dynamic model. The dynamic simulation is carried out in PSS/E [60]. The 57 online units have dynamic models. The generator model used is the round rotor generator model (GENROU) [61]. The following table 7 indicates the different exciters used in the dynamics data.

**Table 7 : Different Exciter Models Used in the System**

| Exciter Code | Description |
|---|---|
| ESAC1A | 1992 IEEE type AC1A excitation system model. |
| ESAC8B | Basler DECS model. |
| ESAC3A | 1992 IEEE type AC3A excitation system model. |
| ESST1A | 1992 IEEE type ST1A excitation system model. |
| EXAC2 | 1981 IEEE type AC2 excitation system model. |
| EXST1 | 1981 IEEE type ST1 excitation system model. |
| IEEEX1 | 1979 IEEE type 1 excitation system |
| ESST3A | 1992 IEEE type ST3A excitation system model. |
| EXPIC1 | Proportional/integral excitation system model. |

The different governor models used in the system are given below in table 8. The PSS2A type stabilizer is also used for some generators. The PSS2A is the IEEE Dual-Input Stabilizer model.

**Table 8 : Different Governor Models Used in the System**

| Governor Code | Description |
|---|---|
| GGOV1 | GE general purpose turbine-governor model. |
| IEEEG1 | 1981 IEEE type 1 turbine-governor model. |
| WESGOV | Westinghouse digital governor for gas turbine. |
| IEESGO | 1973 IEEE standard turbine-governor model. |
| TGOV1 | Steam turbine-governor model. |

### 4.4.2 Tap-Changer Modeling

. Online tap changers are devices used to adjust the taps of a transformer. The taps of a transformer help change the ratio of the primary to the secondary winding of the transformer. The primary application of tap changers is to boost up the voltage on the lower kV side of the transformer to maintain load voltages. The tap changers are dangerous in a system that is close to voltage instability. Whenever transformer taps are adjusted the reactive power absorbed or injected into the grid on the high kV side of the transformer changes. When the taps are adjusted to increase the voltage on the low kV side, additional reactive power is absorbed from the grid. Since voltage instability in the power system is closely tied to the reactive reserves in the system, tap changer action can take a system closer to voltage instability. Thus, modeling the tap changer action gives a more accurate representation of the system response to low voltage conditions.

The standard OLTC1 model is used to model tap changer action in the system. The OLTC1 model consists of two components – the voltage sensor and the time delay circuit [62]. The voltage sensor senses if the bus voltage is outside the predefined band. The control will operate if the time of voltage excursion from the band exceeds the time delay. The output of the regulator is modified instantaneously because the time delay of the electronic circuit is much smaller than the time-delay.

The time-delay circuit uses a simple integrator timer. The time delay prevents the controller from acting for self correcting voltage violations. A predefined time interval $T_D$ is the minimum period for which the voltage should violate the band. The tap changing action takes place $T_C$ seconds after the time delay is exceeded. This time is the tap changing delay.

The final parameter for the OLTC1 model is the time between consecutive tap changing actions. This delay is called the $T_{SD}$ . For the delay to work well, it must be more than the tap changing delay, so that the effect of the tap changing is observed by the voltage regulator and unnecessary tap changing does not occur.

The settings used in the model for the system considered is $T_D$= 25 s, $T_C$ = 10 s and $T_{SD}$ = 15 s. Online Tap changers are modeled at 26 transformers in the load zone.

### 4.4.3 Wind Park Model

The standard GE 1.5 MW machine model is used [63]. The model is utilized as a user defined model in PSS/E. The wind plant model has 6 components. Table 9 indicates the 6 models and their description.

**Table 9 : Components of Wind Turbine Model**

| Model Code | Description |
|---|---|
| GEWTG1 | Wind Turbine Generator |
| GEWTE1 | Wind Turbine Electrical Control |
| GEWTT | Two Mass Shaft Model |
| GEWTA | Wind Turbine Aerodynamics |
| GEWTP | Pitch controller |
| WGUSTC | Wind Gust Model |

The GEWTG1 model is the wind turbine generator model. The inputs to this model are the real and reactive power commands from the GEWTE1, the electrical control model. The reactive power control is set to remote bus voltage control. The wind

interconnection bus is used as the remote bus to be regulated. The regulated voltage is set to 1.04. The other models are the standard pitch control model (GEWTP) and the aerodynamic model (GEWTA) that handles the mechanical power input from the blades. The two mass shaft model (GEWTT) consists of the generator inertia and the inertia of the blades. The wind gust model (WGUSTC) is used to simulate wind gusts and ramps. Since we are looking at a small time frame (< 5 min), the wind speed is assumed to be constant throughout the simulation.

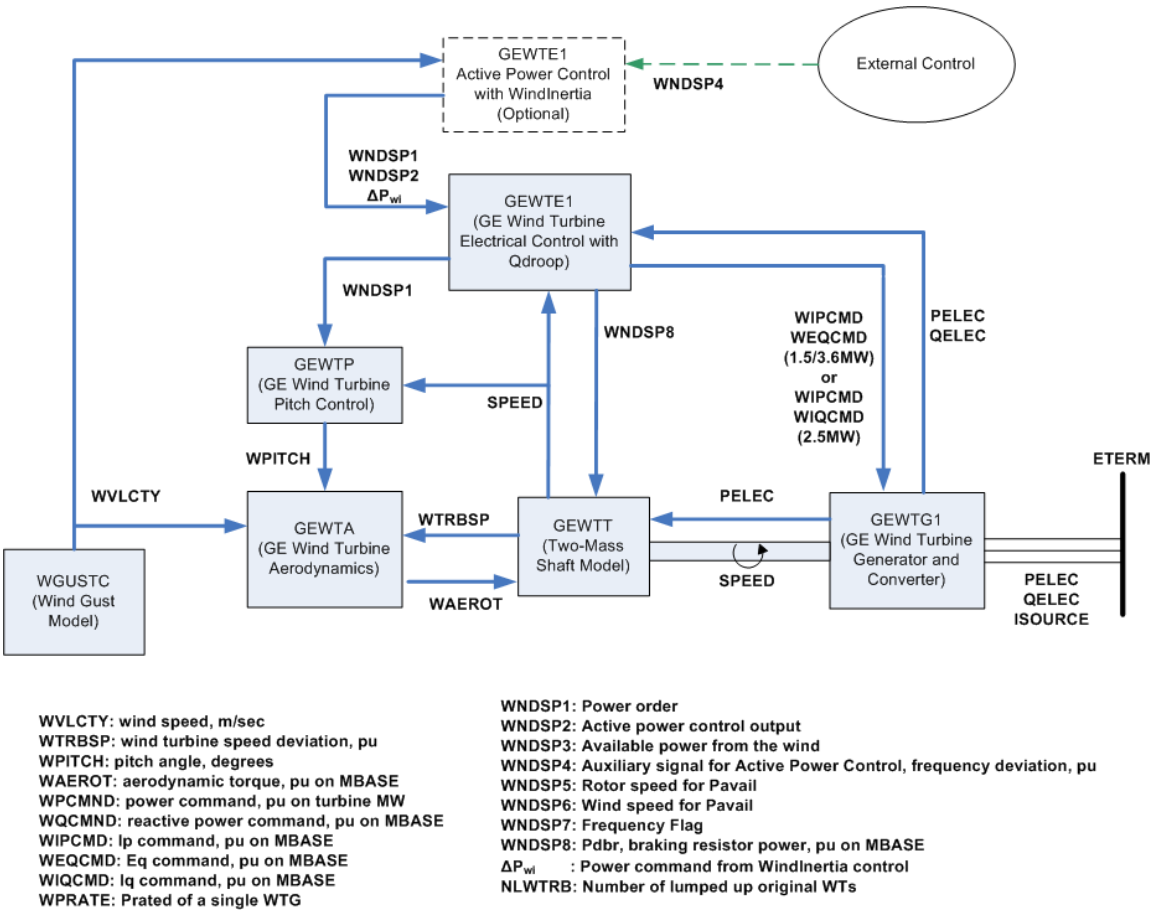


**Figure 30 : Connectivity of Different Components in the GE wind model [64]**

The machine parameters given in Table 1 are the parameters of a standard GE 1.5 MW unit. Thus the model is used entirely as it is including parameters. The only

modification made is the change in reactive power limits based on the real power output. The reactive power limits that are available in p.u. in figure 9 are scaled up to the park maximum power output which is 126 MW. Since the dynamic model is based on p.u. on the MVA base of the plant, the reactive power limits in p.u. are entered in the dynamic model. Two sets of dynamic data are set up – for 100% park output and 5% park output respectively.

## 4.5 Dynamic Simulation Results

The dynamic analysis is done to verify the results obtained from the static voltage stability analysis. To simulate the effect of Under Load Tap Changers (ULTC's), the model is included. The load is modeled as a constant MVA load for the static analysis. The dynamic simulation software's like PSS/E do not allow for constant MVA load model. The load has to be converted to either a constant current model or constant impedance model. The constant impedance model is the least conservative model. The real power load is converted to a constant current load and the reactive load is converted to a constant impedance load. This assumes an intermediate assumption for load behavior and proximity to voltage collapse.

The same cases are used for the dynamic analysis as the steady state analysis. The approximate transfer limits obtained in the static analysis is used as a starting point for the dynamic simulations. The disturbance on the system is the loss of a line with no fault. The most severe contingency in the static analysis is used for the loss of line contingency.

The first case that is run is the case with the wind at 100%. The objective is to look at the load levels at which there are voltage violations either pre contingency or post

contingency. Also, the simulation is extended for 5 minutes to see the effect of the tap changing transformers.

### 4.5.1 Wind Plant at 100%

The maximum load obtained with the static analysis in section 4.3 is 770 MW with the wind farm at maximum output. Thus, the initial load zone load is set to 775 MW. The following plots indicate the voltages at the three monitored buses and the reactive power output from the two wind parks.

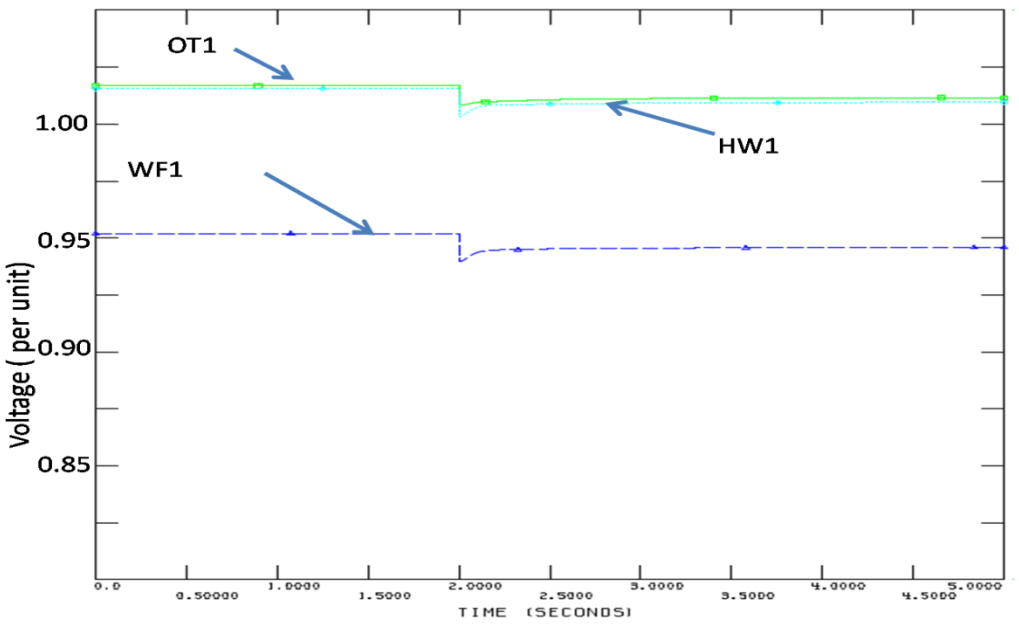


**Figure 31 : 5 Second Voltage Profile – Load = 775 MW Wind 100%**

The figure 31 indicates the 5 second voltage profile at the three buses. Again, as seen in the static analysis, the WF1 bus is the lowest voltage amongst the monitored buses.

The objective of this plot is to see post disturbances voltage. Since the timeframe is just 5 seconds the effect of tap changers is not evident.

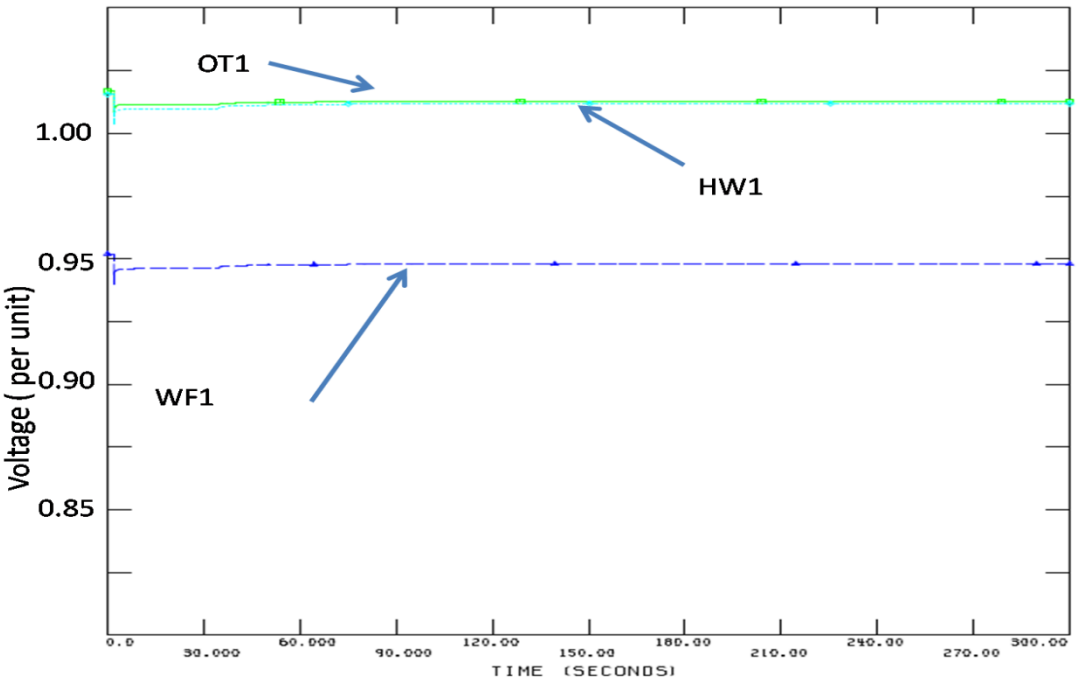


**Figure 32 : 300 Second Voltage Profile – Load = 775 MW Wind 100%**

The next plot in figure 32 indicates the extended simulation for 5 minutes. The voltages begin to rise due to the tap changer action. The system reactive reserves are sufficient and the post disturbance voltage settles very close to the pre disturbance voltage.

Figure 33 indicates the reactive output of the two wind parks. The reactive power output settles at a value below the maximum value of 46.2 MVAr.

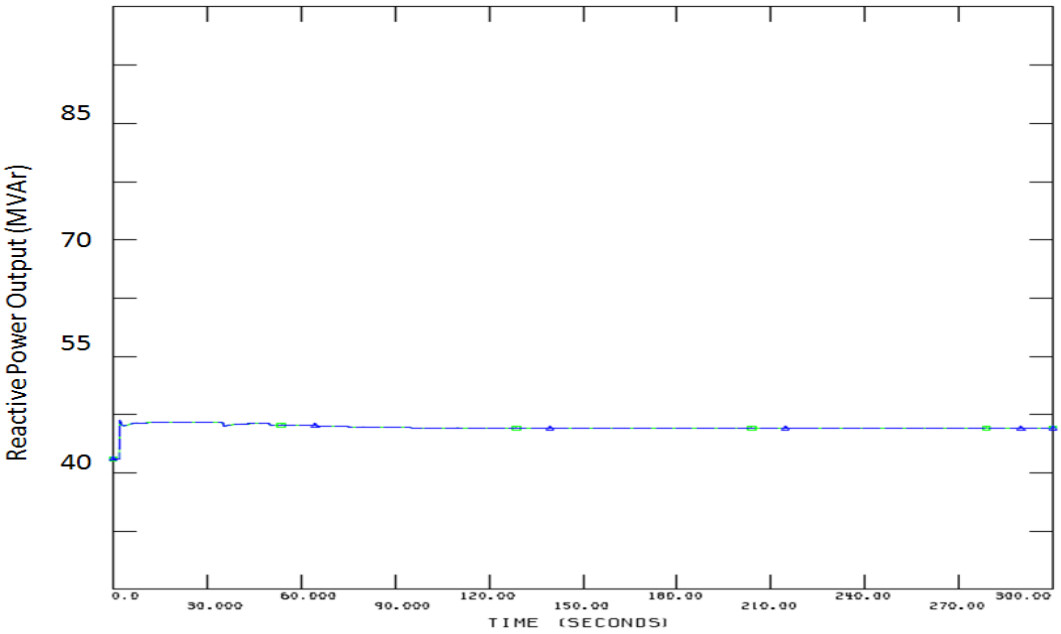


**Figure 33 : 300 Second Reactive Power – Load = 775 MW Wind 100%**

The next load level that is tested is 800 MW. At this load level, the pre contingency voltage at WF1 violates the criteria. But from figures 34 and 35 it is evident that the post disturbance voltages are over 0.9 p.u and there is no criteria violation.

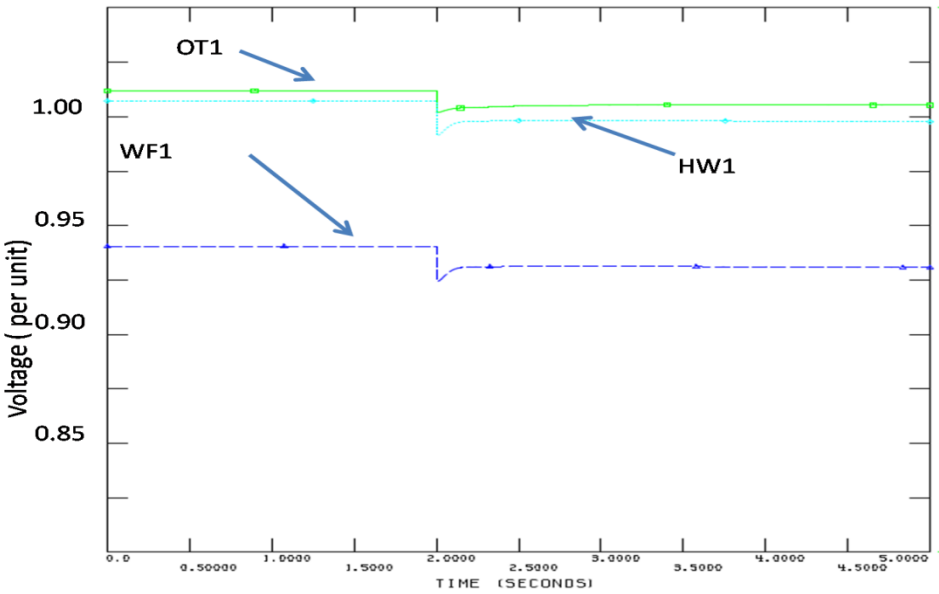


**Figure 34 : 5 Second Voltage Profile – Load = 800 MW Wind 100%**

In figure 35, it is visible that the number of tap changing actions is minimal.

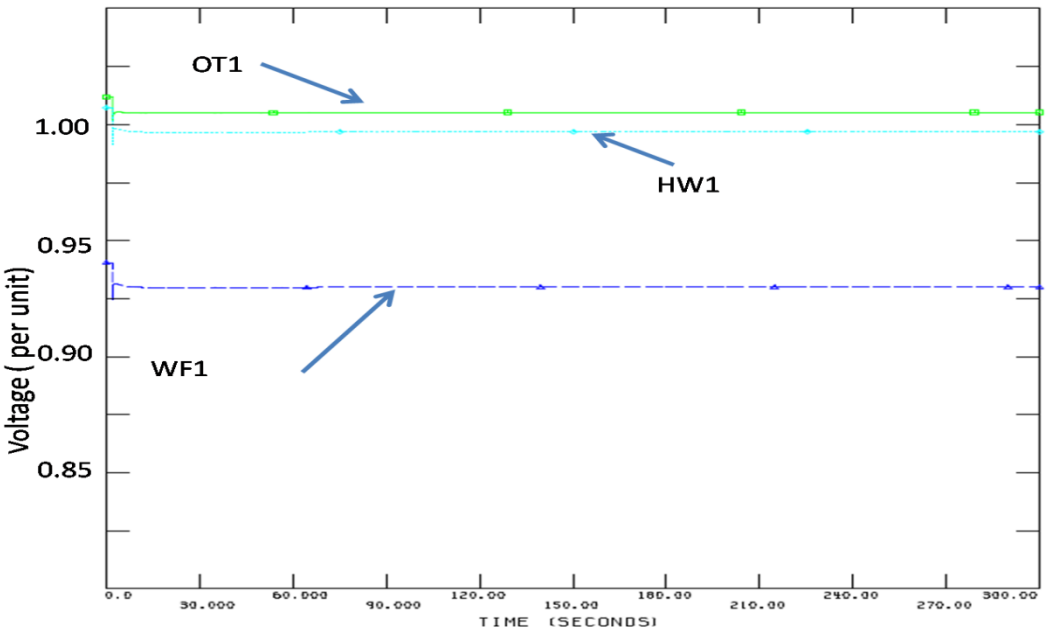


**Figure 35 : 300 Second Voltage Profile – Load = 800 MW Wind 100%**

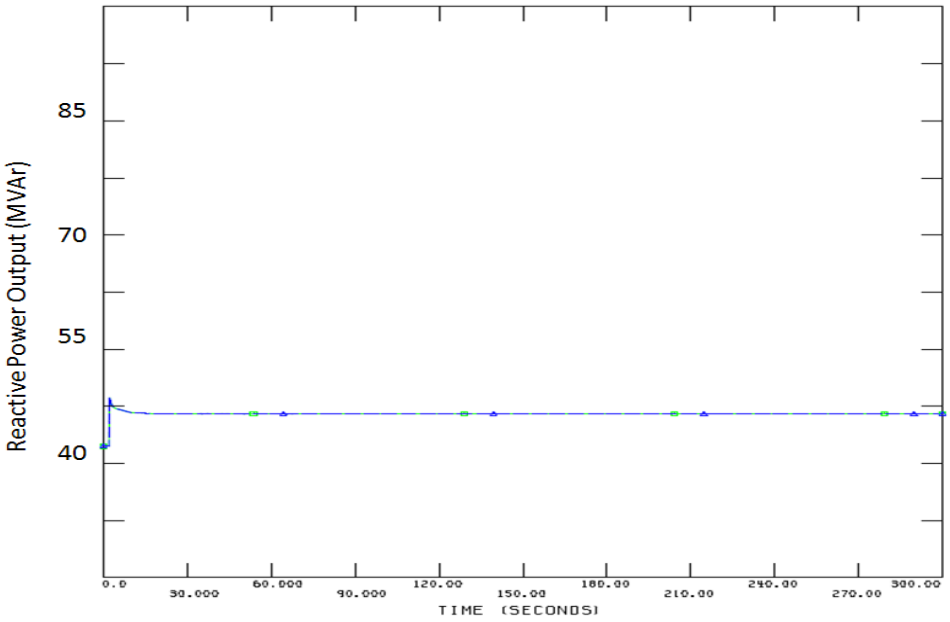


**Figure 36 : 300 Second Reactive Power – Load = 800 MW Wind 100%**

The figure 36 shows the reactive power outputs of the two parks. The wind parks in this case hit their reactive limit, but it remains flat at that level, which indicates the minimal tap changing events.

The load is increased further until there is post contingency voltage violation. At 850 MW, the post contingency voltage just after the disturbance reduces below 0.9 p.u. Figure 37 shows the voltage reduces below the minimum value of 0.9.

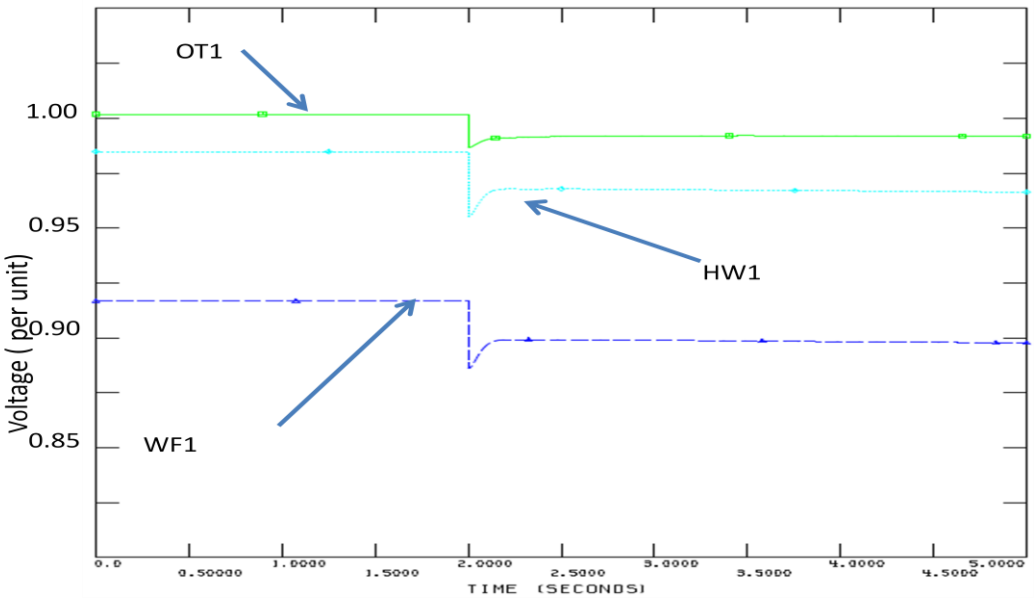


**Figure 37 : 5 Second Voltage Profile – Load = 850 MW Wind 100%**

In figure 38 the 5 minute simulation of the voltages is shown. The voltages at all the buses deteriorate with continuous tap changer action.

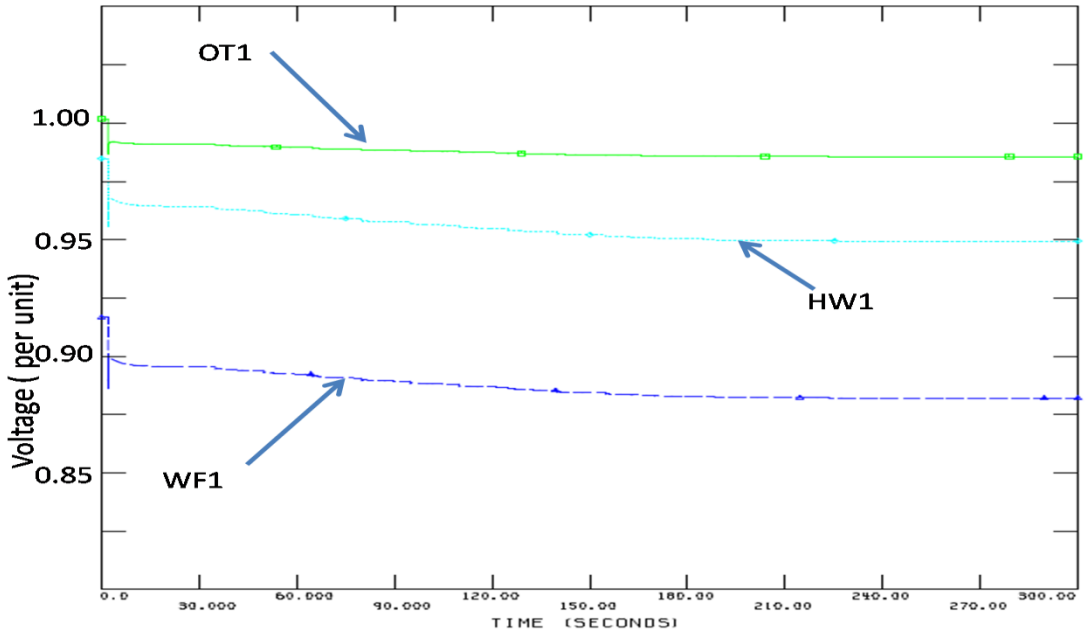


**Figure 38 : 300 Second Voltage Profile – Load = 850 MW Wind 100%**

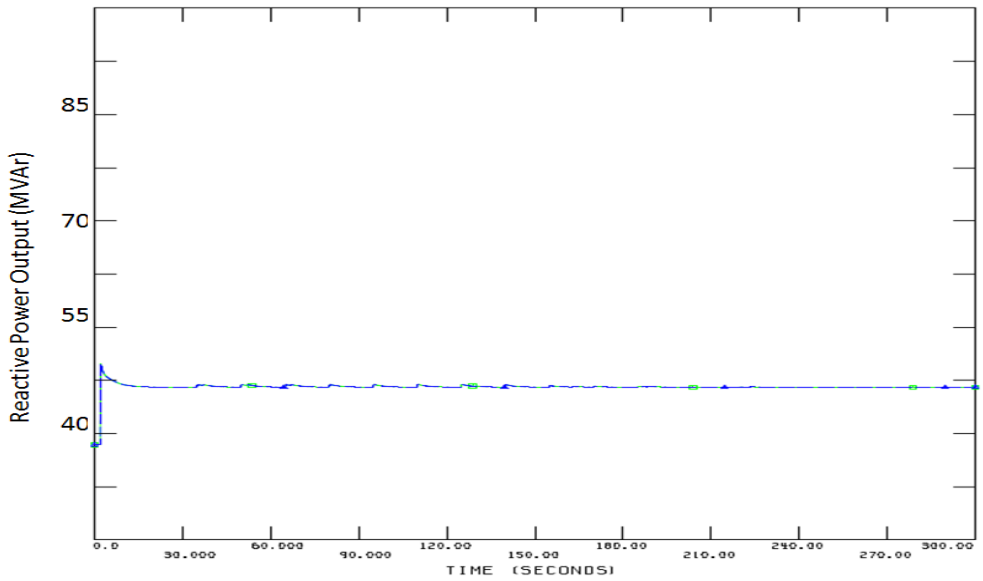


**Figure 39 : 300 Second Reactive Power – Load = 850 MW Wind 100%**

In figure 39 the reactive output of the wind parks is seen for the 850 MW case. Post disturbance the reactive power reaches its maximum value. For every subsequent tap change the reactive power spikes up but then the electrical control of the wind turbine reduces the output to its maximum value and the voltages begin to deteriorate.

### 4.5.2 Wind Park Offline

The next case that is considered is the case with zero wind. The wind parks are offline. The first system load scenario considered is the 775 MW load. The 775 MW load is the maximum secure load that can be served with the wind units at 100%. Figure 40 indicates the 5 second voltage response. The post contingency voltage violates the 0.9 p.u value for two buses.

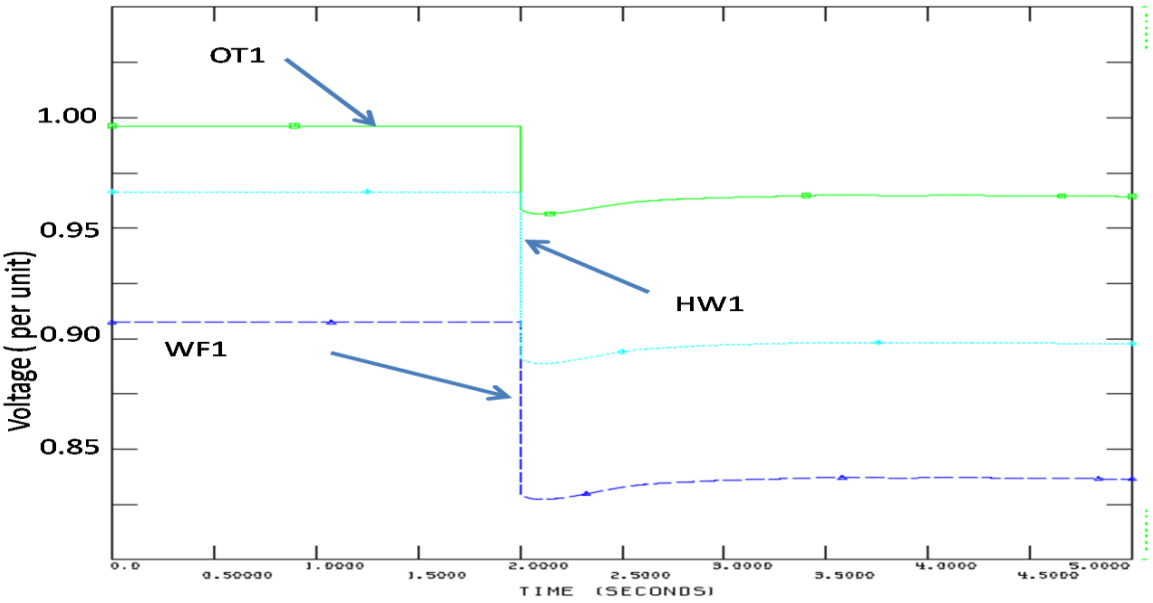


**Figure 40 : 5 Second Voltage Profile – Load = 775 MW Wind Off**

Figure 41 indicates the 5 minute voltage response. There is continuous tap changing action and the voltages continue to deteriorate.

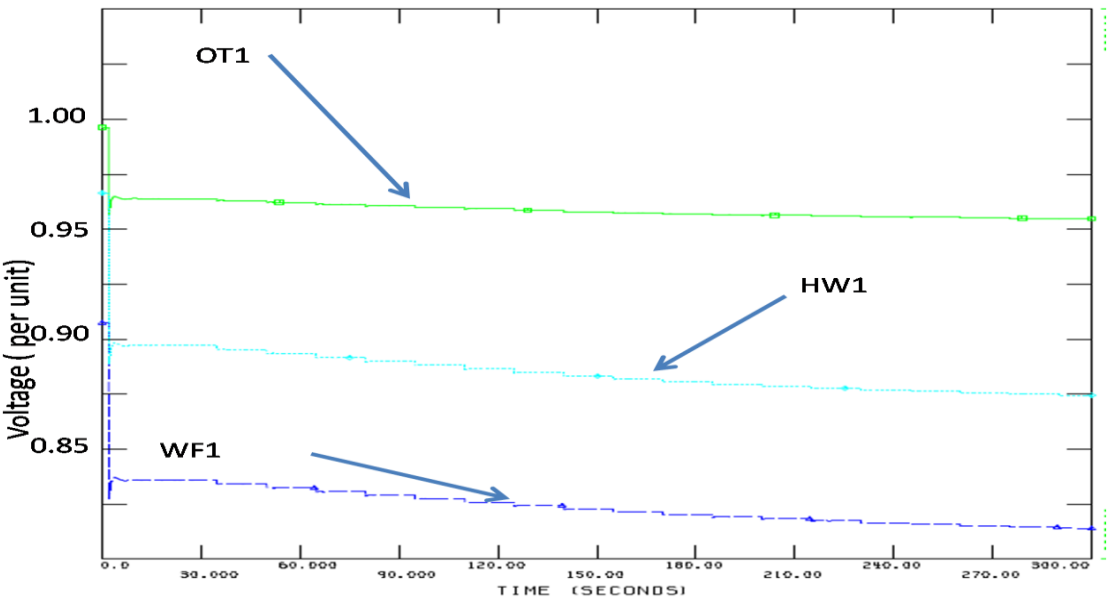


**Figure 41 : 300 Second Voltage Profile – Load = 775 MW Wind Off**

The load is reduced until the voltages are secure for pre and post contingency. This occurs at the system load of 600 MW. The figures 42 and 43 show the voltage profiles for the three buses. WF1 is very close to violating the low voltage pre contingency violation.

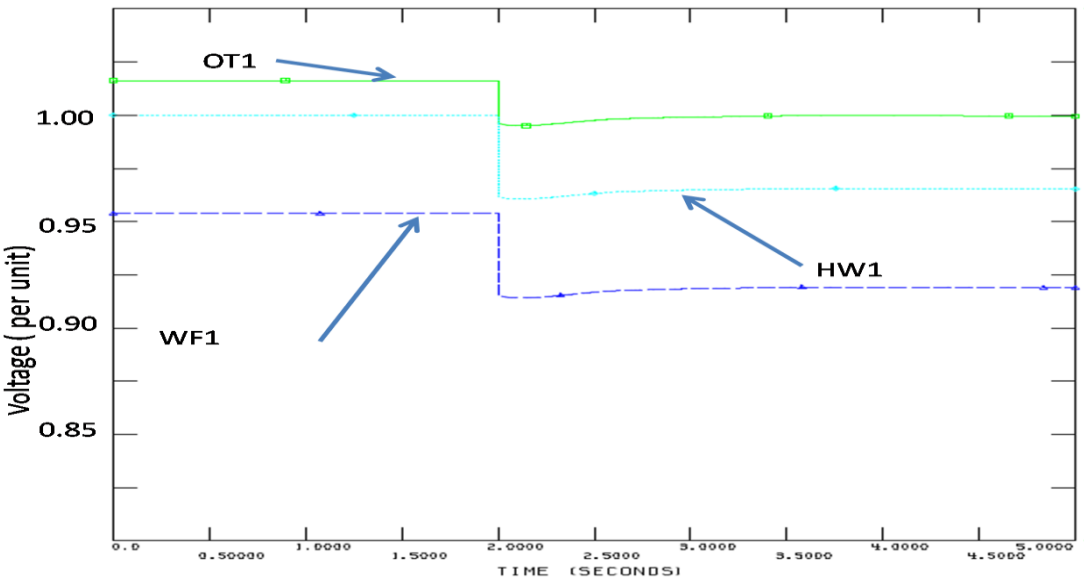


**Figure 42 : 5 Second Voltage Profile – Load = 600 MW Wind Off**

Figure 43 shows the long term voltage profile. The tap changing action takes place but eventually the post disturbance voltage settles down at a secure value.

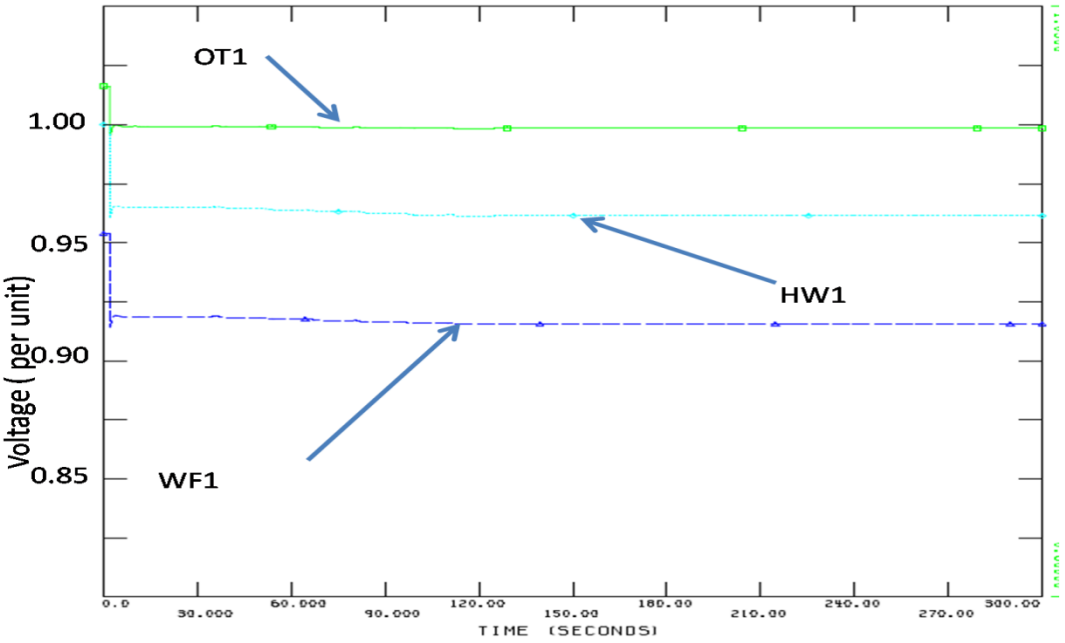


**Figure 43 : 300 Second Voltage Profile – Load = 600 MW Wind Off**

The system is stressed further to a load of 625 MW. At this load level the WF1 bus is violating pre contingency secure voltage criteria.

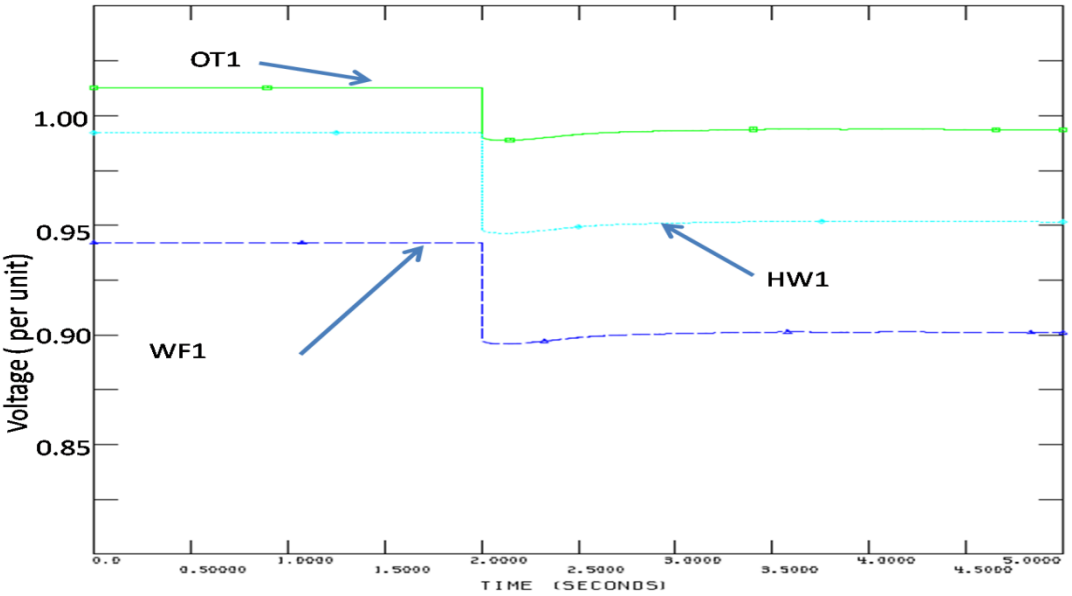


**Figure 44 : 5 Second Voltage Profile – Load = 625 MW Wind Off**

Figure 44 above shows the 5 second voltage response. The immediate voltage after the loss of the line reduces below 0.9 but the voltage begins to recover. But as time progresses, it is evident in figure 45 that with tap changer action the voltage deteriorates and violates the post contingency minimum voltage criteria. Thus 600 MW is the maximum load that can be served by the system if no wind is present.

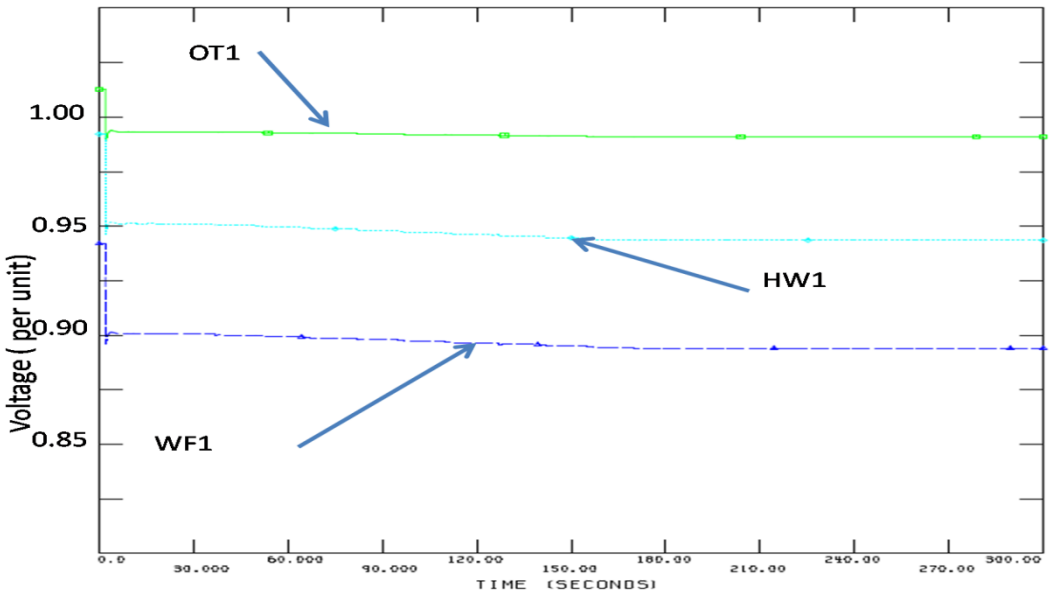


**Figure 45 : 300 Second Voltage Profile – Load = 625 MW Wind Off**

### 4.5.3 Wind Park 5 % - Providing Reactive Power

The final case is the case with 5% wind providing reactive power support to the load pocket. The first load level tested is 825 MW. This load is just beyond the maximum secure load that can be served in this scenario. At this load level, the voltage at WF1 for the pre-contingency case is just below 0.95 p.u as seen in figure 46.

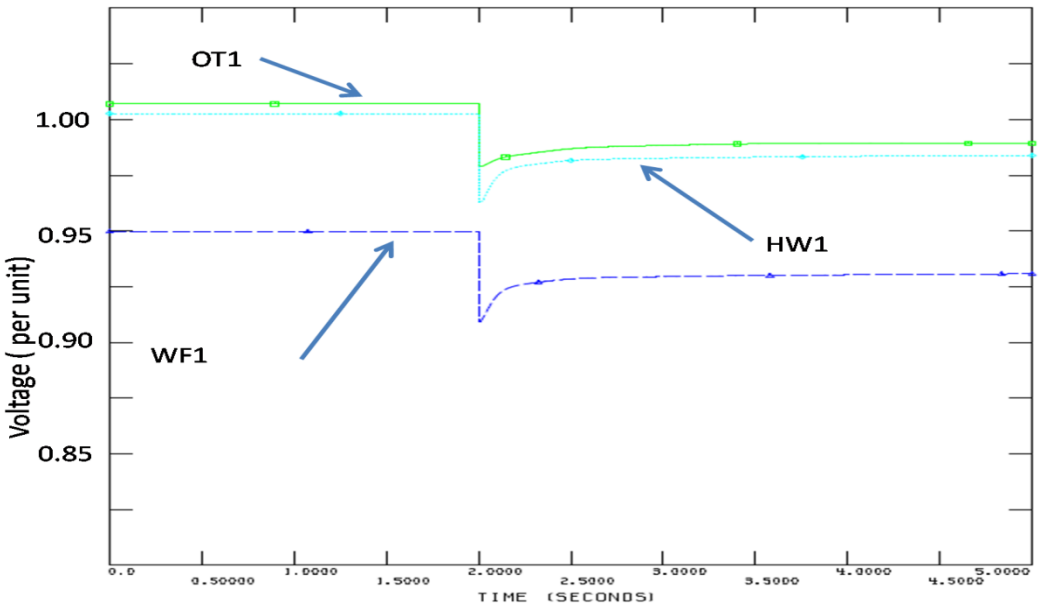


**Figure 46 : 5 Second Voltage Profile – Load = 825 MW Wind – 5%**

The 5 minute simulation in figure 47 again shows that even though there is some tap changer action, the voltage quickly settles to a stable secure post disturbance value.

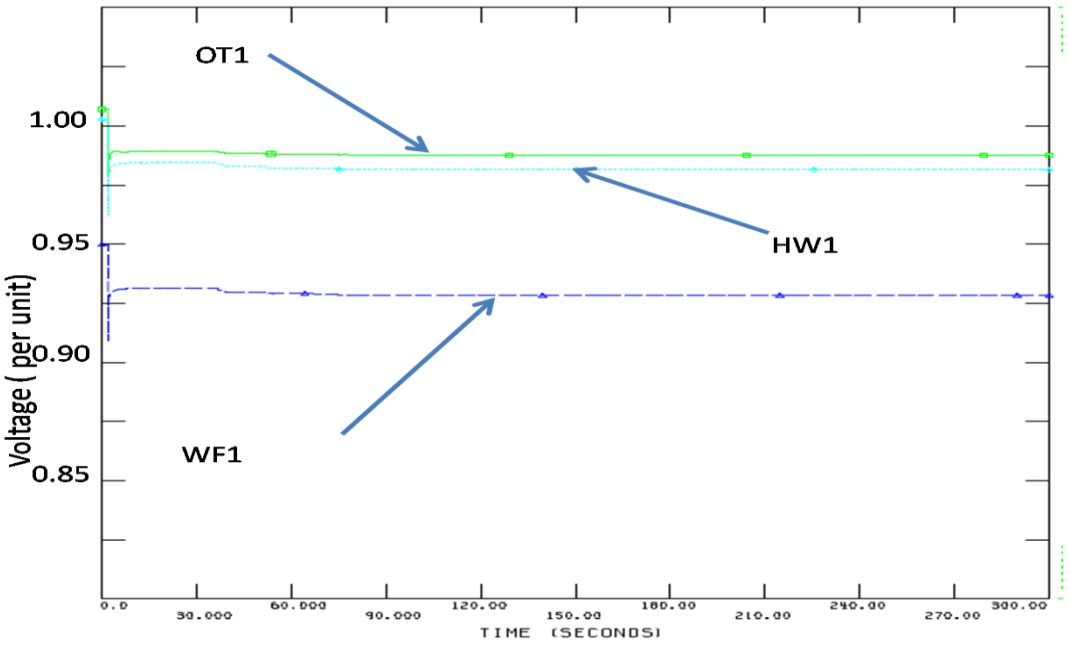


**Figure 47 : 300 Second Voltage Profile – Load = 825 MW Wind – 5%**

The reactive power output from the parks as seen in figure 48, increases with time but is still below the maximum value of 96 MVAr.

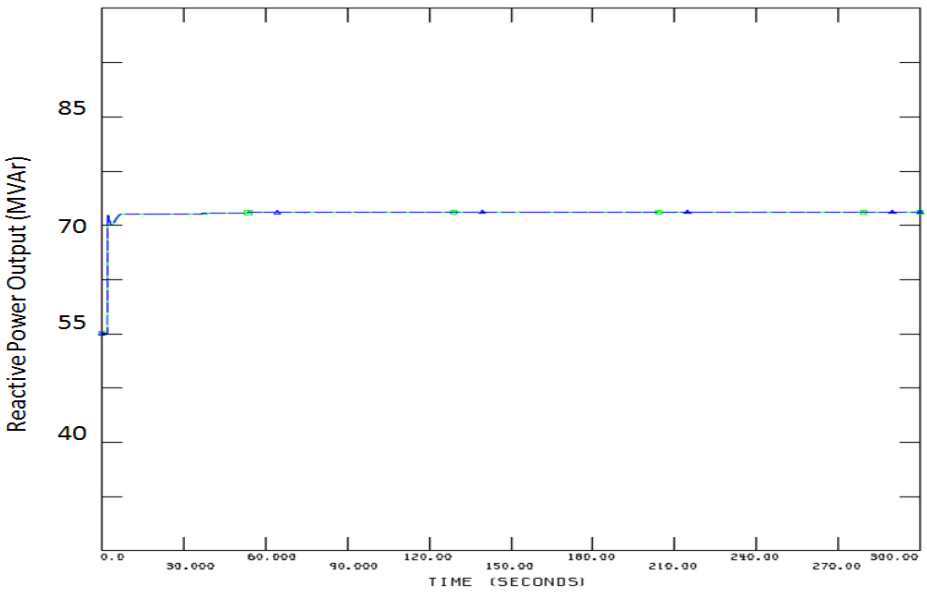


**Figure 48 : 300 Second Reactive Power – Load = 825 MW Wind – 5%**

The next increment of 25 MW results in the pre-contingency voltage going below 0.95 and the post disturbance instantaneous voltage reducing below 0.9 p.u. But in the 5 second simulation in figure 49 the voltage seems to be recovering. But the voltage begins to deteriorate as seen in figure 50 for the extended simulation. The voltages eventually settle at a value greater than 0.9 p.u.

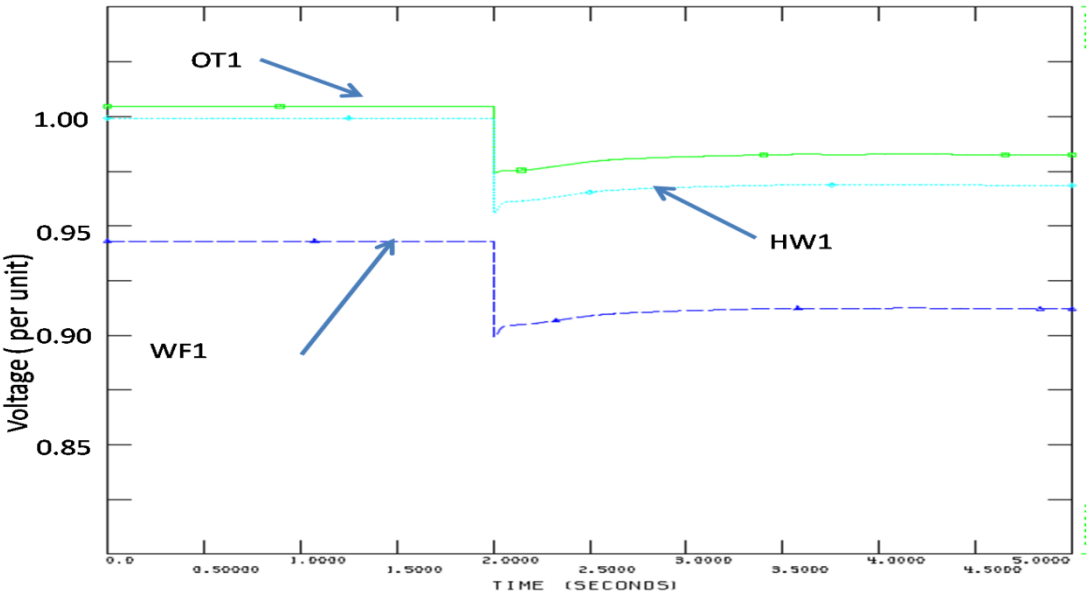


**Figure 49 : 5 Second Voltage Profile – Load = 850 MW Wind – 5%**

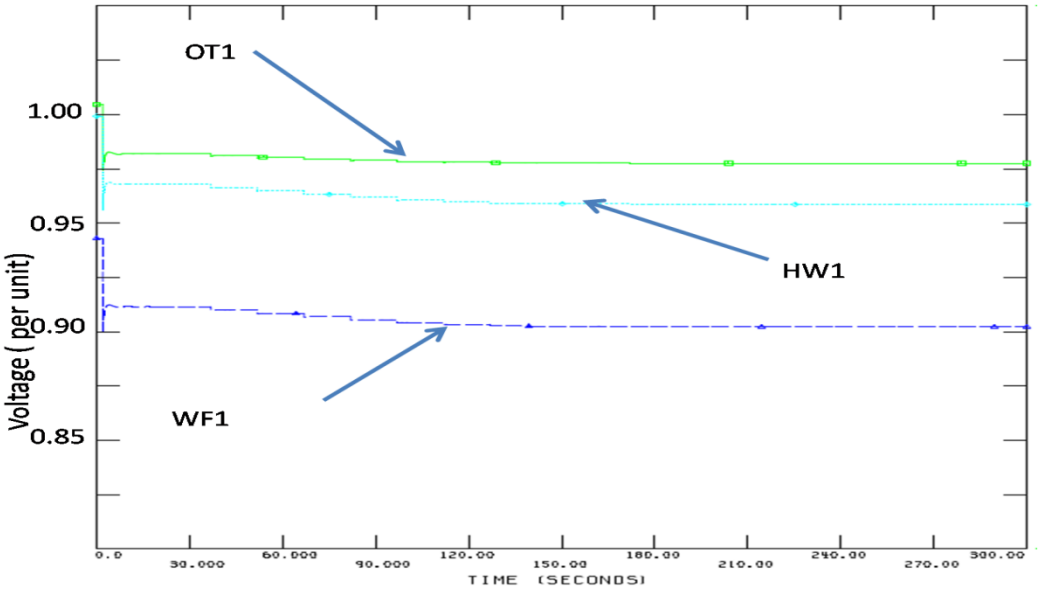


**Figure 50 : 300 Second Voltage Profile – Load = 850 MW Wind – 5%**

The reactive power outputs of the two units are shown in figure 51. Even at this load level the reactive power output of the machine is well below the maximum reactive power limit.

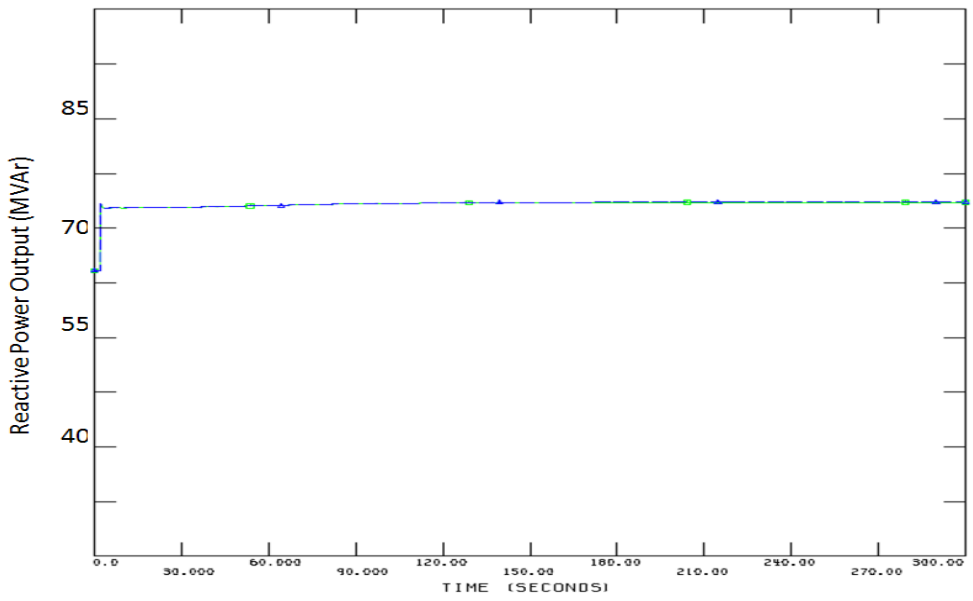


**Figure 51 : 300 Second Reactive Power – Load = 850 MW Wind – 5%**

Thus the dynamic simulation studies further confirm the results from the static analysis. The reactive power capability at low wind levels allows for higher load being served than the wind park at 100% output. Also, the load served by no wind is significantly less than the load that can be served by using the capability curve at low wind levels.

## 4.6 Summary

This section demonstrates the benefit of utilizing the capability curve of an off shore wind park to reliably serve load during low wind periods. The proximity of off shore wind farms to load centers and the reactive power requirements of load pockets makes it favorable to utilize the reactive capability to prevent voltage issues in the load center.

The periods of low wind correspond with periods of high load. High load time periods are times when the system reactive reserves are at their lowest. The accessibility of wind farms as a reactive power source will lead to higher import capabilities into the coastal load pockets from remote generation. In essence the additional reactive capability helps the power system handle the unavailability of wind.

Both steady state and dynamic simulations demonstrate the improved transfer capability into the load pocket. The effect of online tap changers on the post disturbance voltages was also studied.

The results in this section make a strong case for off shore wind generation and the ability to handle wind variability more effectively by utilizing the full reactive capability of a DFIG wind park.

# CHAPTER 5: LARGE SYSTEM IMPLEMETATION-WESTERN IOWA

## 5.1 Wind in Iowa

Iowa is the second ranked state in terms of wind capacity in the United States [65]. The only state ahead of Iowa is Texas. Figure 52 shows the current installed capacity of wind power by state.

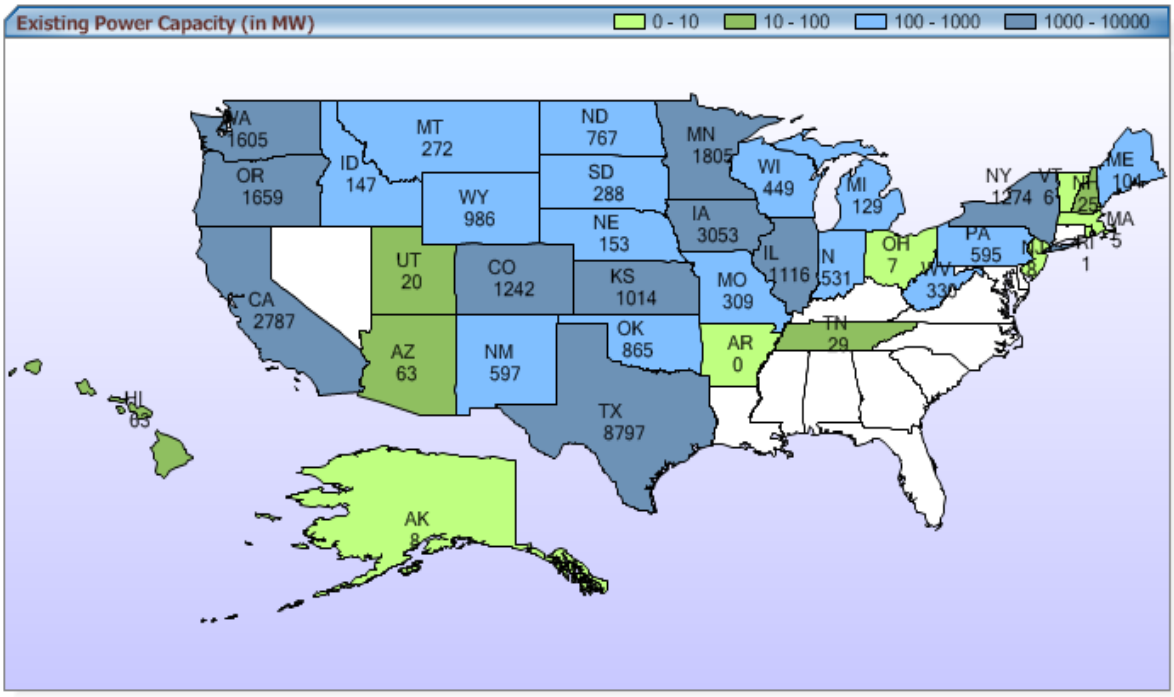


**Figure 52 : Wind Capacity by State in MW's [65]**

Even though a large amount of the wind energy sites have been developed there is potential for more wind power in Iowa. In figure 53, the high yield wind energy sites selected by NREL are shown [66]. It is evident that the western Iowa region has great prospects for wind energy development.

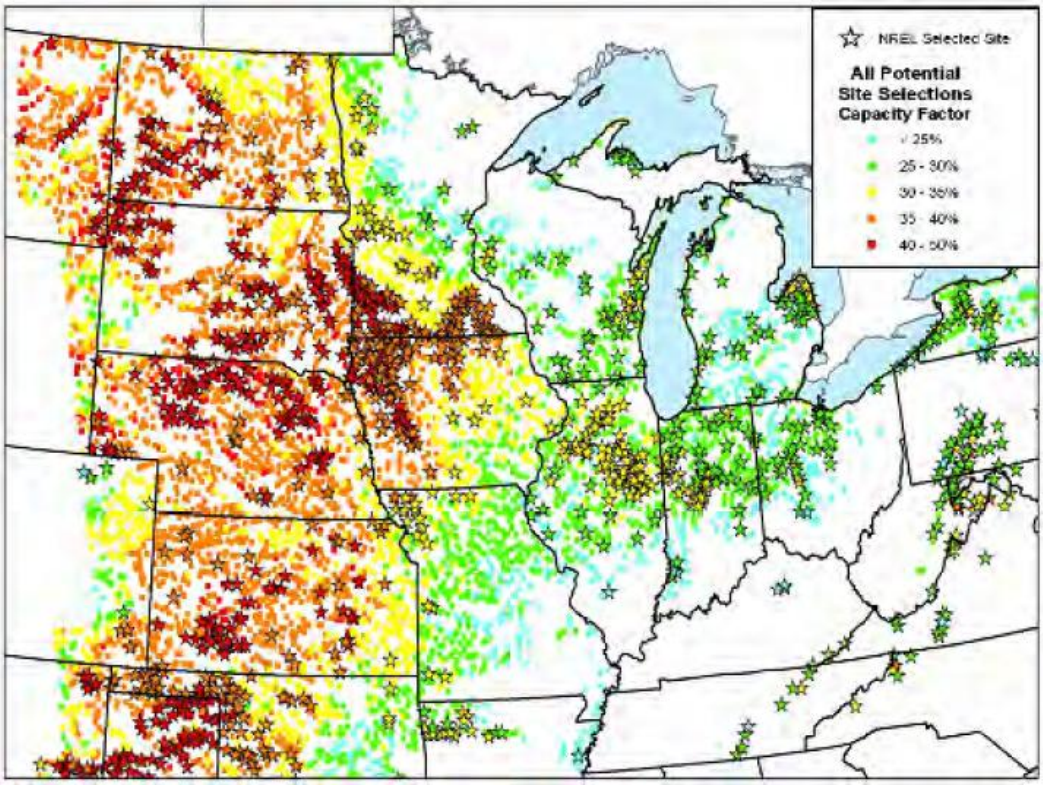


**Figure 53 : Selected NREL Sites for Wind Potential [66]**

With consultation from the local utility in the region - MidAmerican Energy, the three counties of Ida, Pottawattamie and Osceola were identified as high potential sites in terms of incoming wind projects. The utility also considered the load pocket that this additional wind would serve as the Chicago area. The following figure 54 illustrates the three counties on an annual average wind speed map of Iowa [67].

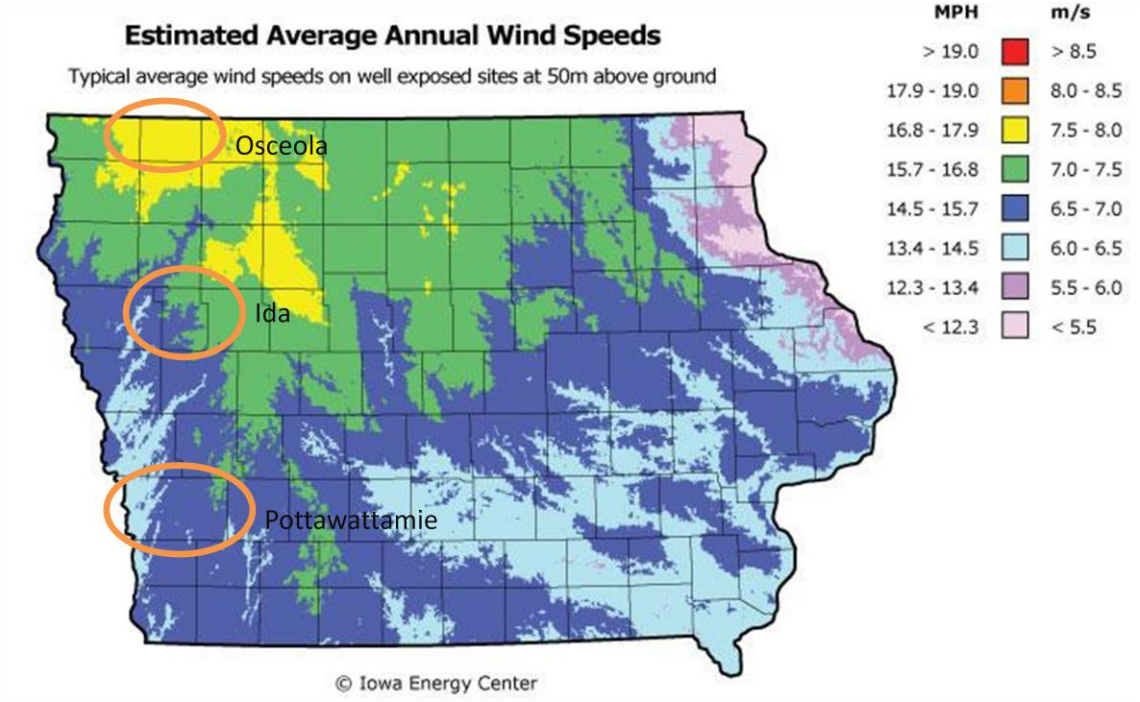


**Figure 54 : High Wind Potential Counties in Iowa [67]**

The intent of the study is to determine how much additional wind generation can be added at these three counties in order to serve load in Chicago. An additional case is run with added transmission to determine the impact of the additional transmission on transfer capability. The Eastern Interconnection system data is used for the analysis.

## 5.2 Modeling Details

The Eastern Interconnection system consists of 22053 buses. The area of study is restricted to the three utilities- MidAmerican Energy and Alliant, the utilities that cover Iowa and Commonwealth Edison (NI), the utility that covers the Chicago area and Northern Illinois. The base case load in the NI area is 22700 MW. The import lines from Iowa to Illinois consist of 345kV lines near the eastern border near the Quad cities area.

The following figure 55 shows the existing 345 kV system running west to east in Iowa. There are three lines coming in from Western Iowa to Central Iowa and then two lines going from Central Iowa to the Iowa/Illinois border.

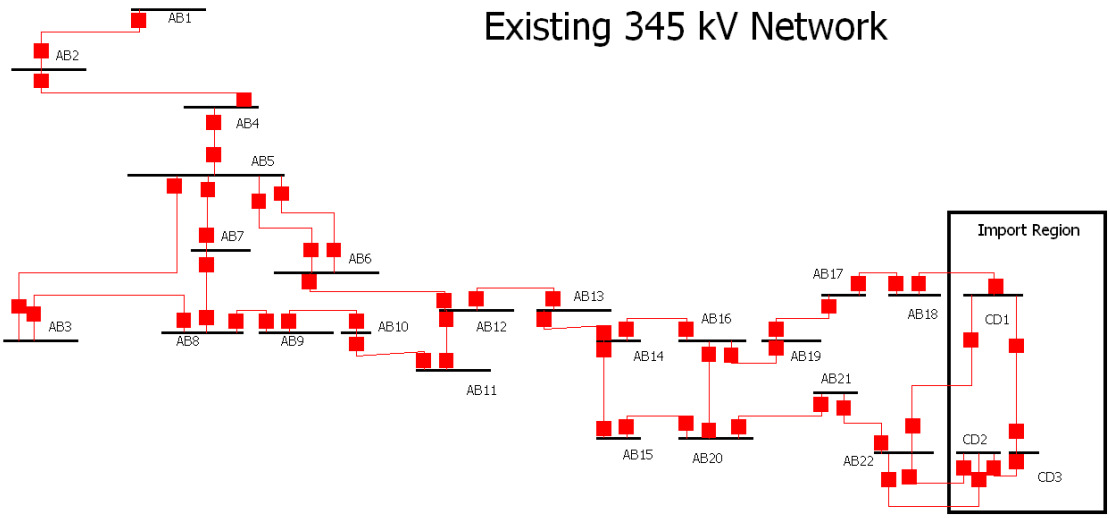


**Figure 55 : Existing 345 kV network West to East in Iowa**

Three new 345 kV buses are tapped off this network to add wind. The three new buses correspond to the three counties discussed in the previous section. The wind is added on the 161 kV network and a 345/161 kV autotransformer is used to step up the wind power to the transmission network. The modified 345 kV system is shown in figure 56.

For the added transmission case, many of the 345 kV lines are doubled up to have the system as shown in figure 57.

In the following sections the maximum wind power output from the three given locations is determined. The criteria used to determine the transfer limit is voltage violation below 0.9 p.u. All 345 kV and 161 kV buses are monitored in the MidAmerican and Alliant System. All single line out contingencies on the 345 kV paths from west to east are considered. The total number of contingencies is 38.

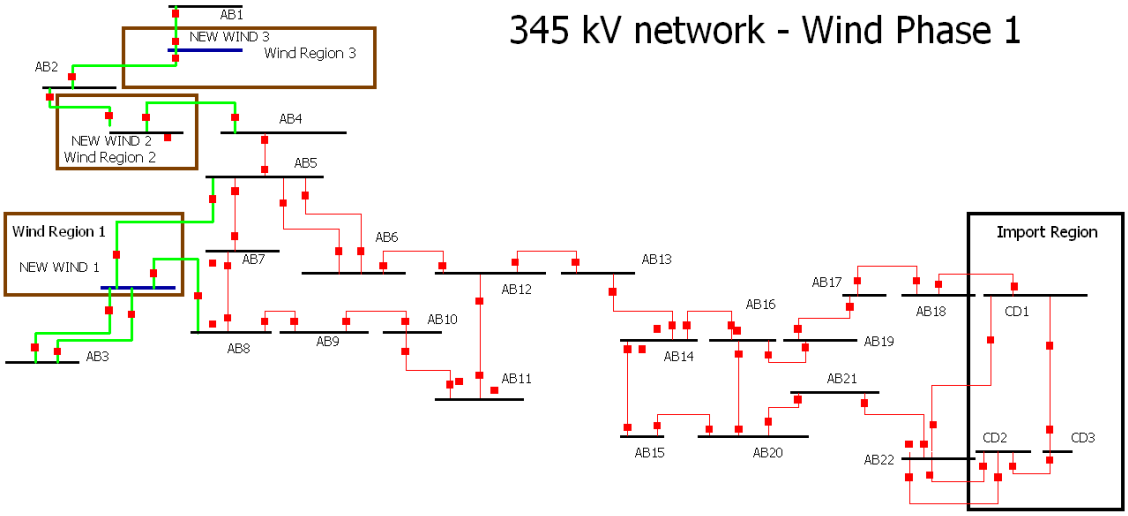


**Figure 56 : Iowa 345 kV network with new 345 kV buses for Wind**

The wind farm parameters and the collector system is the same as used in chapter 4. The intent is to determine the amount of wind power that is deliverable to the import region, if all the wind parks were operating at 100%. The tool used for the analysis is VSAT.

This approach is very similar to the analysis done for new interconnection generators. The generator must be able to deliver its maximum power with all the generators around the new unit operating at full output.

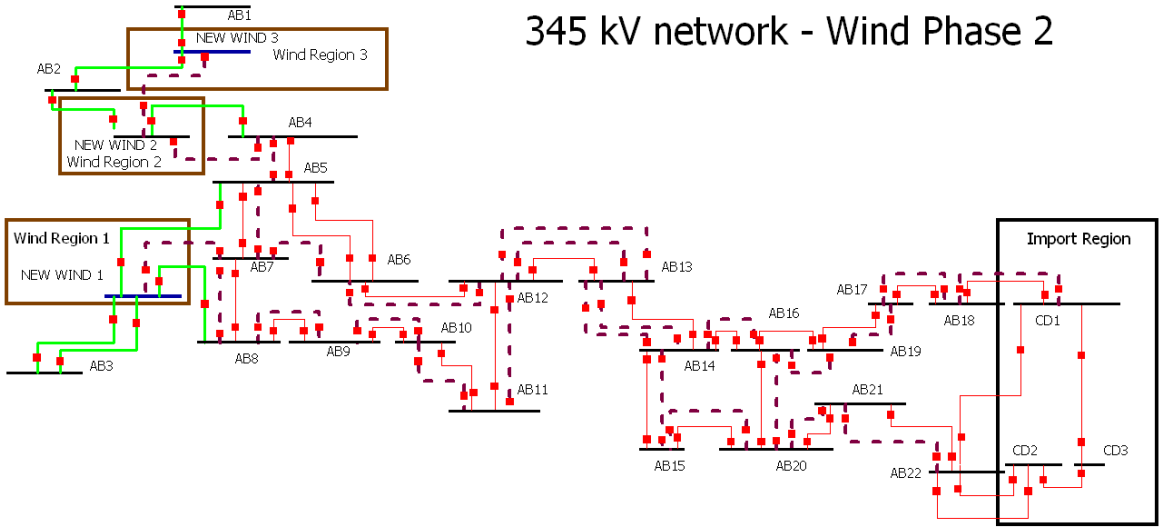


**Figure 57 : Iowa 345 kV network with additional transmission lines**

## 5.3 Wind Phase 1

Three wind parks of 441 MW each are added at the three locations. The first study is to see if the three wind farms were simultaneously operating at 100% output, how much wind power can be delivered to the Import Region. Each wind farm consists of 4 separate aggregated units. Three aggregated units of 126 MW each and one aggregated unit of 63 MW.

To determine the maximum deliverable wind power a unit each is turned on at the three locations and a transfer analysis is done to check for voltage violations. The voltages at 345 kV and 161 kV are monitored. Any post-contingency voltage below 0.9 is considered a criteria violation. The contingencies considered are the loss of any 345 kV line on the West to East path.

The following PV curve demonstrated the limit obtained. The maximum power transfer is obtained with two units on at each location. At a transfer level of 756 MW,

instability is seen. Thus, no more than 250 MW at each location and hence 750 MW total can be accommodated with the current system.

The monitored bus where the voltage violation occurs is a 161 kV bus off one of the buses in the import region. The bus is off the import region bus CD1. The critical contingency in this case is the loss of the line from AB 16 to AB 19. This results into loss of a source into the lines feeding the import bus CD1. This causes post contingency voltage to deteriorate for this contingency.

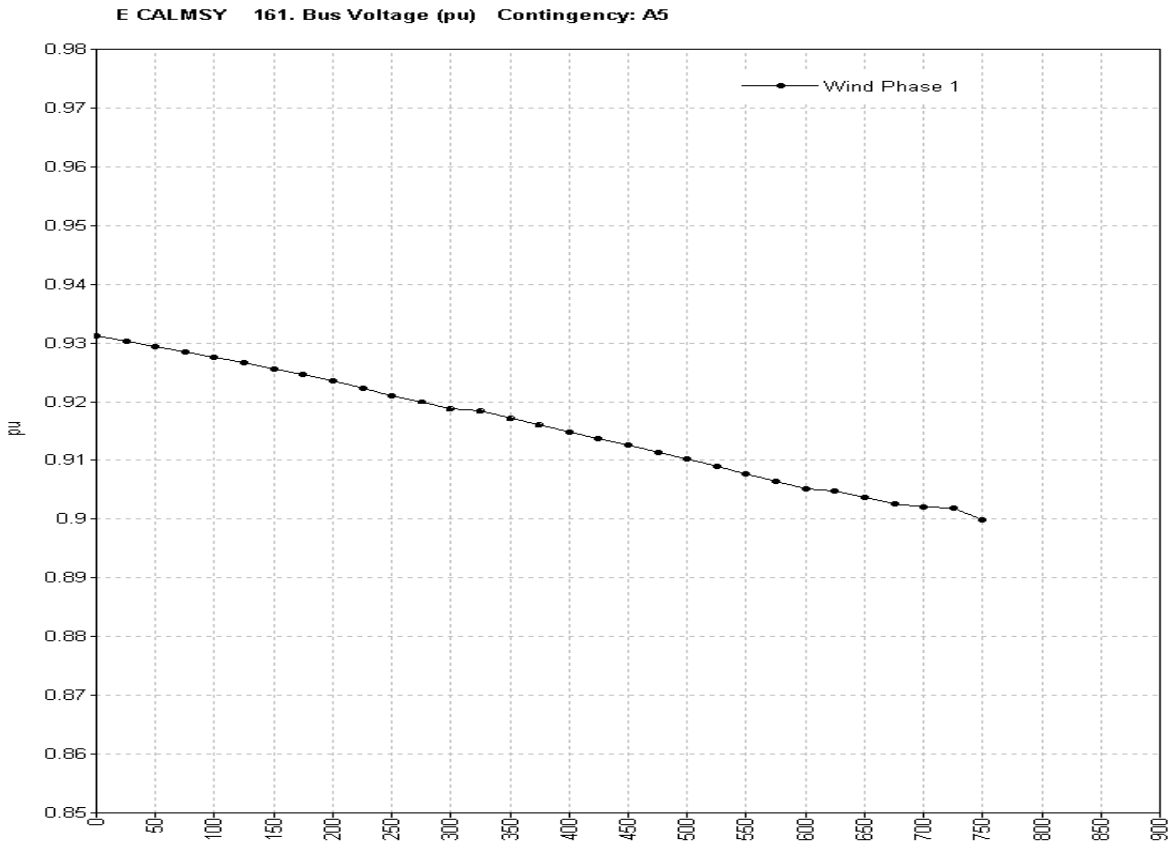


**Figure 58 : Phase 1 - Power Transfer Margin with all 3 regions at 100%**

Figure 58 above indicates the voltage profile at the bus East Calmsy. It is evident that at a power transfer level of 750 MW the voltage at the bus goes below 0.9 p.u. The PV

analysis also shows that the powerflow does not converge beyond the 750 MW transfer level.

## 5.4 Wind Phase 2

The analysis carried out in section 5.3 is repeated for this section. The impact of the additional transmission on the deliverability is studied. No additional reactive power reinforcements are made. In this case the entire power from the three locations is deliverable. The total power transfer margin in this case is 1325 MW.

The voltage violation occurs on the bus Galesbr5. This bus is a 161 kV bus off AB21. The critical contingency here is the loss of the line from AB 20 to AB 21. This direct loss of source to AB21 results in the low voltage at the lower kV bus.

In figure 59 the voltage profile at the monitored bus is plotted with respect to the power transferred from the wind parks. With the reinforced transmission system an additional 600 MW of power can be transferred. The critical contingency and the critical bus are different from the ones in Phase 1.

Again, the voltage violation occurs much before any thermal violations. Thus adding reactive power devices near the border and closer to the load center will help deliver more power to Illinois.

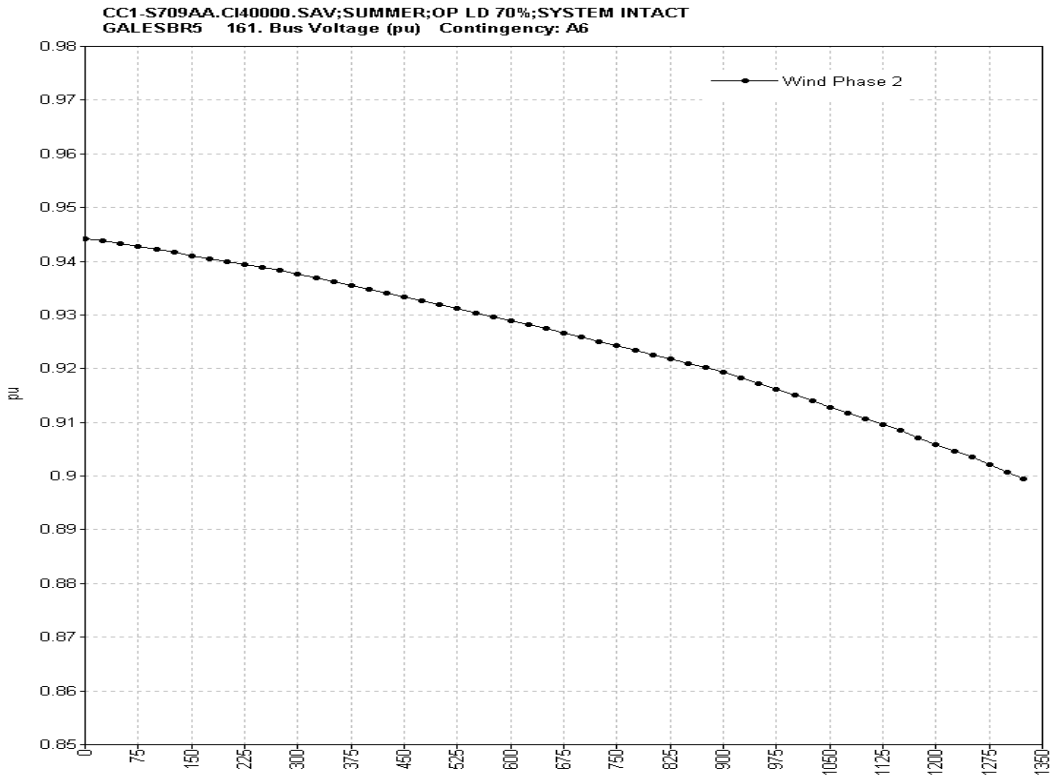


**Figure 59 : Phase 2 - Power Transfer Margin with all 3 regions at 100%**

## 5.5 Impact of Capability Curve at Low Wind Levels

Finally, the impact of using a wind park with low wind speeds to provide reactive power is analyzed. Since the wind parks are very distant from the load center, and the power flow from the wind parks to Chicago passes through the load pocket in central Iowa the additional reactive power does not help increase the transfer margin significantly. The only wind park that has some significant impact is the wind park at location 2. This wind park's reactive power contributes to the power transfer margin because it lies on the path of the power coming from wind region 3. Again the critical contingency is the loss of AB 16 to AB 19. The low voltage bus is the same bus seen in section 5.3.

The two wind parks at region 1 and region 3 are used to transfer power to the load pocket. Figure 60 demonstrates the PV curves plotted for the critical bus at East Calmsy. Two curves are plotted. The red plot is with the wind park at Region 2 off and the black plot is with the wind park producing reactive power. Both the plots violate the minimum voltage around 750 MW. But the system without the wind park at region 2 is closer to instability. The nose point for the case with the wind park producing reactive power is 80 MW higher than the case with the wind park at region 2 off.

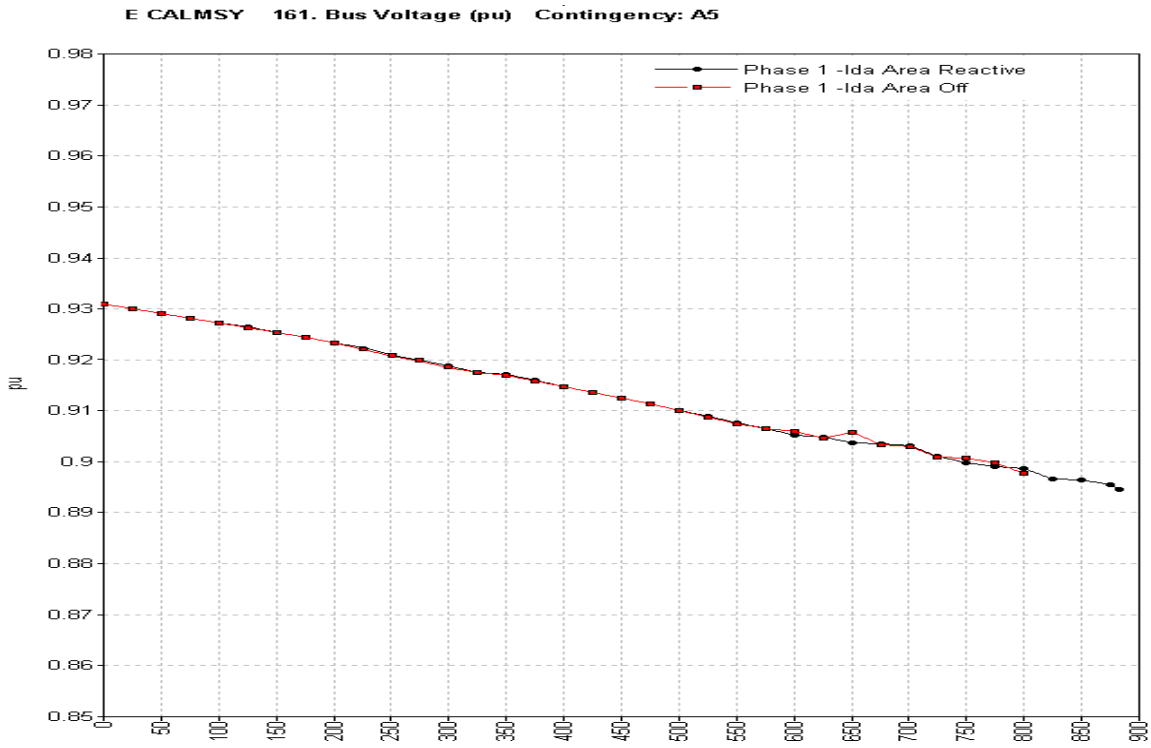


**Figure 60 : Comparison of Power Transfer Margins with/without Region 2 Providing Reactive Power**

## 5.6 Summary of Results

In the above analysis the impact on system voltage performance is analyzed when large scale wind generation is transferred from Western Iowa to Illinois. The maximum power is determined with and without transmission reinforcement. It is seen that the real bottle neck for the west to east power transfer is at the IA/IL border and more reinforcements are needed in that region before more wind can be exported.

The reactive capability of the wind park does not play a big role in increasing power transfer capability. A major reason for this is the distance of the wind farms from the load center and the transmission bottle neck. The way the Iowa system is poised the presence of the central Iowa load center prevents the reactive power from the wind park to help the voltage issues at the IA/IL border.

The wind farms closer to the IA/IL border will play a greater role in increasing transfer capability. In the above analysis only the new wind added is used for reactive power support. Since it is difficult to determine the location of the existing wind farms with respect to the grid and the west to east 345 kV corridor, they could not be used to determine the enhanced performance.

# CHAPTER 6: CONCLUSIONS

## 6.1 Summary of Work

A DFIG capability curve is developed for a 1.5 MW machine. The development of the capability curve is detailed in chapter 2. The DFIG machine in voltage control mode has significant reactive power capability, which can contribute to improved system performance. The FERC mandated requirement of maintaining power factor at the interconnection restricts the wind park from maximizing its contribution to improved voltage performance. DFIG wind parks implementing capability curve control may substantially reduce system losses, especially at low plant output levels. The additional reactive capability leads to larger power transfer capability in the system.

In chapter 3, a novel voltage stability assessment tool that incorporates wind variability is developed. The technique developed is general and is applicable for any type of wind generation technology. The traditional methodology of drawing PV curves to assess static voltage stability margin is modified to address the intermittent nature of wind energy. Given a range of wind variability, the developed tool calculates sets of PV curves plotted along parallel planes, thus giving a three-dimensional VSROp.

The tool is used to determine the VSROp for a 23-bus test system. It is then utilized to compare the effect of utilizing the DFIG capability curve over the FERC-mandated ±0.95 power factor requirement. The results demonstrate that restricted power factor operation could lead to an overly conservative estimate of the power transfer capability of the system, while use of the capability curve causes a substantial increase in the power transfer capability of the system. Also, the results demonstrate that the redispatch

strategy chosen to dispatch against wind is an important factor in determining system voltage stability margins. The critical contingency on the system is shown to vary with varying wind levels.

In chapter 4, a large system implementation of the DFIG capability curve for an off shore wind farm is carried out. The steady state and dynamic analysis indicate that the additional reactive capability at low wind levels helps alleviate voltage margin issues in the coastal load pocket and also helps serve peak load periods by providing reactive support. The employing of capability curve makes a strong case for wind integration by reducing the reliability impacts of variable wind.

In chapter 5, the Western Iowa high wind pocket and the ability to export power from that pocket to the east is analyzed. The transmission bottleneck is determined to be distant from the wind generators, and thus the additional reactive capability does not help improve the power transfer capability. But if the wind units were on a more direct path into the load center, especially in the form of a high kV line from wind parks to the load centers, like the Green Power Express, the impact of the capability curve would be higher.

## 6.2 Significant Contributions

Large scale penetration of wind energy in the system raises significant concerns regarding the reliability implications of large scale variable generation. The work presented in this thesis provides a methodology to utilize the capability curve of the DFIG machine to enhance the voltage performance of the system. By utilizing wind parks as reactive sources during low wind periods can facilitate maintaining balanced system voltages. Not all wind parks will provide a significant impact, but any wind park that has direct access to load

centers or is on a transmission path carrying large amounts of power; will provide a substantial system performance improvement.

Since the general trend for on shore wind is having low wind centers closer to load and high wind regions away from load, the wind parks closer to the load centers can facilitate more power from the remote high wind areas to access the load pockets. This allows for maximum utilization of the transmission system built for large scale wind integration. An example for this can be seen by considering a wind park close to the load center. During periods of high wind at the wind park closer to load, it will provide real power to the load center. When the wind park close to the load has low wind levels, it will provide reactive power which will facilitate maximum transfer of power from the distant wind generation. Since the general trend is that remote wind parks have better capacity factors, there is a high probability that when the wind park close to the load is having low power outputs, the remote wind park will tend to have better wind levels.

In the case of off shore wind parks, their proximity to load pockets makes the ability to provide reactive power to the load pockets a significant benefit in terms of reliability improvement.

Finally, the VSROp methodology is a general method to analyze systems with large scale wind penetration and determine the susceptibility of the system reliability to wind variability. The methodology helps assess if a particular redispatch strategy will adversely impact the system reliability, if the wind ramps up or down. The work demonstrates that the critical contingency and the transfer margin vary with the wind levels on the system. Also the variation in transfer margin is not monotonic, and the system topology and generator levels will impact the variation in transfer margins. This tool

provides a simplified method to obtain a secure region of operation, which can be a useful in an operations environment.

## 6.3 Future Scope

The above work demonstrates the positive impact that utilizing the capability curve of wind parks has on the voltage performance of a power system. The additional benefit is especially amplified for those wind parks that are in close proximity to load centers.

With a large number of conceptual transmission networks being suggested to deliver wind from the central part of the United States to the load centers in the Eastern part of the country, a number of questions come up regarding the level of utilization of these transmission lines and the associated costs of building these lines. An alternative would be to plan the transmission along a string of wind parks. The wind parks closer to load can serve the load when they have high wind speeds, and during low wind periods the reactive support provided by these close to load wind parks will allow the remote wind parks to deliver power to the load. From the load's perspective the transmission corridor will be like a constant source of power. This new philosophy can lead to sharing of the transmission line cost by all the wind parks along the corridor and helps handle the wind variability aspect effectively.

The analysis in section 5 is restricted to a steady state analysis. To make a more complete assessment of the deliverability of the wind from western Iowa to the Chicago load pocket, the steady state analysis should be backed up with dynamic simulations.

The VSROp is a useful tool for large practical systems. But to accurately carry out the analysis detailed information of the reserve generator's location and their capacities must be available. With the deregulated market environment, even though the large system data was available, the details of the generating units on the system, in terms of their fuel type and ramp rates are not available.

With the limited data available, a VSROP was determined for the Midwest area of the power system. An attempt was made to attain maximum penetration of wind power. In this analysis, the location of the wind units was not chosen based on wind speeds. Any location on the system where wind could be integrated successfully was deemed to be a wind site.

The study area constituted of 5600 buses with 11 areas. The total base case load in the study region is 63,600 MW with 6500 MW coming from Wind. With a given set of 50 critical contingencies, the minimum power transfer margin possible is 300 MW. In the total wind region, 3000 MW is varied to determine the VSROp. To compensate for reduced wind, additional units are brought online. The redispatch units are distributed between the load pockets in direct proportion to the load in each area. The existing online units are either ramped up or down in totality to reflect reserves.

The figure 61 shows the two VSROP's for the system. In one case the capability curve is utilized and in the other case the restricted power factor mode is used. It can be seen that the capability curve gives a higher transfer margin throughout the range of wind variability. It is also seen that the critical contingency varies as the wind level varies. For a given wind level, the choice of reactive power dispatch is a decisive factor in determining the critical contingency.

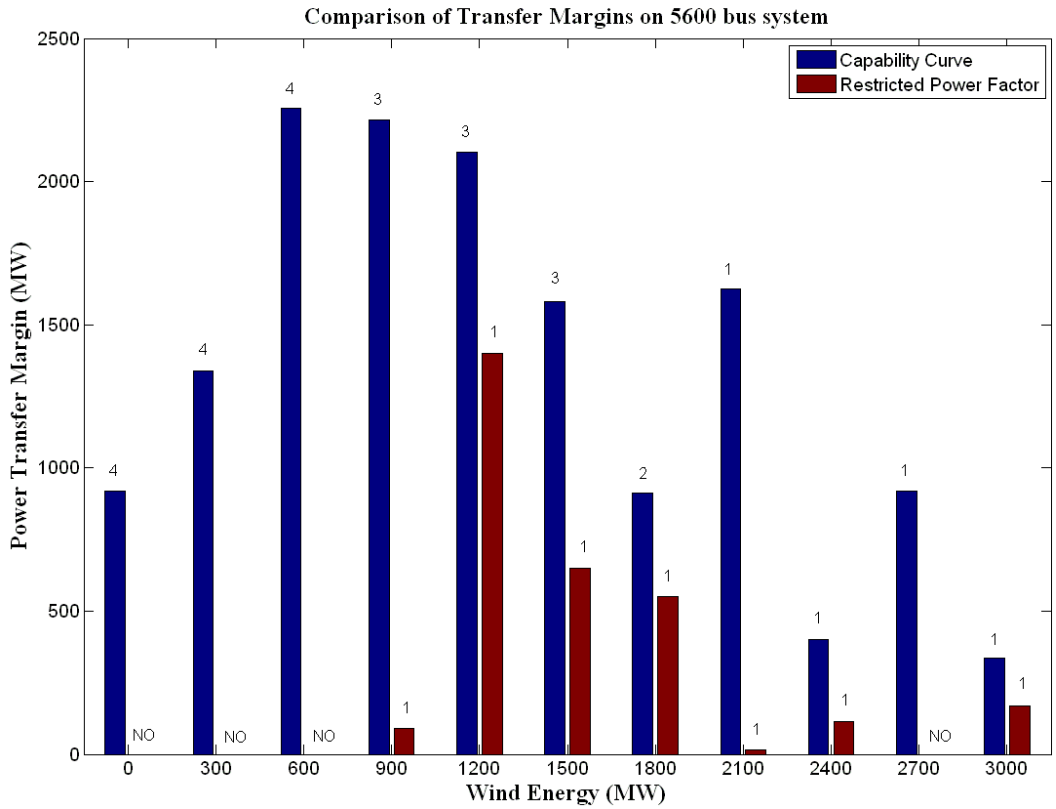


**Figure 61 : Sample VSROP for the 5600 bus Study Area**

The above VSROP is just a basic implementation with the limited data available. Another possible analysis for VSROP is to consider large scale transmission development from Illinois to the Dakotas. Consider initial dispatch with all the wind in Western Iowa on. Then consider the reduction in wind in western Iowa with the power being picked up by the higher capacity wind in the Dakotas. This would be a good way to see the impact of maximum utilization of transmission that is built to deliver wind.

# BIBLIOGRAPHY


1. R. Zavadil, N. Miller, A. Ellis, and E. Muljadi, "Making connections," *IEEE Power & Energy Magazine*, pp. 26–37, November/December 2005.
2. R. Doherty, "Establishing the role that wind generation may have in future generation portfolios," *IEEE Transactions on Power Systems*, vol. 21, no. 3, pp. 1415–1422, August 2006.
3. American Wind Energy Association: 2009: Another Record Year for Wind Energy Installations.
4. Renewable Energy Policy Network for the 21st Century, Global Status Report: 2009.
5. T. Berry, M. Jaccard, "The renewable portfolio standard: design considerations and an implementation survey", *Energy Policy*, vol. 29, no. 4, pp. 263-277, March 2001.
6. L. Bird, M.Bolinger, T.Gagliano, R. Wiser, M. Brown, B. Parsons, "Policies and market factors driving wind power development in the United States", *Energy Policy*, vol. 33, no. 11, pp. 1397-1407 , July 2005.
7. American Wind Energy Association (AWEA), "Legislative Affairs", Retrieved on 17th July, 2008, from Available: http://www.awea.org/legislative/
8. S.Muller, M.Deicke and Rik W. De Doncker, "Doubly Fed Induction Generator Systems for Wind Turbines," *IEEE Industry Applications Magazine*, pp. 26-33, May/June 2002.
9. Website: Institute of Energy Technology-Aalborg University: www.iet.aau.dk/education
10. A.D. Hansen, L H. Hansen, "Wind Turbine Concept Market Penetration over 10 Years (1995-2004)", *Wind Energy*, vol. 10, no.1, pp.81-97, 2007.

11. B. Parsons et al., “Grid Impacts of Wind Power: A Summary of Recent Studies in the United States”, *Wind Energy,* vol. 7, no., pp. 87-108, 2004.
12. Ming Ni, J.D. McCalley, V. Vittal, T. Tayyib, "Online risk-based security assessment," *Power Systems, IEEE Transactions on* , vol.18, no.1, pp. 258-265, Feb 2003
13. P. Kundur, Power System Stability and Control. New York: McGraw-Hill, 1994, pp. 27-33, pp. 209-211.
14. C. W. Taylor, Power System Voltage Stability. New York: McGraw-Hill, 1994, pp. 6-13.
15. V. Ajjarapu, Computational Techniques for Voltage Stability Assessment and Control, New York: Springer Science, 2006, pp. 1-3.
16. A.M. Abed, “WSCC voltage stability criteria, under-voltage, load shedding strategy, and reactive power reserve monitoring methodology,” in Proc. IEEE Power Engineering Society Summer Meeting, vol. 1, Edmonton, AB, Canada, Jul. 1999, pp. 191–197.
17. D. Feng, B.H. Chowdhury, M.L. Crow, L. Acar, “Improving voltage stability by reactive power reserve management,” *IEEE Trans. on Power Systems,* vol. 20, no.1, pp. 338-345, February 2005.
18. T.J.E. Miller, Reactive power control in electric systems, Wiley, New York (1982), pp. 129-131.
19. T. Van Cutsem, “Voltage instability: Phenomenon, countermeasures and analysis methods,” *Proceedings of the IEEE,* vol. 88, no. 2, pp. 208-227, Feb 2000.

20. K. Bhattacharya, J. Zhong, "Reactive Power as an Ancillary Service," *Power Engineering Review, IEEE*, vol. 21, no.5, pp. 64-64, May 2001

21. L. Xu, P. Cartwright, "Direct active and reactive power control of DFIG for wind energy generation," *IEEE Trans. on Energy Conversion*, vol. 21, no. 3, pp. 750-758, Sept. 2006.

22. F.M. Hughes, O. Anaya-Lara, N. Jenkins, G. Strbac, "A power system stabilizer for DFIG-based wind generation," *IEEE Trans. on Power Systems*, , vol. 21, no. 2, pp. 763-772, May 2006.

23. G. Tapia, A. Tapia, J.X. Ostolaza, "Proportional–Integral Regulator-Based Approach to Wind Farm Reactive Power Management for Secondary Voltage Control," *IEEE Trans. on Energy Conversion*, vol. 22, no. 2, pp. 88-498, June 2007.

24. A.Tapia, G. Tapia, J. X. Ostolaza, "Reactive power control of wind farms for voltage control applications", *Renewable Energy*, vol. 29, no. 3, pp. 377-392, March 2004.

25. Federal Energy Regulatory Commission (FERC), Order No. 661 on Interconnection for Wind Farms, June 2, 2005.

26. Federal Energy Regulatory Commission (FERC), Order No. 661A (Order on Rehearing) on interconnection for wind farms, December 12, 2005.

27. T. Lund, P. Sorensen, J. Eek, "Reactive Power Capability of a Wind Turbine with Doubly Fed Induction Generator", *Wind Engineering*, no. 10, pp. 379-394, 2007.

28. H.W. Dommel, W.F. Tinney, "Optimal Power Flow", *IEEE Transactions on Power Apparatus and Systems*, October 1968.

29. H. Wang, C. E. Murillo-Sánchez, R. D. Zimmerman, R. J. Thomas, "On Computational Issues of Market-Based Optimal Power Flow", *IEEE Transactions on Power Systems*, Vol. 22, No. 3, Aug. 2007, pp. 1185-1193.

30. "MATPOWER User's Manual", *MATPOWER 3.2 solver* [Online] Available: http://www.pserc.cornell.edu/matpower/

31. R.Piwko, R. DeMello, R. Gramlich, W. Lasher, D. Osborn, C. Dombek, K. Porter, "What Comes First?," *Power and Energy Magazine, IEEE*, vol. 5, no. 6, pp.68-77, Nov.-Dec. 2007.

32. P. Pinson, C. Chevallier, G.N. Kariniotakis, "Trading Wind Generation From Short-Term Probabilistic Forecasts of Wind Power," *Power Systems, IEEE Transactions on* , vol.22, no.3, pp.1148-1156, Aug. 2007

33. A.Fabbri, T.GomezSanRoman, J. RivierAbbad, V.H. MendezQuezada, "Assessment of the Cost Associated With Wind Generation Prediction Errors in a Liberalized Electricity Market," *Power Systems, IEEE Transactions on* , vol.20, no.3, pp. 1440-1446, Aug. 2005

34. P. Kundur, J. Paserba, V. Ajjarapu, G. Andersson,A. Bose, C. Canizares, N. Hatziargyriou, D. Hill, A. Stankovic, C. Taylor, T. Van Cutsem, V. Vittal, "Definition and classification of power system stability IEEE/CIGRE joint task force on stability terms and definitions," *Power Systems, IEEE Transactions on* , vol.19, no.3, pp. 1387-1401, Aug. 2004

35. B. Gao, G. K. Morison, and P. Kundur, “Toward the development of a systematic approach for voltage stability assessment of large-scale power systems,” IEEE Trans. Power Syst., vol. 11, no. 3, pp. 1314–1324,Aug. 1996.

36. T. Nagao, K. Tanaka, and K. Takenaka, “Development of static and simulation programs for voltage stability studies of bulk power system,” IEEE Trans. Power Syst., vol. 12, no. 1, pp. 273–281, Feb. 1997.

37. P. Kundur, Power System Stability and Control. New York: McGraw-Hill, 1994.

38. C. A. Canizares, A. C. Z. De Souza, and V. H. Quintana, “Comparison of performance indices for detection of proximity to voltage collapse,” IEEE Trans. Power Syst., vol. 11, no. 3, pp. 1441–1447, Aug. 1996.

39. A. Sode-Yome and N. Mithulananthan, “Comparison of shunt capacitor, SVC and STATCOM in static voltage stability margin enhancement,” Int. J. Elect. Eng. Educ., vol. 41, no. 3, Jul. 2004.

40. IEEE/PES Power System Stability Subcommittee, Voltage Stability Assessment: Concepts, Practices and Tools, special publication, final draft, Aug. 2003.

41. C. W. Taylor, Power System Voltage Stability. New York: McGraw-Hill, 1994.

42. A.M. Abed., "WSCC voltage stability criteria, undervoltage load shedding strategy, and reactive power reserve monitoring methodology," *Power Engineering Society Summer Meeting, 1999. IEEE* , vol.1, no., pp.191-197 vol.1, 18-22 Jul 1999

43. L. Bao, Z. Huang, W. Xu, "Online voltage stability monitoring using VAr reserves," *Power Systems, IEEE Transactions on* , vol.18, no.4, pp. 1461-1469, Nov. 2003

44. EPRI Final Report EL-461 0, “Extended Transient-Midterm Stability Package: Final Report”, Prepared by Ontario Hydro, November 1992.

45. J. Deuse and M. Stubbe, "Dynamic simulation of voltage collapses," *Power Systems, IEEE Transactions on* , vol.8, no.3, pp.894-904, Aug 1993

46. W.W. Price, D.B. Klapper, N.W. Miller, A. Kurita, and H. Okubo, "A Multiple Faceted Approach to Power System Voltage Stability Analysis," *CIGRE,* paper 38-205, 1992.

47. T. Van Cutsem, **Y.** Jacquemart, J.-N. Marquet, and P. Pruvot, "A Comprehensive Analysis of Mid-term Voltage Stability," paper 94 SM 51 1-6 PWRS, presented at IEEE/PES Summer Meeting, San Francisco, CA, July 24-28, 1994.

48. B. Gao, G.K. Morison, and P. Kundur, "Voltage stability evaluation using modal analysis," *Power Systems, IEEE Transactions on* , vol.7, no.4, pp.1529-1542, Nov 1992

49. T. Van Cutsem, "A method to compute reactive power margins with respect to voltage collapse," *Power Systems, IEEE Transactions on* , vol.6, no.1, pp.145-156, Feb 1991

50. F. L. Alvarado and T. H. Jung, “Direct detection of voltage collapse conditions,” in *Bulk Power System Voltage Phenomenon I\—Voltage Stability and Security* Potosi, MO, pp. 5.23-5.38.

51. V. Ajjarapu and C. Christy, "The continuation power flow: a tool for steady state voltage stability analysis," *Power Systems, IEEE Transactions on*, vol.7, no.1, pp.416-423, Feb 1992.

52. I. Dobson and L. Lu, "Using an Iterative Method to Compute a Closest Saddle Node Bifurcation in the Load Power Parameter Space of an Electric Power System," Bulk Power System Voltage Phenomena, Voltage Stability and Security, NSF Workshop, Deep Creek Lake, MD, August 1991.

53. U.S. Department of Energy, Energy Efficiency and Renewable Energy, (2008, July). 20% Wind Energy by 2030: Increasing Wind Energy's Contribution to U.S. Electricity Supply

54. North American Electric Reliability Corporation, Integration of Variable Generation Task Force,(2008,April), Accommodating High Levels of Variable Generation.

55. A.A. Chowdhury and D.O. Koval, "Modeling Non-Dispatchable Wind Energy Sources in Generating Capacity Reliability Planning", Proceeding (442) European Power and Energy Systems - 2004, available online - http://www.actapress.com/PaperInfo.aspx?PaperID=17989&reason=500

56. W. Musial and S. Butterfield, "Future for Offshore Wind Energy in the United States", *EnergyOcean 2004*,Palm Beach, Florida, June 28-29, 2004

57. Web site for AWS Truewind, Accessed May 19, 2004. http://www.awstruewind.com/inner/windmaps/windmaps.htm

58. Cape Wind Associates Website: http://www.capewind.org/ accessed on January 23, 2006.

59. ISO New England – Regional System Plan 2009. Available Online : http://www.iso-ne.com/trans/rsp/2009/rsp09_final.pdf

60. "Installation Guide and User Manual", *VSAT version 9.0*

61. "Program Operation Manual", PSS/E Version 30, Siemens PTI.

62. "Program Application Guide", PSS/E Version 30, Siemens PTI

63. K. Clark, N.W. Miller, J.J. Sanchez-Gasca, "Modeling of GE Wind Turbine-Generators for Grid Studies", *Version 4.3* April 8, 2009.

64. Y. Kazachkov, P-K. Kweng, K. Patil, "PSS/E Wind Modeling Package for GE 1.5/3.6/2.5 MW Wind Turbines*", Issue 5.1.0*, July, 2009

65. American Wind Energy Association, AWEA, Website : http://www.awea.org/projects/

66. National Renewable Energy Laboratory(NREL), Website : www.nrel.gov

67. Iowa Energy Center, Website : http://www.energy.iastate.edu/Renewable/wind/maps/annual.htm

## ACKNOWLEDGEMENTS

I am extremely grateful to my major professor, Dr Ajjarapu for providing me an opportunity as a research assistant. My work here at ISU under his guidance will go a long way in shaping my future and helping me achieve my objectives. I would like to extend a special thanks to Dr McCalley and Dr Vaidya, for their contributions towards this work and their wonderful classroom teaching. I would also like to show my gratitude towards all the ISU faculties, especially in the energy and power systems group who have made this stay at ISU a great learning experience. I am indebted to my many fellow graduate students, who have constantly contributed to my educational career at ISU.